West Pacific climate and circulation over the last 160 kyr: A palaeontological and geochemical multiproxy reconstruction within the inflow path of the Indonesian Throughflow

Dissertation

zur Erlangung des Doktorgrades

der Mathematisch-Naturwissenschaftlichen Fakultät

der Christian-Albrechts-Universität

zu Kiel

Vorgelegt von

Timothé Bolliet

2010

West Pacific climate and circulation over the last 160 kyr: A palaeontological and geochemical multiproxy reconstruction within the inflow path of the Indonesian Throughflow

Dissertation

zur Erlangung des Doktorgrades

der Mathematisch-Naturwissenschaftlichen Fakultät

der Christian-Albrechts-Universität

zu Kiel

Vorgelegt von

Timothé Bolliet

2010

Referent: Prof. Dr. Wolfgang Kuhnt

Koreferent: Prof. Dr. Ralph Schneider

Tag der Disputation: 19/07/2010

Zum Druck genehmigt:

Der Dekan:

EIDESSTATTLICHE ERKLÄRUNG

Hiermit erkläre ich an Eides statt, dass die vorliegende Dissertation mit dem Titel ‘West Pacific climate and circulation over the last 160 kyr: A palaeontological and geochemical multiproxy reconstruction within the inflow path of the Indonesian Throughflow’, abgesehen von der Beratung durch meine akademischen Lehrer, in Inhalt und Form meine eigene Arbeit darstellt. Ferner habe ich weder diese noch eine ähnliche Arbeit an einer anderen Hochschule im Rahmen eines Prüfungsverfahrens vorgelegt.

Kiel, den 19.07.2010

Timothé Bolliet

Contents

List of Figures

Chapter I: Introduction

Chapter II: Mindanao Dome variability over the last 160 kyr: Episodic glacial cooling of the West Pacific Warm Pool

Chapter III: Deglacial re-organization of Pacific intermediate water masses during terminations I and II

Chapter IV: Monsoon variability and deep oceanic circulation in the western equatorial Pacific over the last climatic cycle: insights from sedimentary magnetic properties and sortable silt.

Chapter V: A mid-Holocene transition in the nitrogen dynamics of the western equatorial Pacific: Evidence of a deepening thermocline?

Acknowledgements

The first person I would like to thank is my primary supervisor Prof. Dr. Wolfgang Kuhnt for having offered me this position and for having guided, advised and supported me during my entire PhD program. For the same reasons, I would like to thank Dr. Ann Holbourn who has been available at any moment of those years for giving me particularly precious work direction, petinent remarks, as well as for encouraging me or sometimes persuading me to relax a bit. If by chance any student seriously interested in doing a PhD in micropaleontology or paleoceanography was reading this manuscript, I really would give her or him the advise, from my personal experience, to try to work under the supervision of Wolfgang and Ann.

I also would like to thank all the people who help me in my work: Jian Xu, Brigitte Salomon, Karin Kißling, Nils Andersen, Dieter Garbe-Schönberg, Pieter Grootes, Catherine Kissel, Carlo Laj, Markus Kienast, Luc Beaufort, Noëlle Buchet, Michael Sarnthein and of course all the HIWI team. My name is on this manuscript, but it would have never been possible to do it without all those persons. I also sincerely thank Guillaume Leduc for all the scientific discussions we had and who tremendously helped me in my work. Once again, if by chance any director of earth science institute looking for a serious researcher is reading this text, I really would advise her or him to hire Guillaume. This man is just amazing. He knows all the papers, manages 497 various projects simultaneously and can discuss about the past, present and future climate at any timescale and in any location.

I am particularly grateful to my friends Anke and Markus who have been supporting me since the first moment. Well, actually Anke even took care of me before the first moment of my PhD as I was (surprisingly...) late on my arrival day in Kiel, so she already had to wait for me before knowing me. Thank you very much for all the very nice moments I had with you two, all the laughs, the “battles of the best”. Those are precious and *good quality* moments. I will not forget them.

I will not forget all the great moments Veronica and I had as well. I am very glad to know you my friend, and I wish you to success in your PhD. I will miss your elegant jokes and drawing of mouches.

I also would like to thank Mrs *“Lova Lova”* Franzisca very much. You made considerable work as a HIWI but I also would like to thank you for our friendship, for

all the funny or serious discussions we had, and for all you did for helping me with the obscure german administration. Keep on being cool. I wish you all the best for the future.
I finally would like to thank all the colleagues and friends from the Institut für Geowissenschaften (yes, my skills in German considerably increased during these almost 4 years) for all the nice conversations we had during lunch and parties: Rina, Steffi, Laura, Birgit, Janne, Uta, Emma, Yiming and Thomas, as well as Mohamed, Liya, Slava and Opeyemi.

And now, it´s time to write en Francais. J´ai également beaucoup de personnes à remercier dans la langue de Molière.
Je remercie donc pour commencer ma famille qui m´a toujours supporté pendant cette thèse, particulièrement lors de mes (régulières) périodes de doute. Merci mille fois, et par la même occasion, merci à l´inventeur du télephone.
J´aimerais également remercier tout le groupe francais de l´institut: Nabil, avec qui j´ai vraiment passé de mémorables moments, particulièrement notre voyage à Shanghai. Je te souhaite une grande carrière scientifique, et vu ta motivation, je ne me fais pas trop de soucis. Envoie moi une photo quand tu auras une enorme Audi.
Johan, peu de chances que tu lises ce manuscrit mais je te souhaite également une belle carrière et j´espère que ton projet Parisien se déroulera bien.
J´aimerais remercier Elfi également, pour sa bonne humeur perpetuelle et son dynamisme qui font plaisir à voir. Je te souhaite une très bonne fin de thèse également.
Je tiens à remercier une deuxième fois Guillaume mais cette fois c´est l´ami que je remercie, pas le collègue. Nos fous rires et conversations surréalistes vont me manquer.
Je remercie chaleureusement toute ma bande d´amis en France, et notamment Amandine, Benoît et Nelly pour m´avoir rendu visite dans le grand Nord.
Un merci aussi à toute la faune sauvage de FA également.

Enfin, j´aimerais particulièrement remercier Camille, simplement pour tout le bonheur que tu m´as apporté ces derniers mois.

Abstract

Understanding the Earth´s present day climate and predicting its future evolution require investigation of high resolution sedimentary archives providing critical information of past oceanic and atmospheric variability. This study is based on two continuous marine sedimentary successions (Cores MD06-3067 and MD06-3075), recovered close to Mindanao Island (Philippines). The Indo-Pacific region represents a major source of heat and moisture, which are redistributed to the high latitudes by atmospheric and oceanic circulations; thus this region is a major actor in regulating global climate. The two cores investigated in this work are located within the inflow path of the Indonesian Throughflow. This ocean current provides a critical link within the thermohaline circulation by transferring relatively cold and fresh upper water from the equatorial western Pacific to the Indian Ocean through the complex seaways of the Indonesian archipelago, in turn affecting atmospheric and oceanic circulation within the entire Pacific and Indian Oceans.

Our data indicate that Core MD06-3067 (1575 m water depth) provides an essential archive of atmospheric and surface to mid-depth oceanic circulation for the western equatorial Pacific over the last 160 kyr. Paleotemperature reconstruction performed on surface and deep-dwelling species of foraminifera from this core indicates large-amplitude variations in sea surface and thermocline temperatures and major fluctuations of the upper ocean thermal contrast occurring on glacial-interglacial and suborbital timescales. These variations in upper-ocean thermal contrast are interpreted as reflecting changes in the activity of a major regional upwelling system (Mindanao Dome). Enhanced activity of the Mindanao Dome during the last glacial maximum and MIS 4 compared to MIS 6 is revealed by anomalously cold surface waters and increased productivity, indicated by coccolith and benthic foraminiferal assemblages. In contrast, high sea surface temperature resulting from episodic decreases in the activity of the dome coincide with Antarctic warm events A1-4. These fluctuations in upwelling activity appear related to latitudinal migrations of the Intertropical Convergence Zone, inducing fundamental changes in monsoonal wind regimes and oceanic circulation patterns.

Oxygen and carbon stable isotopes analysis performed on benthic foraminifera from Core MD06-3067 in the open west Pacific Ocean indicate long-term influence of mid-

depth water originating from the Southern Ocean, interrupted during terminations I and II by abrupt incursions of ^{13}C-depleted water masses coming from the North Pacific. These sudden shifts in the intermediate and deep water circulations close to Mindanao island indicate major re-organization of the latitudinal extent of the mid-depth water masses in the whole Pacific basin, related to glacial/interglacial climatic transitions. Comparison with stable isotope records from the deeper Core MD06-3075 (1878 m), located in the more marginal Davao Gulf, indicates a highly contrasted evolution of the mid-depth circulation at these two sites over the last termination. Lower benthic $\delta^{13}C$ values in Core MD06-3075, particularly during MIS2, reflect poorer ventilation and/or differences in carbon export flux at this more proximal location within the Davao Gulf. There is no evident incursion of North Pacific intermediate or deep water during deglaciation, possibly due to the relative isolation of the Davao Gulf from the open Pacific Ocean and/or to different sourcing of deep and intermediate waters at this site.

Zusammenfassung

Für das Verständnis des heutigen globalen Klimas und für Vorhersagen der zukünftigen Klimaentwicklung ist die Erforschung hochauflösender sedimentärer Archive früherer mariner und atmosphärischer Klimavariablität eine unabdingbare Voraussetzung. Die hier vorgelegte Arbeit beruht auf zwei kontinuierlichen marinen Sedimentabfolgen (MD06-3067 und MD06-3075), die in der Nähe von Mindanao (Philippinen) gekernt wurden. Die Indo-Pazifische Region stellt heute eine bedeutende Quelle von Wärme und Feuchtigkeit dar, die von dort durch atmosphärische und marine Zirkulation in hohe Breiten transportiert werden; dadurch wird diese Region zu einem bedeutenden Faktor für das globale Klimagleichgewicht. Die beiden untersuchten Kerne liegen im Einstrombereich des indonesischen Durchstroms. Dieser Ozeanstrom transportiert heute relativ kühle und süsse oberflächennahe Wassermassen in einer komplexen Passage durch den indonesischen Archipel vom äquatorialen Westpazifik in den indischen Ozean und stellt damit nicht nur ein kritisches Bindeglied in der globalen thermohalinen Zirkulation dar, sondern beeinflußt damit auch die atmosphärischen und ozeanischen Strömungsmuster sowohl im Pazifik als auch im indischen Ozean.

Kern MD06-3067 aus 1575 m Wassertiefe stellt ein ausgezeichnetes Archiv der Zirkulation in der Atmosphäre und der oberflächennahen- bis intermediären Wassermassen im westlichen äquatorialen Pazifik während der letzten 160 000 Jahre dar. Paläotemperatur-Rekonstruktionen an oberflächennah und in größeren Wassertiefen um 100 m lebenden planktonischen Foraminiferen zeigen bedeutende Schwankungen der Meeresoberflächen- und Thermoklinen-Temperaturen auf glazialen-interglazialen und suborbitalen Zeitskalen. Diese Variabilität in den Temperaturen des oberen Ozeans wird als Ausdruck der Aktivität des bedeutenden regionalen Auftriebssystems (Mindanao Dome) gedeutet. Verstärkte Aktivität des Mindanao Dome Auftriebs während des letzten glazialen Maximums und des marinen Isotopenstadiums (MIS) 4 im Vergleich zu Interglazialen und MIS 6 wird durch ungewöhnlich kalte Oberflächenwassermassen und erhöhte Produktivität (Coccolithen und benthische Foraminiferengemeinschaften) angezeigt. Hohe Oberflächentemperaturen, die mit einer Abschwächung der Aktivität des Mindanao Dome in Zusammenhang stehen, entsprechen den Antarktischen Warm-Ereignissen

A1-4. Diese Schwankungen der Auftriebsaktivität werden mit meridionalen Verschiebungen der intertropischen Konvergenzzone in Zusammenhang gebracht, die grundlegende Änderungen des lokalen Monsun-Windregimes und der daraus resultierenden ozeanischen Zirkulationsmuster nach sich ziehen.

Sauerstoff und Kohlenstoffisotopenanalysen an benthischen Foraminiferen des Kerns MD06-3067 im offenen West Pazifik zeigen den langfristigen Einfluß intermediärer Wassermassen aus dem Südozean, der nur kurzfristig während der Glazialen Terminationen I und II durch abruptes Einströmen ^{13}C-armer Wassermassen aus dem Nord-Pazifik unterbrochen wurde. Diese plötzlichen Änderungen der intermediären und Teiefenwasserzirkulation vor Mindanao belegen bedeutende Fluktuationen der meridionalen Ausdehnung intermediärer Wassermassen im Pazifik während glazialer-interglazialer Klimawechsel. Ein Vergleich mit benthischen stabilen Isotopensignalen des tieferen Kerns MD06-3075 (1878 m), der innerhalb des Davao Golfs gelegen ist, zeigt deutliche Unterschiede in der Entwicklung der intermediären Zirkulation zwischen diesen beiden Lokationen. Niedrigere $\delta^{13}C$-Werte in Kern MD06-3075, speziell während MIS2, spiegeln eine geringere Ventilation und/oder höheren Kohlenstoffffluß an dieser proximaleren Lokalität im Davao Golf wieder. Es gibt hier keine Hinweise auf den Einfluß von nordpazifischem Zwischenwasser während der glazialen Termination, was wahrscheinlich an einer Barriere zum offenen Pazifik und damit an einer unterschiedlicher Herkunft der tiefen und intermediären Wassermassen an dieser Lokalität liegt.

CHAPTER I: Introduction

Understanding the Earth's current climate and predicting future trends over the next centuries rely heavily on studies of past climate archives. The main target of this work is to investigate past climatic and oceanographic conditions in a sensitive area of the equatorial western Pacific Ocean during the late Pleistocene and Holocene (160 ka to present day). This area is critical in driving major regional climatic features such as El Niño-Southern Oscillation (ENSO) and the East Asian monsoon, and also acts as a major link in the global thermohaline circulation, which regulates global climate. This work provides a contribution to understand the climatic evolution of the equatorial western Pacific Ocean, and results may also help to optimize and validate circulation models monitoring the past, present and future regional and global climate.

1 – Climate and oceanography of the western equatorial Pacific Ocean

The western equatorial Pacific Ocean plays a critical role in the transfer of heat and moisture to the high latitudes. Trade winds over the Pacific basin drive warm sea surface waters towards the western part of this ocean, and create a pool of warm waters, the West Pacific Warm Pool (WPWP). This region constitutes the most important moisture source of the world with an enormous convection zone over the warm surface waters (Graham and Barnett, 1995). The heat and humidity originating from the WPWP and other tropical convection zones are then transferred to higher latitudes by the atmospheric circulation, and especially via Hadley cells (Bjerknes, 1969; Ropelewski and Halpert, 1986).

This scenario can be significantly modified, due to the ENSO variability, engendering the eastwards migration of the WPWP towards the center or the eastern part of the Pacific basin, and thus shifting the convection zone eastwards (El Niño events). Conversely, during La Niña events, the WPWP gets warmer and extends up to south East Asia, leading to enhanced rainfall over this region, whereas the upwelling along the equatorial western coast of the American continent is increased (McPhaden, 1999). The equatorial western Pacific Ocean is also affected by the East Asian monsoon, with a reversal of the trade winds between summer and winter monsoon and increased rainfall during summer (Xie and Arkin, 1997). This reversal of the Monsoon regime is due to the migration of latitudinal position of the ITCZ over the western equatorial Pacific Ocean, creating a significant seasonality of the winds and rainfall in this area (Fig. 2a and 2b) (Sadler, 1975; An et al., 2000). In the

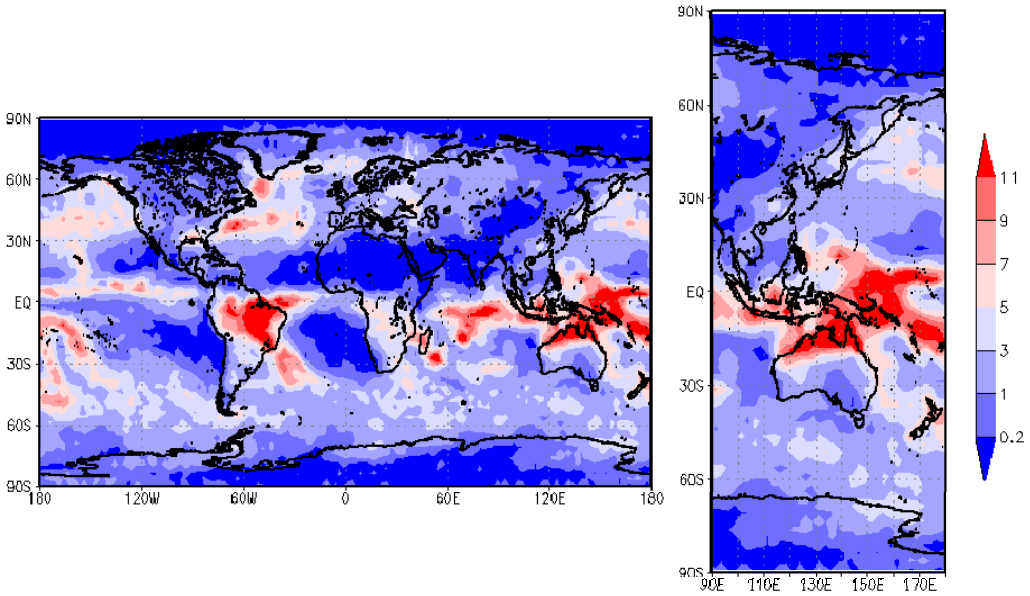

Fig. 1 – a) Winter position of the ITCZ revealed by monthly precipitation rates (mm/day) on a worldwide (left) and regional (right) scale. Data for february 2004 from Global Precipitation Climatology Project (http://cics.umd.edu/~yin/GPCP/main.html). Note the rainbelt reaching north of Australia, whereas low precipitation prevails over India and China during the South Indian and East Asian monsoons.

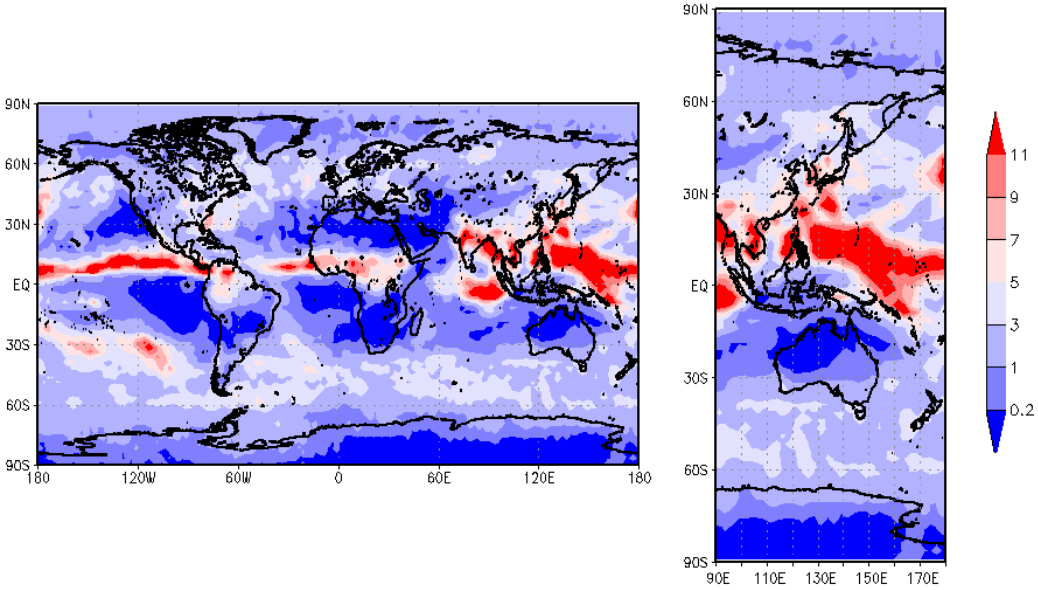

Fig. 1 – b) Summer position of the ITCZ revealed by monthly precipitation rates (mm/day) on a worldwide (left) and regional (right) scale. Data for august 2004 from Global Precipitation Climatology Project (http://cics.umd.edu/~yin/GPCP/main.html). Note high precipitation rates over India and WPWP associated to the South Indian and East Asian summer monsoons, in contrast to the relative aridity off north Australia.

Australasian region, the migration of the ITCZ reaches its maximal amplitude with a winter/summer latitudinal difference of nearly 30°, from northern Australia during boreal winter up to Taiwan in summer (Waliser and Gautier, 1993).

The East Asian monsoon is generated by a thermal contrast between air masses over the East Asian continent and the western Pacific Ocean water. This induces a regional gradient of pressure leading to an intensification of trade winds over the area. Relatively cold and dry winds originate from Siberia and go southward to East China and WPWP during the winter monsoon (An, 2000). In contrast, the summer monsoon is characterised by winds originating from large convection cells over the warm seas around northern Australia and the WPWP, and transferring this heat and humidity towards northern China

1.1 – Study area and local oceanography

The oceanic upper circulation in the west Pacific involves currents originating locally (Mindanao Current, North Equatorial Counter Current; Mindanao and Halmahera Eddies) or from the two major gyres located in the north and south of this ocean (North and South Pacific Equatorial Currents). The upper circulation in the Indo-Pacific region is mostly driven by the North Equatorial Current (NEC) originating from the southern side of the clockwise North Pacific gyre and flowing westwards along latitude 15°N. On reaching the WPWP, this current is divided into two branches flowing northward and southward. The northern branch transfers relatively warm water from the western Pacific Ocean to higher latitudes, reaching the eastern coast of Japan. The southern branch flows along the eastern coast of Philippines and creates the Mindanao Current (MC), also further divided into two branches. One of these branches joins the North Equatorial Counter Current (NECC) flowing eastward over the entire tropical Pacific, and also includes water originating from the South Equatorial Current (SEC) passing along the northern coast of Papua-New Guinea during boreal summer (Ueki et al., 2003). The second branch of the Mindanao Current is the most important in terms of volume and forms the main flux of the Indonesian Throughflow (ITF, solid blue arrows on Fig. 4) flowing through the Indonesian archipelago to the Indian Ocean.

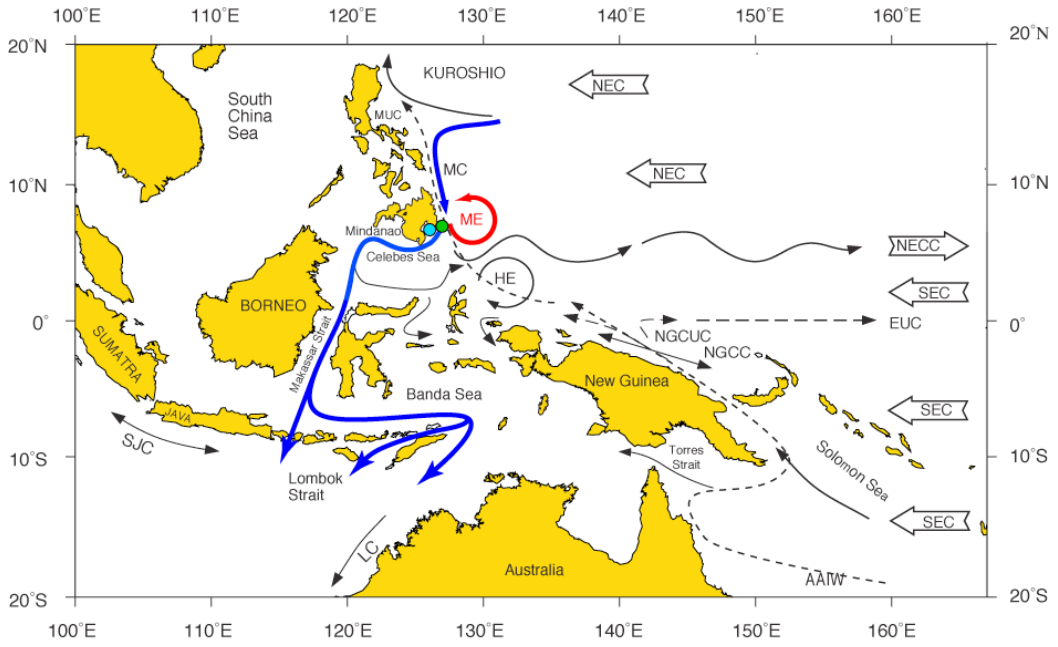

Fig. 2 – Main oceanic currents of the Western Equatorial Pacific Ocean (modified from Fine et al., 1994). NEC: North Equatorial Current; NECC: North Equatorial Counter Current; SEC: South Equatorial Current; EUC: Equatorial Undercurrent; NGCC: New-Guinea Coastal Current; NGCUC: New-Guinea Coastal Undercurrent; MUC: Mindanao Undercurrent; AAIW: Antarctic Intermediate Water; SJC: South Java Current; LC: Leeuwin Current; MC: Mindanao Current; ME: Mindanao Eddy; HE: Halmahera Eddy. Solid blue arrows indicate the main path of the Indonesian Throughflow. Green and blue dots indicate the position of Cores MD06-3067 and MD06-3075, respectively.

This study is based on two marine cores (MD06-3067 and MD06-3075) located along the southeast (MD06-3067; 06°30.86' N 126°29,86'E; 1575 m water depth) and south (Davao Gulf, MD06-3075; 06°28.57' N 125°49,92'E; 1878 m water depth) coasts of Mindanao Island, Philippines. Marine sediments are among the most complete climatic archives available, providing a precise and precious picture of the local and global evolution of short- and long-term climate. Located in the heart of the WPWP, these cores were taken in order to reconstruct the evolution of the regional atmospheric and oceanic circulation and particularly the poorly known inflow part of the ITF.

1.2 – Indonesian Throughflow

The ITF represents a vital link in the global thermohaline circulation, transferring a considerable amount (around 16Sv; Gordon, 2003) of relatively cold and fresh thermocline waters from the North Pacific to the eastern Indian Ocean through the Indonesian archipelago. Today, the main flux originates from the Mindanao

current, and reaches further south the Makassar Strait, where it meets during summer monsoon an important flux of relatively fresh water coming the Java Sea. Before reaching the Indian Ocean, this northern branch of the ITF is joined in the Banda Sea by a minor contributory originating from the SEC and flowing along the northern coast of Papua-New Guinea. Several studies have shown that the ITF regulates the water properties of both the Indian and western Pacific Oceans and thus, affect the intensity of the South Indian and East Asian monsoons (MacDonald, 1993; Hirst and Godfrey, 1993; Murtugudde et al., 1998; Wajsowicz and Schneider, 2001; Wajsowicz, 2002; McCreary and Lu, 2001; Schott and McCreary, 2001; Lee et al., 2002; Schott et al., 2002; Song et al., 2004; Song and Gordon, 2004).

Recent oceanographic surveys revealed the presence of an eddy (Mindanao Eddy, ME) associated to a doming system (Mindanao Dome, MD) close to the eastern coast of Mindanao Island. Core MD06-3067 thus has a strategic position, and provides the first available climate archive located within the influence zone of the ME/MD couple, providing new critical information about the history of the circulation in this area. The ME and MD remain poorly known, and most previous studies are based on oceanographic in situ measurements. In fact, only rare papers were published concerning the activity of the ME and MD (Masumoto and Yamagata 1991; Tozuka et al., 2002), and the past evolution of this complex system remains virtually unknown. Nevertheless, those publications provided essential information about the ME and MD and the mechanisms responsible for their formation. The ME is a cyclonic small gyre (about 250 km diameter) with a center moving between 7 an 8°N (Heron et al., 2006), which creates a doming in deeper water layers by Ekman pumping. The formation of the ME is due to the separation of the waters from the MC into two branches, one flowing towards the Makassar Strait, and the second one flowing eastwards and then joining the Pacific North Equatorial counter current. According to previous studies, the ME is mainly induced by the winter monsoon (Udarbe-Walker and Villanoy, 2001; Tozuka et al., 2002) with probable additional influence of Rossby waves (Yaremchuk and Qu, 2004). Due to this linkage with the wind direction and strength, both the ME and MD exhibit a strong seasonality leading to a possible temporary shutting down of their activity (Tozuka et al., 2002). The doming does not act as a typical upwelling such as the ones associated with large oceanic gyres. In fact, in situ observations indicate that upwelled waters do not reach the surface, and that the effect of the doming is only detected in water masses deeper

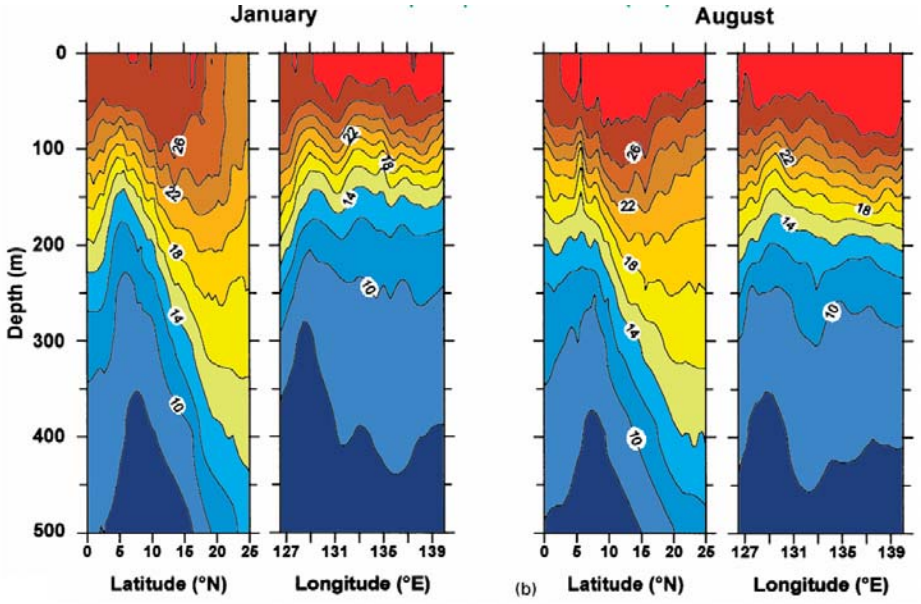

Fig. 3 – Meridional and zonal monthly mean temperature (°C) sections in the western equatorial Pacific Ocean for January and August. Note the shoaling of the isotherms centered at 128°E; 7°N due to the action of the Mindanao Dome. Modified from Udarbe-Walker and Villanoy (2001).

than 75 m (Udarbe-Walker and Villanoy, 2001). This parameter might have an important influence on the ITF, as the MD is located directly on the path of this current transferring North Pacific waters from 100 to 500 m water depth.

Until now, most publications monitoring the modern (Godfrey, 1996; Gordon et al., 2001, Vranes and Gordon, 2005; Vranes et al., 2002) and past (Zuraida et al., 2009; Xu et al., 2006 and 2008; Holbourn et al., 2005, Visser et al., 2003) activity of the ITF focused on the central or outflow paths of the ITF. Within this context, Core MD06-3067 provides a unique opportunity to monitor the evolution of water masses properties directly within the inflow path of the ITF and influence zone of the ME and MD. In contrast, Core MD06-3075, located inside the Davao gulf, allows to track local climatic changes from an area possibly more influenced by terrestrial influx from Mindanao Island. These cores can thus provide essential information on the climatic and oceanographic evolution of the region.

1.3 – Intermediate circulation

Our knowledge of the intermediate (around 500 to 1500 m water depth) and deep circulations in the western equatorial Pacific Ocean was considerably increased during the last decades by several critical publications (Reid, 1965; Tsuchiya, 1968;

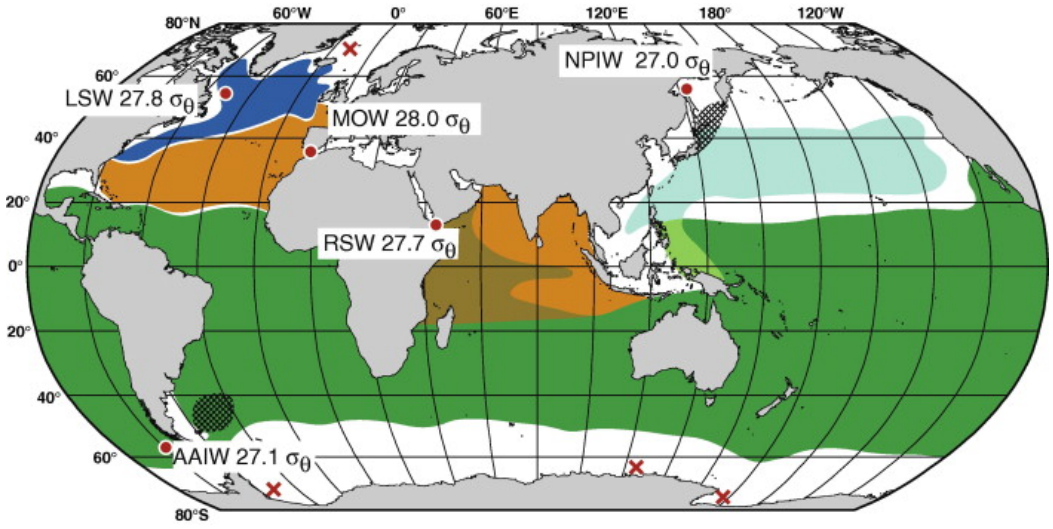

Fig. 4 – Schematic of low salinity (blue, green and blue-green) and high salinity (orange) intermediate water masses, after Talley (1999). The overlap of Red Sea Water and AAIW is shown in brown; the overlap of NPIW and AAIW is shown with an intermediate shade of green. Red dots represent intermediate water sources; these are sites of open ocean convection (LSW and AAIW), or sill overflow (MOW and Red Sea Water), or shelf brine rejection (NPIW). Potential density at each source is listed. Red X's represent deep and bottom water sources.

Nitani, 1972; Hu et al., 1989 and 1991; Fine et al., 1994; Qu et al., 1998, 1999 and 2004; Xie et al., 2009).

Additional high resolution studies based on various water-mass tracers provided further information about this circulation system (Xie et al., 2009). Today, the intermediate circulation in the Pacific is dominated by two well distinct water masses, Antarctic Intermediate Water (AAIW) and North Pacific Intermediate Water (NPIW) (Fig. 4). Those two water masses are formed at high latitudes and spread equatorwards over the entire width of the Pacific basin via the South and North Pacific gyres. The AAIW is a fresh water mass (potential density 27.2–27.3 σθ) mainly formed in the southeastern Pacific (Talley, 1999) and dominating the intermediate circulation of the whole southern Pacific basin. It has been shown that AAIW could also be found in low latitude areas (Tsuchiya, 1981), notably in the western equatorial Pacific up to the latitude of Mindanao (Reid and Mantyla, 1978; Tsuchiya and Talley, 1996; Reid, 1997; Wijffels et al., 1998; Qu et al., 2004; Fig 4). North Pacific Intermediate Water (NPIW) is defined as the subsurface salinity minimum centered on the 26.8 σθ potential density surface (Talley et al., 1991). This water mass is generally produced in the Bering Sea (Takahashi, 1998), the Sea of Okhotsk (Talley, 1991) and in the Alaskan Gyre (Van Scoy et al., 1991). The NPIW is mainly found in the northern part of the Pacific basin, generally not extending at lower latitudes than 20°N.

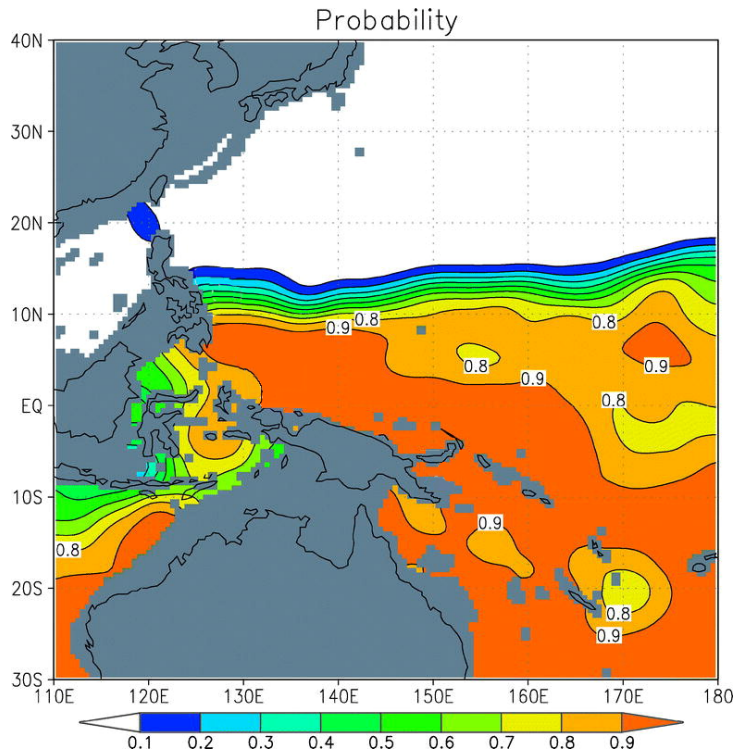

Fig. 5 – Probability of AAIW in the Australasian region, defined as the percentage of salinity profiles that contain at least one salinity minimum at the potential density range of 27.0–27.4 σθ (modified from Qu et al., 2004).

However, several studies observed a tongue of NPIW in the western equatorial Pacific extending down to around 3°N (McCreary and Lu, 2001; Reid and Mantyla, 1978; Talley et al., 1993 and 1999; Lukas et al., 1991; Wijffels et al., 1995; Qu et al., 1998 and 1999; Fig. 5). Additionally to those two major low-density water masses, North Pacific Tropical Waters (NPTW) characterized by high salinity ($34.75 < S < 35.25$) are also found in the western equatorial Pacific Ocean on potential density surfaces of around 24.0 σθ (Qu et al., 1999, Fig. 6). According to Tsuchiya (1968) and Fine et al., (1994) these water masses are mainly formed in the WPWP and result from excessive evaporation. About 100 km offshore of the eastern coast of Mindanao, oceanographic surveys detected a northward subthermocline flow (Mindanao undercurrent, MUC, Hu et al., 1991; Lukas et al., 1991) below the Mindanao Current.

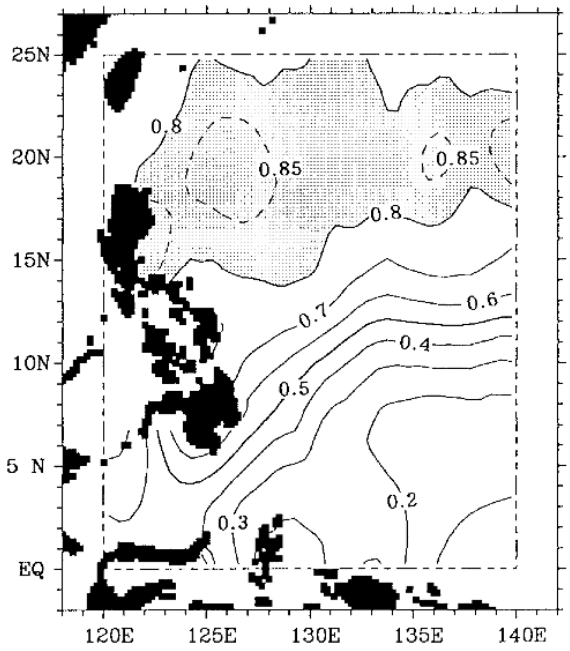

Fig. 6 – Distributions of probability of NPIW around the Philippines (Qu et al., 1999), defined as a salinity minimum (<34.45 psu) in potential density range of 26.4-27.0 σθ.

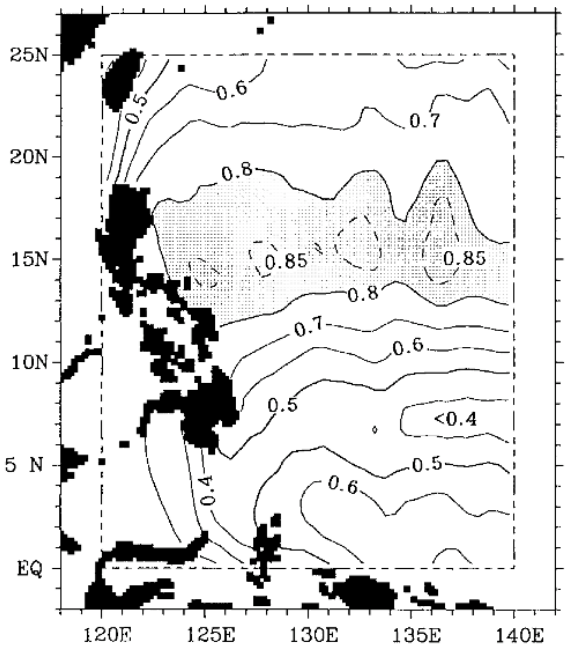

Fig. 7 – Distributions of probability of NPTW around the Philippines (Qu et al., 1999), defined as a salinity maximum (34.85 psu) in potential density range of 23.0-25.0 σθ.

Additional studies estimated the flow to be constrained between 700 and 1300 m water depth (Qu et al., 1998) and to carry AAIW and NPIW (Wang and Dunxin, 1998 a and b). However, the consistency of this current remains still debated (Qu et al., 1998 and 1999; Kashino et al., 2005).

The Mindanao area then appears to not be only a water mass crossroad for the upper circulation, but also for intermediate waters (Fig. 9). In fact, this region constitutes a unique overlapping zone of AAIW and NPIW, making the position of Cores MD06-3067 and MD06-3075 crucial for reconstructing the past influence of those two water masses, possibly due to some fluctuations in their production rate as well as possible reorganization of their distribution.

2 – Late Pleistocene Climate Evolution of the Western Equatorial Pacific.

The late Pleistocene and the Holocene are probably the most documented periods for paleoclimatology and paleoceanography. These two periods correspond to the most recent history of the Earth, providing theoretically the best records in terms of preservation and resolution. The western equatorial Pacific Ocean has been intensively studied during the last decades, providing essential although sometimes controversial information on regional climate and oceanography.

2.1 – Glacial-interglacial cycles

The reconstruction of glacial conditions in the tropics has provided a major challenge for many years, especially concerning Sea Surface Temperatures (SSTs). During the last three decades of the 20th century, many experiments were done to estimate glacial SSTs in the tropics. One of the major programs, the "Climate: Long-range Investigation, Mapping, and Prediction" (CLIMAP) concluded from assemblages of species of various fossil groups that glacial conditions in the tropical Pacific were 1 to 2°C colder than the present conditions. However, pollen records and snow lines reconstructions from regional highlands revealed a glacial cooling possibly reaching 8°C (Webster and Streten, 1978; Stuijts et al., 1988; Van der Kaars and Dam, 1995), not consistent with the moderate glacial/interglacial contrast estimated from SSTs (Rind and Peteet, 1985), and leading to major interrogations concerning the estimation errors of terrestrial and/or marine records (Wang et al., 1998).

At the beginning of the 21st century, with the development of geochemical techniques of SST reconstructions (Mg/Ca from foraminifera, alkenones), estimations of the conditions in the tropical Pacific during the LGM were significantly revised. Lea et al., (2000) and Stott et al., (2002) estimated a contrast of 2.8° ± 0.7°C and 2 (summer species) to 3°C (winter species) between the LGM and the Holocene, revealing that the tropics could have been much more affected by the last glacial/interglacial transition than the suggestion of the CLIMAP. Following this work, several publications confirmed a warming of around 3°C in the Indo-Pacific area (Oppo and Sun, 2005; Xu et al., 2008; Stott et al., 2007a: Visser et al., 2003; de Garidel-Thoron et al., 2007) even if the all proxies did not show homogenous results (de Garidel-Thoron et al., 2007), and some studies noticed local discrepancies, with a possible 4.5-5°C warming in the marginal seas (South China Sea, Sulu Sea; Wang et al., 1998). Archives spanning termination II in this region are less common, but suggest slightly larger amplitude of the warming between MIS 6 and MIS 5e than during the last deglaciation (3.5 to 4.2°C; Visser et al., 2003, Lea et al., 2000; Oppo and Sun, 2005; Xu et al., 2006; de Garidel-Thoron et al., 2005).

However, although a consensus is emerging on the considerable impact of glacial/interglacial cycles on the climate of the tropics, the role played by low-latitudes during the last deglaciation remains controversial (Lea et al., 2000; Kienast et al., 2001; Seltzer, et al., 2002a and b; Clark et al., 2002; Visser et al., 2003; Stott et al., 2007a).

This work provides new surface and thermocline seawater temperature reconstruction from foraminiferal Mg/Ca covering the two last glacial interglacial cycles. The position of Core MD06-3067 on the path of the inflow part of the ITF and also within the influence zone of the MD provides new information on the amplitude of the warming for the two last terminations in a zone of the WPWP possibly affected by upwelling waters and variations in the ITF structure. It thus allow us to monitor the unknown past intensity of the MD through the last two glacial/interglacial cycles, by reconstructing the structure of the water column using surface and thermocline analysis.

2.2 – ENSO

ENSO is a major actor in the current and late Pleistocene climate regulation (Clement et al., 2001) and understanding its present and past dynamics still remains one of the most critical topics in paleoclimatology. However, multiproxy reconstructions did not provide consistent results on the amplitude of ENSO during the last glacial period. In fact, Tudhope et al., (2001) firstly suggested the persistence of ENSO over glacial/interglacial cycles through the last 130 ka, and proposed a reduction of the amplitude of this phenomenon during cold periods, whereas Stott et al., (2002) noticed a possible enhancement of ENSO during glacials. No clear consensus emerged as well concerning the dominant phase (El Niño or La Niña) of ENSO during the last glacial period. In fact, Koutavas et al., (2002) suggested El Niño-like conditions during Ice age and a dominance of La Niña during the Mid Holocene. One year later, Martinez et al., (2003) proposed a possible dominance of La Niña during MIS 2. Recently, Leduc et al., (2009) highlighted the role of the variability of the latitudinal position of the ITCZ rather than ENSO to explain past rapid changes in the precipitation pattern in the tropical Pacific. To explain such divergences in reconstructions of the past climate in the Pacific, Rosenthal and Broccoli, (2004) pointed out the possible biases introduced by the proxies used. The previously cited paleoclimate reconstructions are based on various proxies (corals, $\delta^{18}O$ and Mg/Ca from foraminifera, faunal assemblages), which may not exhibit similar sensitivity to climatic changes. It is thus necessary to carefully take into account the reliability of those proxies in recording ENSO signals (Rosenthal and Broccoli, 2004; Leduc et al., 2009).

Another major bias may be induced by interactions between the numerous large-scale climatic phenomenons of the Indo-Pacific region. In fact, ENSO, the East Asian and the Australian monsoons as well as the movement of the ITCZ exhibit close relationships increasing the complexity of extracting a clear and precise signal of each of those individual phenomena from the climatic background. The interactions between those different climatic phenomena also affects the creation of a homogenous picture of the past climate of the western equatorial Pacific, as it is necessary to consider that results observed locally might not be representative of the whole Indo-Pacific region. Within this context, results from Cores MD06-3067 and MD06-3075 might not reflect the paleoclimatology and paleoceanography of the whole Indo-

Pacific region, but may be considered as archives of local conditions in a critical area of atmospheric and oceanic circulation.

2.3 – Role of Indonesian Throughflow

Studies on the Indonesian Throughflow are relatively recent, starting in the second part of the 20th century (Wyrtki, K., 1961). The interest for the ITF increased when some major publications showed the importance of this Throughflow for the climate of the Australasian region, as well as for the entire Indian Ocean (Gordon, 2003; Hirst and Godfrey, 1993; MacDonald, 1993). Several authors described the complex modern oceanography of the Australasian region using *in situ* measurements or models (Tozuka et al., GRL, 2007; Qu et al., 1999 journ physical oceanography; Wainwright et al., 2008 GRL; Gordon and McClean, 1999. Gordon et al., 2003), but the evolution of the ITF during the late Pleistocene still remains poorly known. Holbourn et al., (2005), Xu et al., (2006) and Zuraida et al., (2009) highlighted the importance of the Australian austral summer monsoon and the local oceanic circulation in driving the productivity over the last 460 kyrs in the Timor Sea, which is the outflow part of the ITF.

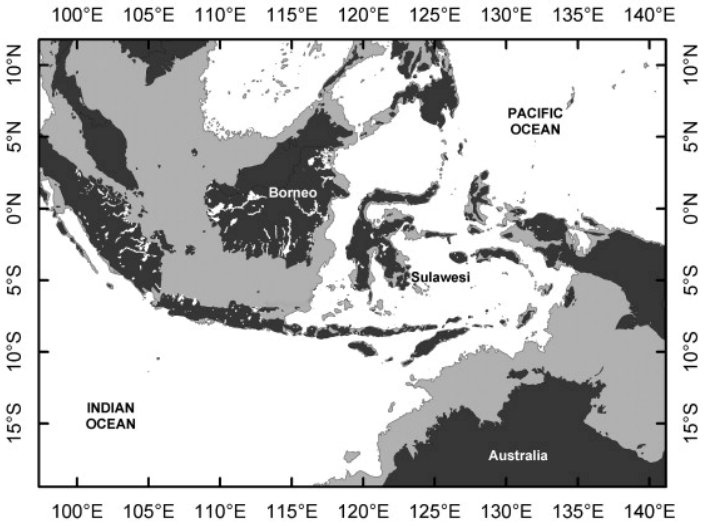

Fig. 8 – Map of the Australasian region showing the repartition of exposed land for today (black areas) and for the LGM with a 120 m-lower sea level (grey areas). Modified from Visser et al., (2004).
Data from http://ingrid.ldgo.columbia.edu/SOURCES/.WORLDBATH/.bath/.

De Deckker et al., (2002) and Visser et al., (2004) described the possible geography of the Australasian region during the last glacial maximum, revealing considerable changes in the amount of exposed land, which covered almost twice the surface of this region today (Fig. 8). The 120 m lower sea level period implies a closure of several of the shallow seas of the Indonesian archipelago, and an interruption of the flux of fresh surface water from the South China Sea, joining today the flow of the ITF in the south of the Makassar Strait. This glacial interruption of the connection between the marginal seas of the Indonesian Archipelago, as well as the tremendously increased surface of emerged land suggest considerably contrasted glacial/interglacial regional wind and rain patterns in the Indo-Pacific region (Müller et al., 2000; de Deckker et al., 2002; Zuvela-Aloise, 2005; de Garidel-Thoron et al., 2007). However, the impact on the ITF during the LGM remains controversial. Modelling results indicating major changes in the vertical structure of the ITF rather than a significant reduction in the amount of transported water (Zuvela-Aloise, 2005), whereas other studies indicate a possible weakening of the ITF (Müller and Opdyke, 2000; Gingele et al., 2001). Xu et al., (2006) reconstructed the evolution of the vertical profile of the ITF during termination II, indicating a shift from a surface- to a thermocline-dominated flow between MIS 6 and MIS 5e. They suggested this change to be related to a restriction of the surface flow through the southern exit of the Makassar Strait. Xu et al., (2008) compared the structure of the ITF over terminations I and II, and noticed that the two deglaciations were accompanied by changes in the structure of the dominant flow of the ITF, shifting from surface to thermocline after the establishment of the connection between the South China Sea and the Makassar Strait, from 9.5 to 10.2 Ka (Ding et al., 2002; Sathiamurthy and Voris, 2006). Zuraida et al., (2009) also reported important changes in the structure of the ITF with a cooling of thermocline waters during the early MIS 3 related to a flux of freshwater coming from the Java Sea as well as to an intensification of the SE Asian winter monsoon. They also highlighted the possible influence of the northern hemisphere climatic variability on the ITF. In fact periods of weakening of the relatively cool and fresh thermocline flow in the Timor Sea coincide with slow-down of the thermohaline circulation during Heinrich events due to cooling of the northern hemisphere. Dürkop et al., (2008) also reported a linkage between northern Hemisphere and ITF waters in the Timor Sea during MIS 3 with planktonic oxygen isotope recording Dansgaard–Oeschger warm events 8, 12, 14 and 16–17, whereas the benthic oxygen isotope record indicates a

clear influence of Antarctica and southern ocean deep water over the local deep circulation. Those publications thus provided essential information of past climatic and oceanographic conditions in the central and outflow parts of the ITF. Our study focuses on the long-term paleoceanography and paleoclimatology of the inflow part of the ITF based on data from Cores MD06-3067 and MD06-3075.

3 – Proxies for Paleoclimate Reconstruction

3.1 – Foraminifera

For this study, we analyzed the following planktonic and benthic foraminiferal species:

– *Globigerinoides ruber* (white) is a planktonic species most commonly found in warm to temperate waters (temperature range, 14–32 °C; optimum temperature, 23.0 °C, as determined by culture experiment; Bijma et al., 1990), which secretes a test made of low magnesium calcite ($CaCO_3$). It is mainly found in a water-depth interval ranging from 0 to 50 m (Ravelo et al., 1990) and is thus restricted to the mixed layer (de Garidel-Thoron et al., 2005). It therefore constitutes an ideal species to record surface water properties. Even if it generally dominates during boreal summer, no notable seasonality in its abundance has been detected from sediment traps (Kawahata et al., 2002)

– *Pulleniatina obliquiloculata* is a deep dwelling planktonic species secreting a shell made of calcite and living mostly in subtropical areas between 10°N and 10°S. The water depth distribution of this species varies according to different publications, but is generally found between 60 and 175 m of water depth (Ravelo and Fairbanks, 1992; Cleroux et al., 2007), following the depth of the thermocline. Core tops studies in the Timor Sea indicated a depth habitat below 100 m for *P. obliquiloculata* (Zuraida et al., 2009) coinciding with the relatively deep thermocline generally observed in the Australasian region (Fig. 9) and supporting the use of this species as a proxy for thermocline water properties.

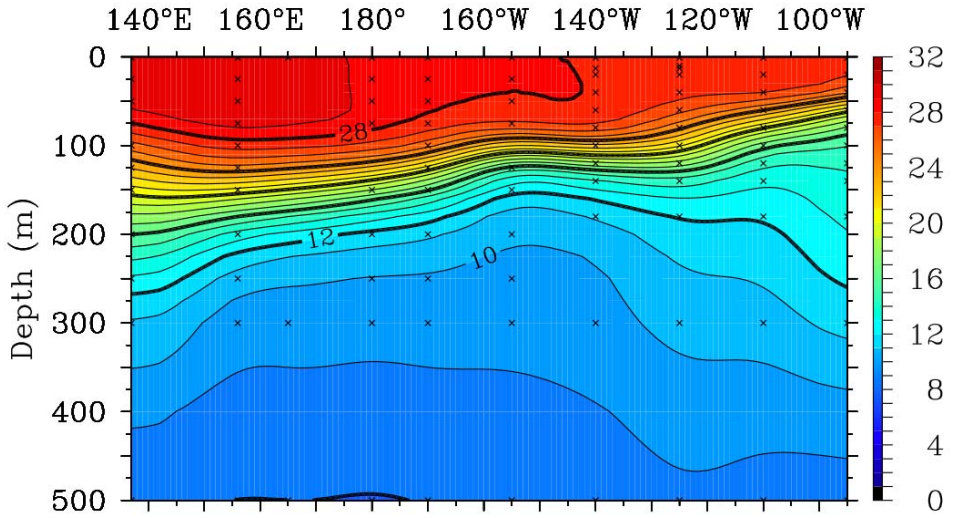

Fig. 9 – Monthly mean upper water temperature (°C) in the equatorial Pacific (5°N) for June 2007. Note the deepening of the thermocline in the western part of the basin. Data from TAO/NOAA

– Benthic foraminifera are found at the water-sediment interface with a distribution, ecology and morphology closely linked to biological (organic flux) and chemical (oxygen and redox conditions) parameters within this interface (Jorissen et al., 1995; Van der Zwaan et al., 1999). Epibenthic foraminifera live on the substratum and their distribution is controlled by bottom water conditions, whereas infaunal species are generally found in the upper centimetres of the sediment with a specific distribution depending on physiochemical conditions within this layer (Corliss, 1985). In this study we present results from geochemical analysis for oxygen and carbon isotopes performed on *Uvigerina proboscidea* (shallow infaunal habitat), *Cibicidoides mundulus*, *Cibicidoides pachyderma* and *Planulina wuellerstorfi* (epifaunal) reflecting the physical and geochemical properties of bottom waters. Benthic foraminifera were also counted and we used percentage abundances of four main groups (globocassidulinids, globobuliminids, miliolids and *Bolivinita quadrilatera*), which are indicative of high and intermediate carbon export flux reaching the seafloor (Kuhnt et al., 1999; Holbourn et al., 2005; Dürkop et al., 2008).

3.2 – Geochemical analysis

3.2.1 – Sea surface and thermocline temperature:

Seawater palaeotemperature was reconstructed by measuring the ratio of Magnesium and Calcium (Mg/Ca) in the shells of *Globigerinoides ruber* and *Pulleniatina obliquiloculata* for surface and thermocline waters, respectively. This technique, developed in the late 1990s and (Nürnberg, 1995; Nürnberg et al., 1996 a,b) and refined some years later (Lea et al., 1999; Elderfield and Ganssen, 2000; Anand et al., 2003; Rosenthal et al., 2004; Barker et al., 2005; Greaves et al., 2005), is based on the progressive substitution of Calcium atoms by Magnesium within $CaCO_3$ of the shells of foraminifera, correlated to an increase in seawater temperature. Several publications have shown the robustness of this technique for seawater temperature reconstruction using calibration on modern samples (Rosenthal et al., 1997; Dekens et al., 2002; Annand et al., 2003; Xu et al., 2006; Zuraida et al., 2009). The accuracy of *G. ruber* for tropical SST reconstruction was successfully tested by Dekens et al., (2002) and the equation used during this study for reconstructing surface water paleotemperature from *G. ruber* shells was established by Anand et al., (2003):

$$Mg/Ca = 0{,}38\ (\pm 0{,}02)\ e^{0{,}090\ T}\ (\pm 0{,}003)$$

This equation is equivalent to a 9.0 ± 0.3% change in Mg/Ca for a 1°C change in temperature. This equation was formulated by calibrating Mg/Ca from $\delta^{18}O$-derived temperature using 12 planktonic species (surface and thermocline) taken from sediment traps in the Sargasso Sea with a significant (R = 0.93) relationship to temperature. According to these authors, the accuracy of this equation is 1.2°C.

The reconstruction of thermocline water past temperature was performed using the specific equation for *P. obliquiloculata* derived by Anand et al., (2003):

$$Mg/Ca = 0{,}328\ (\pm 0{,}007)\ e^{0{,}090\ T}\ (\pm 0{,}003)$$

This relationship was established using an estimated depth of calcification of 50 to 100 m for this species from a comparison of foraminiferal $\delta^{18}O$ with calcite in equilibrium with seawater, corresponding to the depth of the thermocline. This calibration for *P. obliquiloculata* was further tested in the WPWP by Xu et al., (2006).

The cleaning procedure for removing contaminants fixed on shells was performed using the protocol elaborated by Martin and Lea (2002) including a reductive step for the removing of metal oxides. We applied no correction for the reductive step included in our cleaning protocol, which generally results in a small decrease in Mg/Ca leading to temperature underestimation of up to 0.6°C (Rosenthal et al., 2004). All the measurements for MG/Ca analysis were performed on an ICP-OES (Spectro Ciros SOP) with cooled cyclonic spray chamber and microconcentric nebulization (200 $mL.min^{-1}$) at the Institute of Geosciences, Kiel University.

3.2.2 – Oxygen and carbon stable isotopes as a climate proxy in Foraminifera.

3.2.2.1 – Oxygen isotopes

The interest in measuring the stable oxygen isotopes for paleoclimate reconstruction was firstly suggested by Urey, (1947), who noticed the influence of temperature on the fractionation of oxygen between seawater and carbonate.

Since this discovery, the measurement of $\delta^{18}O$ has been intensively used during the second half of the 20th century and optimized during the last decades, particularly the work of Shackleton, (1967) introducing the notion of changes in the $\delta^{18}O$ of seawater through time, and Schrag et al., (1996) suggesting the influence of the local hydrology (precipitation-evaporation) on $\delta^{18}O$ of seawater, also known as "salinity effect".

This study presents new high resolution results for $\delta^{18}O$ from Core MD06-3067 performed on *G. ruber*, *P. obliquiloculata* and benthic foraminifera revealing the evolution of surface, thermocline and bottom water properties, respectively, for the last 160 kyrs. This correspond to a total of around 400, 450 and 500 datapoints for surface, thermocline and deep-water mass proxy, respectively, for Core MD06-3067, with a 2-cm resolution from MIS 4 up to the Holocene, and one measurement every 10 cm for older samples. Replicates $\delta^{18}O$ measurements were performed on 70 samples for *G. ruber,* around 80 for *P. obliquiloculata* and 35 for benthic species.

$\delta^{18}O$ Measurements were also performed with a 10 cm resolution on the upper 18 meters of Core MD06-3075 for benthic species (200 samples; 22 replicates), and on the whole core for planktonic (*G. ruber;* 330 samples; 25 replicates).

Core MD06-3064 (6°28.23'N, 126°27.82') was sampled for $\delta^{18}O$ analysis on *G. ruber* (30 samples) and *P. obliquiloculata* (32 samples) over the first two meters. This core

constitutes a well-preserved archive of the Holocene climate and oceanography in ITF inflow part. Also, this core exhibits no artificial elongation and oversampling due to the piston coring system on the contrary to Cores MD06-3067 and MD06-3075.

3.2.2.2 – Carbon isotopes

The interest in using carbon isotopes for paleoceanography was firstly noted at the end of the 20th century by Shackleton (1977) and Broecker (1982a). The use of carbon isotopes is, as for oxygen isotopes, based on the ratio of two carbon isotopes (^{12}C and ^{13}C) noted $\delta^{13}C$. $\delta^{13}C$ in calcite reflects the relative amount of ^{12}C and ^{13}C in deep sea water, primarily controlled by the recycling of organic matter.

$\delta^{13}C$ is generally used as a proxy of ventilation of oceanic water (Duplessy et al., 1988). In fact, deep-water masses get enriched in ^{13}C through time due to the "carbon rain" i.e. organic matter falling from the upper water column and later recycled on the seafloor. It is thus possible to reconstruct the evolution of this carbon flux and to recognize possible major switches in the nature of deep-water masses revealed by abrupt changes in the $\delta^{13}C$.

$\delta^{13}C$ of benthic foraminifera is also sensitive to variations in the carbon global inventory due to climatic changes as suggested by Shackleton et al., (1977) and Duplessy et al., (1984). Several factors have to be taken into account in order to avoid severe biases in $\delta^{13}C$ records. In fact, influence of pore water on infaunal benthic foraminifera, as well as possible microhabitat effects particularly in high productivity areas (possible presence of a organic fluff layer on the seafloor; Lutze and Thiel, 1989; Mackensen et al., 1993) can interfere with the isotopic signal from bottom waters, and most of the benthic $\delta^{13}C$ studies preferably use epibenthic species.

3.2.2.3 – X-Ray fluorescence

X-Ray fluorescence (noted XRF) emerged in field of geosciences at the end of the 20th century with the work of Ramsey et al., (1995) and Jansen et al., (1998) and was rapidly optimized during the last decade. This non-destructive analysis provides intensities measurements for 9 light (Al, Si, P, S, K, Ca, Ti, Mn and Fe) and 7 heavy (Rb, Sr, Zr, Ag, Sn, Te, Ba) elements, reported in counts per seconds. XRF analysis was performed on Cores MD06-3067 and MD06-3075 at a 1 cm resolution in the

Marum Center, University of Bremen (Germany) on an Avaatech scanner. In this study we used XRF results as a tracer of land-derived flux revealed by titanium intensities (Jansen et al., 1992; Arz et al., 1998) normalized by calcium and using a log-ratio as suggested by Weltje and Tjallingii, (2008). According to Arz et al., (1998), titanium as well as iron contents in the sediment originate from continental silliciclastic rocks and especially clay minerals.

3.2.2.4 – Coccoliths counting.

The use of coccolithophorids in paleoceanography gained more interest during the last decades. In fact, as these micro-algae which constitute the major part of the phytoplankton and are found in all the oceans over the world, and thus coccoliths assemblages provide precise information on the physico-chemical parameters of the water masses, as the different species exhibit specific ecological preferences (Andruleit et al., 2002). Another utilization of coccoliths in paleoceanography is the estimation of primary production directly linked to the relative abundance of *Florisphaera profunda* (Beaufort et al., 1997). In fact, Beaufort et al., (1997) calibrated the inverse relationship proposed by Molfino and McIntyre, (1990) between the primary production and the relative abundance of this species within the assemblages of coccoliths modulated by fluctuations in the depth of the nutricline. In fact, a deepening (shoaling) of the nutricline would lead to a decrease (increase) of the nutrient concentration within the upper photic zone, engendering a rise in the percentage of *F. profunda* within the coccoliths population.

The reconstruction of past primary production was performed using the equation proposed by Beaufort et al., (1997)

$$PP = 617 - [279 * \log (\%FP + 3)]$$

Where PP represents the primary production ($gC.m^{-2}.year^{-1}$) and $\%FP$ is the relative abundance of *F. profunda* within the coccoliths assemblage. The counting of coccoliths for this study was done by using a system of automatic recognition of coccoliths specimen (SYRACO) using the protocol described by Dollfus and Beaufort, (1999) and Beaufort and Dollfus, (2004). This analysis was performed every 10 cm on Core MD06-3067, corresponding to 154 datapoints.

CHAPTER II: Mindanao Dome variability over the last 160 kyr: Episodic glacial cooling of the West Pacific Warm Pool

Mindanao Dome variability over the last 160 kyr: Episodic glacial cooling of the West Pacific Warm Pool

Timothé Bolliet[1], Ann Holbourn[1], Wolfgang Kuhnt1, Carlo Laj[2], Catherine Kissel[2], Luc Beaufort[3], Markus Kienast[4], Nils Andersen[5], Dieter Garbe-Schönberg[1].

[1] Institute of Geosciences, Christian-Albrechts-University, Ludewig-Meyn-Str. 10-14, D-24118 Kiel, Germany.

[2] Laboratoire des Sciences du Climat et de l'Environnement (LSCE), Laboratorie mixte CEA–CNRS, Avenue de la Terrasse, Gif-sur-Yvette Cedex 91198, France.

[3] CEREGE, Aix-Marseille Université, CNRS, IRD; Europôle Méditerranéen de l'Arbois, BP 80, 13545 Aix-en-Provence, France.

[4] Department of Oceanography, Dalhousie University, 1355 Oxford Street, Halifax NS B3H 4J1, Canada.

[5] Leibniz Laboratory for Radiometric Dating and Stable Isotope Research, Christian-Albrechts-University, D-24118 Kiel, Germany.

Paleoceanography, 26, PA1208, doi:10.1029/2010PA001966.
Received 29 March 2010; accepted 28 December 2010; published 26 February 2011.

Abstract

We present sea surface, upper thermocline and benthic $\delta^{18}O$ as well as temperature and paleoproductivity proxy data from IMAGES Core MD06-3067 (6°31 N, 126°30 E, 1575 m water depth), located in the western equatorial Pacific Ocean within the flow path of the Mindanao Current. Our records reveal considerable glacial interglacial as well as suborbital variability in the Mindanao Dome upwelling over the last 160 kyr. Dome activity generally intensified during glacial intervals resulting in cooler thermocline waters, whereas it substantially declined during interglacials, in particular in the early Holocene and early MIS 5e, when upwelling waters did not reach the thermocline. During MIS 3 and MIS 2, enhanced surface productivity together with remarkably low SST and low upper ocean thermal contrast provide evidence for episodic glacial upwelling to the surface, whereas transient surface warming marks periodic collapses of the Mindanao Dome upwelling during Heinrich events. We attribute the high variability during MIS 3 and MIS 2 to changes in the El Niño Southern Oscillation state that affected boreal winter monsoonal winds and upper ocean circulation. Glacial upwelling intensified, when a strong cyclonic gyre became established, whereas El Niño-like conditions during Heinrich events tended to suppress the cyclonic circulation, reducing Ekman transport. Thus, our findings demonstrate that variations in the Mindanao Dome upwelling are closely linked to the position and intensity of the tropical convection and also reflect far-field influences from the high latitudes.

1 – Introduction

The West Pacific Warm Pool (WPWP) plays a critical role within the ocean climate system, as the accumulation of warm water in the western equatorial Pacific Ocean represents one of the main sources of moisture and heat for the mid to high latitudes. The WPWP is strongly affected by large-scale climatic features including the El Niño Southern Oscillation (ENSO) and the East Asian monsoon. Thus, the spatial and temporal evolution of the WPWP is closely linked to latitudinal oscillations in the mean position of the Intertropical Convergence Zone (ITCZ) and to changes in the equatorial Pacific surface ocean. Previous studies indicated that the WPWP showed considerable variability in the past and that some of the changes had major repercussions for global climate evolution (Beaufort et al., 2001; Stott et al., 2002, 2004 and 2007; Dannenmann et al., 2003; Oppo et al., 2003; Rosenthal et al., 2003; Wang et al., 2004; Thevenon et al., 2004; Oppo and Sun, 2005; de Garidel-Thoron et al., 2001 and 2007; Zhang et al., 2007 and 2009). However, the temporal and spatial evolution of the WPWP remains the focus of vigorous debate and its long term history is still poorly known. A major obstacle has been the difficulty in recovering continuous high-resolution sedimentary successions along the western Pacific coast, as the narrow continental shelf and strong prevailing currents generally inhibit long-term accumulation of sediments.

Here, we present new Mg/Ca based paleotemperature reconstructions, stable isotope and paleoproductivity proxy data in a sedimentary core recovered in the central part of the WPWP within the flow path of the Mindanao Current. We measured stable isotope and Mg/Ca in two planktonic foraminifers living at different water depths within the upper water column. *Globigerinoides ruber* (sensu stricto white) is a near surface dweller, whereas *Pulleniatina obliquiloculata* reflects conditions within the upper thermocline (Hemleben et al., 1989; Ravelo and Fairbanks, 1992; Xu et al., 2006; Farmer et al., 2007; Cléroux et al., 2007; Zuraida et al., 2009). A consistent habitat depth at ~ 100 m for *P. obliquiloculata* is supported by Mg/Ca derived temperature estimates and by calculation of calcification temperatures from $\delta^{18}O_{carbonate}$ and $\delta^{18}O_{seawater}$ measurements in the Timor Sea, which closely match regional WOA05 annual average temperature at 100 m water depth (Locarnini et al., 2006; Zuraida et al., 2009). Furthermore, a habitat depth of 60–80 m was estimated for *P. obliquiloculata* in the upwelling area off South Java (Mohtadi et al.,

2009), indicating that habitat depth does not change significantly under upwelling conditions.

Core MD06-3067 is located at a water depth of 1575 m in the open western Pacific Ocean (6.5°N, 126.5°E), approximately 45 km east of Mindanao Island (Laj et al., 2006; Fig. 1). This 15.5 m long sediment core provides a unique opportunity to closely track past variations of the upper water column in a highly sensitive part of the WPWP, and in particular to relate regional hydrological changes to the activity of the Mindanao Current (MC), SE Asian climate evolution and high latitude climate variability over the last 160 kyr.

2 – Regional oceanography and climate

The Pacific North Equatorial Current (NEC) contributes to the zonal transfer of heat across the Pacific Ocean, and therefore influences the short- and long-term variability of the WPWP. Today, the NEC splits into two branches near the eastern coast of the Philippine islands (15°N; Toole et al., 1990). The northern branch eventually forms the main part of the Kuroshio Current, whereas the southern branch gives rise to the MC, which transfers waters in the upper 300 m along the southeastern coast of the Philippine islands, and ultimately contributes to the Indonesian Throughflow (ITF) transport (Fig. 1).

East of Mindanao Island, a stationary eddy (Mindanao Eddy, centered at 7°N, 130°E and measuring 200 to 300 km in diameter; Fig. 1), is embedded in the regional circulation system, and is characterized by seasonal mid-gyre upwelling (Takahashi, 1959; Masuzawa, 1968; Lukas, 1988; Lukas et al., 1991; Masumoto and Yamagata, 1991; Gordon and McClean, 1999; Qu et al., 1999; Tozuka et al., 2002; Firing et al., 2005). This cyclonic feature, which is mainly driven by the MC, engenders local and seasonal upwelling. Oceanographic observations indicate that upwelled waters are present up to 75 m water depth, but do not reach the surface (Udarbe-Walker and Villanoy, 2001; Tozuka et al., 2002), thus, forming a dome (Mindanao Dome) rather than upwelling sensu stricto (Fig. 2).

The Mindanao Dome is characterized by strong seasonality, as shown by oceanographic observations indicating that dome activity increases markedly during winter (Toole et al., 1990; Masumoto and Yamagata, 1991; Wijffels et al., 1995). The origin and dynamics of the Mindanao Eddy, which induces the Mindanao Dome, are still poorly known. Some studies indicate that changes in the ITCZ position and East Asian winter monsoon variability are the main factors controlling this cyclonic feature (Masumoto and Yamagata, 1991; Tozuka et al., 2002).

The area south and east of Mindanao is affected by monsoonal variability with marked seasonality in the position of the ITCZ driving local wind and rainfall patterns (Fig. 2A-B), even though there is no true dry/wet season due to the relative high amount of precipitation falling over this area during the whole year (Becker et al., 2010). This may explain the small amplitude in salinity change of surface and thermocline waters between summer and winter (Fig. 2G-J).

Early and late boreal summer are the most humid seasons, whereas precipitation is

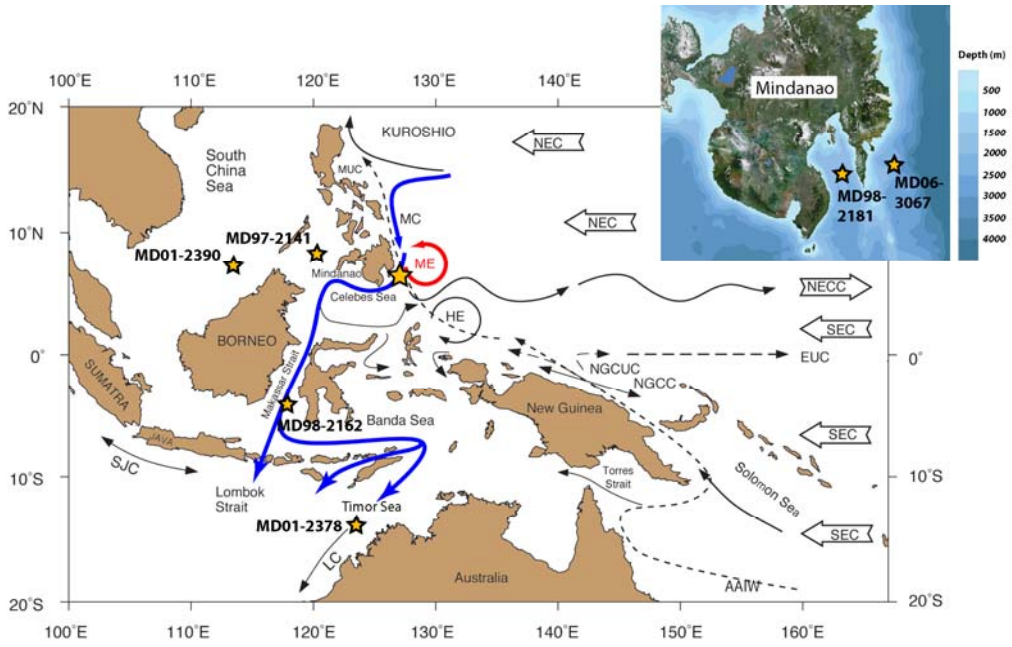

Figure 1. Location of Core MD06-3067 (orange star), bathymetry, and regional circulation in the Australasian area (modified from Fine et al., 1994). Solid blue lines indicate main path of Indonesian Throughflow. Red circular arrow indicates Mindanao Eddy generating Mindanao Dome. NEC is North Equatorial Current, NECC is North Equatorial Counter Current, SEC is South Equatorial Current, EUC is Equatorial Undercurrent, NGCC is New Guinea Coastal Current, NGCUC is New Guinea Coastal Undercurrent, MUC is Mindanao Undercurrent, AAIW is Antarctic Intermediate Water, SJC is South Java Current, LC is Leeuwin Current, MC is Mindanao Current, ME is Mindanao Eddy, and HE is Halmahera Eddy. Positions of cores discussed in this study are also shown: Core MD97-2141 (de Garidel-Thoron et al., 2001; Dannenmann et al., 2003; Oppo et al., 2003; Rosenthal et al., 2003), Core MD01-2390 (Steinke et al., 2010), Core MD98-2181 (Stott et al., 2002; Saikku et al., 2009), Core MD98-2162 Visser et al., (2003), and Core MD01-2378 (Xu et al., 2006, 2010).

Figure 2. Climatology of the Australasian region.

(a) Surface winds direction during boreal winter(January), averaged from 1948 to 2010 (modified from NCEP/NCAR Reanalysis Project, NOAA/ESRL Physical Sciences Division) (Kalnay et al., 1996). Pink shading indicates winter position of ITCZ. Grey star marks position of Core MD06-3067.

(b) Surface winds during boreal summer (July), averaged from 1948 to 2010. Note reversal of trade winds over core location and northward shift of ITCZ position during boreal summer.

(c) SST during boreal winter (January–March) (Locarnini et al., 2006).

(d) SST during boreal summer (July–September) (Locarnini et al., 2006).

(e) Thermocline (100 m depth) temperature during boreal winter (January–March) (Locarnini et al., 2006). Note cold sector east of Mindanao Island due to Mindanao Dome.

(f) Thermocline (100 m depth) temperature during boreal summer (July–September) (Locarnini et al., 2006). Note reduced cold area east of Mindanao Island due to decrease in Mindanao Dome activity during boreal summer.

(g) Sea surface salinity during boreal winter (January–March) (Antonov et al., 2006). Grey star marks position of Core MD06-3067.

(h) Sea surface salinity during boreal summer (July–September) (Antonov et al., 2006).

(i) Thermocline (100 m depth) salinity during borealwinter (January–March) (Antonov et al., 2006). Note insignificant impact of Mindanao Dome on local thermocline salinity.

(j) Thermocline (100 m depth) salinity during boreal summer (July–September) (Antonov et al., 2006).

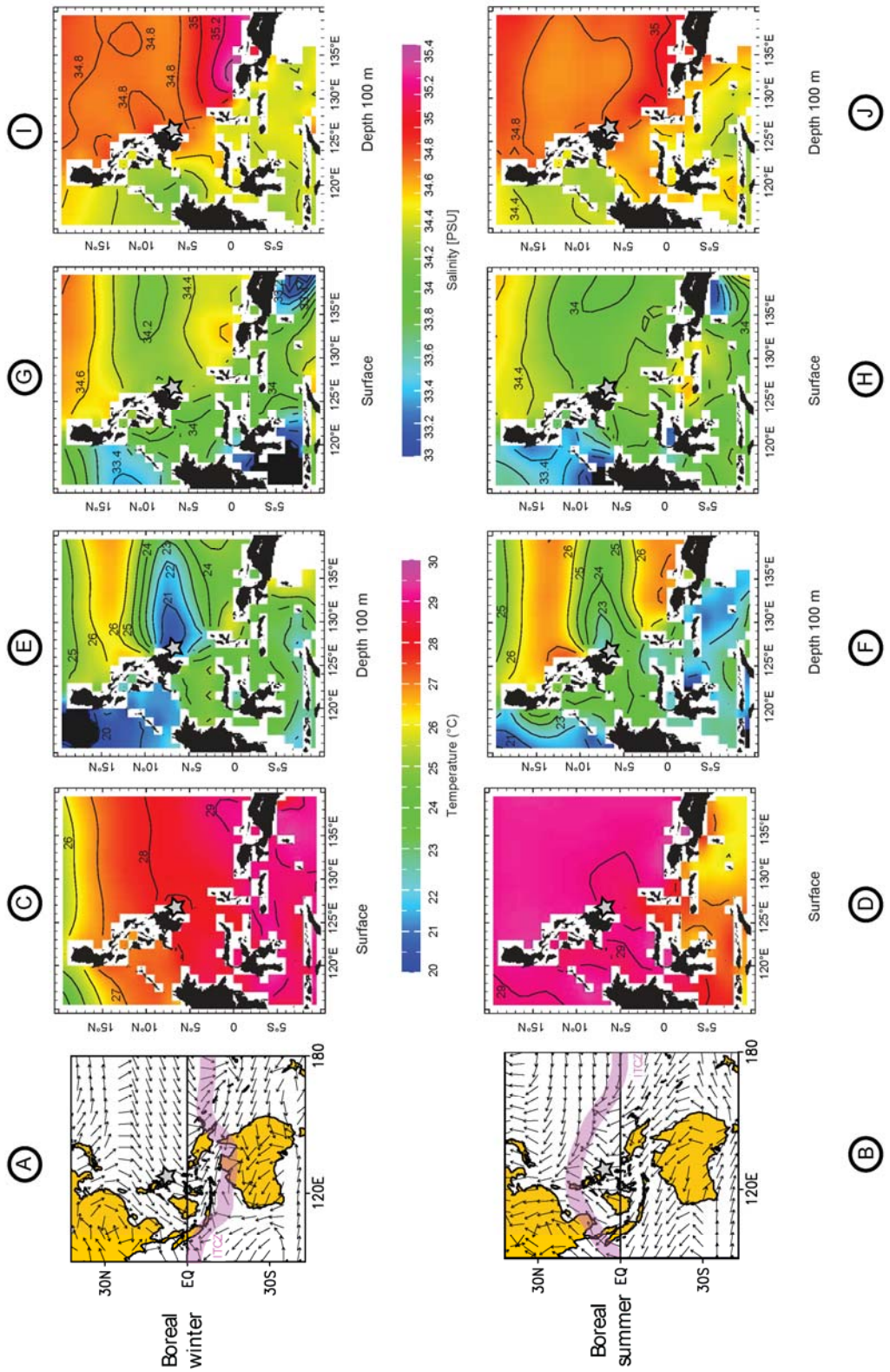
A
B
C
D
E
F
G
H
I
J
Boreal winter
Boreal summer
30N
EQ
30S
120E
180
ITCZ
Surface
Depth 100 m
Temperature (°C)
Salinity [PSU]
5°S
0
5°N
10°N
15°N
120°E
125°E
130°E
135°E

reduced by ~ 50 % during boreal winter and spring. Seasonality is also evident in wind stress data, with stronger winds during boreal summer and winter compared to spring and fall: West to Southwest winds are dominant from June to September, whereas East to Northeast winds blow from December to March (Fig. 2A-B).

The Mindanao region is also influenced by ENSO, with El Niño events marked by clear decreases in rainfall, due to eastward migration of the convection and precipitation cells over the Pacific basin (Lyon et al., 2006). In contrast, La Niña periods are characterized by enhanced precipitation over the western equatorial Pacific Ocean and surrounding land areas. ENSO is also reflected by changes in the seasonal wind pattern, as boreal winter monsoonal winds are weaker during El Niño events and boreal summer monsoonal winds decrease during La Niña periods (Wang et al., 2000; Sakai and Kawamura, 2009).

3 – Material and methods

IMAGES (International Marine Global Change Studies Program) Core MD06- 3067 (6°31 N, 126°30 E, 1575 m water depth) was recovered with the Calypso Giant Piston Corer on board R/V Marion-Dufresne during the IMAGES cruise "Marco Polo 2" in June 2006 (Laj et al., 2006). The core is 15.53 m long and consists mainly of homogenous dark olive gray, silty clay, except for the upper two meters that are composed of brown to olive gray silty clay.

3.1 – Sampling strategy

Core MD06-3067 was initially sampled 148 at 10 cm intervals equivalent to ~ 1 kyr time resolution (155 samples of 1 cm thickness, equivalent to ~ 40 cc) for planktonic and benthic stable isotopes and Mg/Ca analysis. The younger part of the core (MIS 4 to Holocene) was subsequently sampled at 2 cm (~ 200 yrs time resolution) intervals. Samples were dried, weighed, then washed over a 63 μm sieve. Residues were dried on a sheet of filter paper, then weighed and sieved into 63 – 150 μm, 150 – 250 μm, 250 – 315 μm and >315 μm fractions. About 15 to 50 tests of the planktonic foraminifer *G. ruber* (sensu stricto white) and 10 to 40 tests of the upper thermocline dweller *P. obliquiloculata* were picked from the 250-315 μm size fraction. For the initial analysis, 10 to 20 specimens were selected for stable isotope analysis and 10 to 20 (*P. obliquiloculata*) and 20 to 30 (*G. ruber*) specimens for Mg/Ca measurement. For the high resolution analysis, all foraminifers were crushed together, then divided into aliquots for stable isotope and Mg/Ca analyses. In rare occasions, when the number of tests was low, we analyzed foraminifers from an adjacent sample, equivalent to a 2 cm thick interval. For benthic isotopes, 3 to 5 specimens of *Planulina wuellerstorfi* and/or *Cibicidoides mundulus* were selected from the >250 μm size fraction, except in a few samples where only 1-2 specimens were available. In rare occasions where neither of these species was present, we analyzed *Uvigerina proboscidea*, then deducted 0.64 ‰ from the $\delta^{18}O$ values, as suggested by Shackleton and Opdyke (1973).

3.2 – Stable Isotopes

All samples were gently crushed into large fragments, agitated in ethanol for 2-3 seconds in an ultrasonic bath, decanted, then dried at 40°C. Stable carbon and oxygen isotopes were measured with a Finnigan MAT 251 mass spectrometer at the Leibniz Laboratory, Kiel University. The system is coupled online to a Carbo-Kiel Device (Type I) for automated CO_2 preparation from carbonate samples for stable isotopic analysis. Samples were reacted by individual acid addition (99 % H_3PO_4 at 73 °C). Standard external error is better than ±0.07 ‰ for $\delta^{18}O$ as documented by the performance of international and laboratory-internal carbonate standard materials. Replicate $\delta^{18}O$ measurements on 70 samples of *G. ruber* and on 76 samples of *P. obliquiloculata* indicate external reproducibility of ±0.10 ‰ and ±0.12 ‰, respectively. Replicate $\delta^{18}O$ measurements on 31 samples of benthic foraminifers show an external reproducibility of ±0.07 ‰.

3.3 – Radiocarbon dating

For accelerator mass spectrometry (AMS) ^{14}C dating, about 900-1500 well preserved tests of the planktonic foraminifer *G. ruber* were picked from the >250 μm size fraction in samples between 10 and 420 cm. In two samples (KIA 33257, 11 cm and KIA 33790, 210 cm), where the abundance of this species was low, we analyzed *Globigerinoides sacculifer* and *G. ruber* together. In one sample (KIA 33258, 60 cm), we analyzed mixed planktonic species, due to low numbers of *G. sacculifer* and *G. ruber*. AMS ^{14}C dating was performed at the Leibniz laboratory, Kiel University, following the protocol described by Nadeau et al., (1997) and Schleicher et al., (1998). For samples younger than 13 ka, a reservoir age of 480 yrs was subtracted from the conventional ages before conversion to calendar ages. For older samples, we applied a reservoir age of 630 yrs following Saikku et al., (2009). Conventional ages were converted to calendar ages following the protocol established by Fairbanks et al., (2005).

3.4 – Mg/Ca Analysis

Foraminifers were weighed with an ultraprecision balance (Sartorius ME5 OCE, repeatability ± 1 micrograms, linearity ± 4 micrograms), gently crushed to expose inner chamber walls, then put into vials for cleaning. The cleaning procedure used for removing contaminant phases includes oxidative and reductive steps following methods outlined by Martin and Lea, (2002). Prior to analysis, full dissolution of the test fragments was obtained with 1 ml 0.1 N nitric acid and ultrasonication, and aliquots were diluted in such a way that the final solution contained ~ 50 (25-75) mg l-1 Ca. Only freshly prepared subboiled HNO3 was used and all work was done in class100 clean benches. The dissolved samples were analyzed on a radial viewing simultaneous ICP-OES (Spectro Ciros SOP CCD, Spectro Analytical Instruments, Germany) at the Institute of Geosciences, Kiel University, applying an intensity calibration method (de Villiers et al., 2002) and bracketing standards. Batches of 6 unknown samples were bracketed by a synthetic normalization standard. At least 10 % of unknown samples were replicate measurements of samples analysed hours before, or during previous day analytical sessions. Typical external error is 0.1 % rel. (1sigma) for Mg/Ca. Carbonate certified reference material (ECRM 752-1, BAM RS3; Greaves et al., 2008) was analysed for monitoring analytical accuracy. Matrix effects caused by the easily ionisable element Ca were investigated and found to be negligible. Samples with a recovery in Ca concentration of less than 20 % were rejected. Fe/Ca, Al/Ca and Mn/Ca ratios were additionally monitored to test cleaning efficiency, and samples showing a significant correlation between Fe/Ca, Al/Ca, Mn/Ca and Mg/Ca values were excluded, following Schmidt et al., (2004). Replicate measurements of 66 samples of *G. ruber* and 39 samples of *P. obliquiloculata* (measured two to four times) indicated relative standard deviation of 0.18 and 0.11 mmol/mol, which is equivalent to a SST deviation of ±0.48 and ±0.52°C, respectively.

Foraminiferal Mg/Ca ratios were then converted into temperatures using the equations of Anand et al., (2003) that provide an accuracy of ±1.2°C in estimating calcification temperature (T in °C):

Mg/Ca=0.38 (± 0.02) exp 0.090 (± 0.003) T for *G. ruber*

Mg/Ca=0.328 (± 0007) exp 0.090 (± 0.003) T for *P. obliquiloculata*

The equation for *G. ruber* (350-500 microns) was previously used in othe regional studies, and gives similar results as the equation of Dekens et al., (2002) without

dissolution correction. We applied no correction for the reductive step included in our cleaning protocol, which generally results in a small decrease in Mg/Ca leading to temperature underestimation of up to 0.6°C (Rosenthal et al., 2004). Bian and Martin (2010) validated the use of a reductive step in the cleaning procedure for Mg/Ca analysis, and demonstrated the potential of reductive cleaning to improve the Mg/Ca data.

Carbonate dissolution is unlikely to have affected the Mg/Ca ratio of our samples due to the relatively shallow water depth of 1575 m of Site MD06-3067. Nonetheless, potential effects of carbonate dissolution on Mg/Ca were monitored by comparing average weights of individual shells of *G. ruber* (201 samples) and *P. obliquiloculata* (190 samples) with Mg/Ca data obtained from the same samples. Shell weights of *G. ruber* remain relatively constant throughout, while *P. obliquiloculata* shells exhibit more variability in weight (Suppl. Fig. 2). Yet, systematic variations are not observed and there is no correlation between shell weights and Mg/Ca ratios (Suppl. Fig. 2A, B). We use this as an indication that our Mg/Ca data were not affected by carbonate dissolution. Peak occurrence of benthic foraminifers with extremely fragile, thin walled tests (globobulimids) in intervals, where Mg/Ca is episodically low, further indicates that carbonate dissolution is not a cause of Mg loss. Although the deeper dweller *P. obliquiloculata* exhibits more variability in individual shell weight, no significant link with cold/warm phases is detected.

3.5 – Calculation of δ^{18}Osw

We calculated surface and thermocline seawater $\delta^{18}O$ composition (δ^{18}Osw vs. VSMOW) from paired Mg/Ca and $\delta^{18}O$ measurements of *G. ruber* and *P. obliquiloculata*, respectively. For this we used the equation of Bemis et al., (1998):

$\delta^{18}Osw = 0.27 + (T(°C) – 16.5 + 4.8\times\delta^{18}O\ (V\text{-}PDB))/4.8$

A core top δ^{18}Osw value of 0.07 ‰ was calculated for surface water from an average of the last three Holocene measurements in Core MD06-3067. This value is in agreement with the regional average of 0.1 ‰, in the global δ^{18}Osw database (LeGrande and Schmidt, 2006).

A modern δ^{18}Osw value of 0.39 ‰ for thermocline water was calculated from the salinity value at 100 m water depth at the location of Core MD06-3067 (34.9 psu; World Ocean Atlas 2005; Antonov et al., 2006) using the empirical relation by Fairbanks et al., (1997):

$$\delta^{18}Osw = + 0.273 \times S - 9.14$$

Where S is the salinity (psu) and $\delta^{18}Osw$ is expressed in per mil (‰) relative to VSMOW. The $\delta^{18}Osw$ value of 0.27 ‰ that we derive from paired late Holocene *P. obliquiloculata* $\delta^{18}O$ and Mg/Ca agrees well with the estimated water column $\delta^{18}Osw$ value, and supports the upper thermocline habitat depth of this species.

A correction for relative past changes in sea level on the $\delta^{18}Osw$ of the global ocean (following Waelbroeck et al., 2002) was applied to the surface and thermocline $\delta^{18}Osw$ records of Core MD06-3067.

3.6 – Seasonality of sea surface and upper thermocline proxies

Sediment trap data indicate a peak of *G. ruber* fluxes during the summer months in the Panama Basin (Thunell and Reynolds, 1984). Combined sediment trap and plankton tow studies in the South China Sea also show higher percentage abundances of *G. ruber* during the summer months, while total fluxes are enhanced during the boreal winter monsoon, suggesting that the seasonality of *G. ruber* is less pronounced than for other surface dwelling species such as *G. sacculifer* (Lin et al., 2004; Lin and Hsieh, 2007). A recent study within the monsoon driven South Java upwelling (Mohtadi et al., 2009) indicates a similar seasonality of flux rates for *G. ruber* and *P. obliquiloculata*. Flux rates of both species are less influenced by upwelling seasonality than typical upwelling indicators such as *G. bulloides, G. glutinata* and *N. pachyderma* (dextral).

3.7 – Paleoproductivity proxies

3.7.1 – Coccoliths

We sampled Core MD06-3067 for coccolith counts at 10 cm intervals (155 samples), corresponding to a temporal resolution of ~ 1 kyr. A few milligrams of sediment were evenly spread on a glass slide, then 40 digital photos were taken for each slide with a camera mounted on a Leica DMRBE transmitted light microscope with a 50X oil immersion objective. Counting of coccoliths was performed with an automated system of coccolith recognition (SYRACO, SYstème de Reconaisance Automatique de COccolithes) using a neural network algorithm (see details in Dollfus and

Beaufort, 1999; Beaufort and Dollfus, 2004). A total of 14 taxa were identified, of which six represent an average of 89 % of the total assemblage: *Emiliania huxleyi, Florisphaera profunda, Gephyrocapsa ericsonii, Gephyrocapsa muellerae, Gephyrocapsa oceanica* and *Helicosphaera* spp. Within these taxa, the average number of coccoliths recognized by the system is ~ 1600 specimens before visual correction and ~ 1100 specimens after corection. Primary productivity was estimated using the equation of Beaufort et al., (1997), based on the empirical relationship between the relative abundances of *F. profunda* and productivity:

$PP = 617 - [279 * \log(Fp + 3)]$

where PP is the primary productivity and Fp is the relative abundance of *F. profunda*. This equation was established by comparing Indian Ocean core-top data with modern productivity based on satellite chlorophyll, and is considered representative for the Pacific Ocean (Beaufort et al., 2001)

3.7.2 – Benthic foraminifers

Benthic foraminifers were picked and counted in the size fraction >250 μm from 111 samples (10 or 20 cm intervals). In samples, where benthic foraminiferal abundance was high, a quantitative split was picked, and census counts were then reconverted to whole samples. Numbers of benthic foraminifers picked per sample generally vary between 150 and 600 (average of 348) specimens except in rare samples, where foraminiferal abundance was low and fewer specimens were picked.

We used percentage abundances of four main groups that are indicative of high and intermediate carbon export flux to the seafloor (Kuhnt et al., 1999; Holbourn et al., 2005). Counts of globocassidulinids include *Globocassidulina subglobosa* and *G. elegans*. Globobuliminids include *Globobulimina pupoides, G. ovata, G. pyrula* and *G. pacifica*. Miliolids include *Pyrgo murrhina, P. serrata* and *Pyrgo* spp. *Bolivinita quadrilatera* is a mesotrophic indicator species that shows marked variations in abundance in Core MD06-3067.

4 – Results

4.1 – Chronology

The benthic $\delta^{18}O$ record from Core MD06-3067 indicates recovery of a complete succession from the Holocene down to MIS 6 (Fig. 3A-B). Interglacial MIS 5e and MIS 1 and glacial periods (MIS 6 and MIS 2) as well as Antarctic warm events A1-A4 (between 38 and 58 ka BP) can be clearly identified. The age model is based on seven AMS ^{14}C dates in the upper part of the core (11-420 cm) and on correlation of the benthic $\delta^{18}O$ between 253 and 1550 cm in Core MD06-3067 with the $\delta^{18}O$ record from the EPICA Dronning Maud Land ice core (EDML1 chronology, Ruth et al., 2007). AMS ^{14}C dates and tie points used to derive the age model are given in Table 1 and shown on Fig. 3.

AMS ^{14}C dates at 260 and 280 cm (samples KIA 35211 and KIA 35212; Table 1) were not used because ages for surface water appear influenced by upwelling of deeper, older water during the last glacial period. These two AMS ^{14}C dates are older by ~ 1800 and ~ 3000 yrs, respectively, than ages derived from our age model (Fig. 3). Stott et al., (2007) and Saikku et al., (2009) suggested that the benthic $\delta^{18}O$ signal in a nearby location within the Mindanao embayment (Core MD98-2181; Fig. 1) records Antarctic climate variations with a delay of ~ 1000 years. To maintain coherency with these studies, we removed 1000 years from the ages that were derived from graphical correlation of benthic $\delta^{18}O$ with the $\delta^{18}O$ record from the EPICA ice core.

An interpolated curve was fitted through the $\delta^{18}O$ tie points and AMS ^{14}C data points using a Stineman function (Smooth function in KaleidaGraph). This function fits a curve that passes through the data points and matches the slopes at these points. The output of the function then has a geometric weight applied to the current point and ±10 % of the data range. The resulting smoothed curve was then sampled at relevant intervals. The age model in the lower part of the core (1335-1550 cm corresponding to MIS 6) is based on linear extrapolation from the lowest tie point (onset of Termination II at 1335 cm) to the base of the core, assuming a constant sedimentation rate of 10 cm/kyr, which is consistent with glacial sedimentation rates during MIS 2. The Laschamp geomagnetic excursion was used to test the robustness of our age model. This event is centered at ~ 511 cmb.s.f. in Core MD06-3067 (Laj et al., in prep.), which corresponds in our age model to ~ 40.8 ka. This is consistent with the

radiometric age of 40.4 ± 2 ka (2s) obtained from the lava flow at the Laschamp locality (*Guillou et al.,* 2004) and more recently refined to 40.7 ± 0.95 ka (2s) (Singer et al., 2009). The relative position of the Laschamp event (40.8 ka) and Heinrich event H4 (39.8-38.5 ka) in our record (Fig. 3B) also agrees with the GICC05 ice core chronology (Svensson et al., 2008).

Sedimentation rates remain relatively constant, with an average rate of 10 cm/kyr, except within the upper two meters of the core, where the rate increases to 35 cm/kyr (Fig. 3A). This higher apparent rate is due to the piston coring system, as illustrated by the vertical alignment of magnetic particles (Kissel et al., 2010), which can cause expansion of the upper core section and on occasion causes oversampling (i.e. lateral sediment intake) in the upper part of the core (Széréméta et al., 2004).

4.2 – Benthic $\delta^{18}O$

The benthic oxygen isotope record shows glacial-interglacial fluctuations with amplitudes of ~ 1.7 ‰ over both Terminations I and II (from 4.1 to 2.4 ‰ for Termination II and from 4.2 to 2.5 ‰ for Termination I, Fig. 3B). $\delta^{18}O$ values fluctuate between 3.2 and 4 ‰ during MIS 3, and reach 3.8 ‰ during MIS 4, which is 0.8 ‰ more than for MIS 5a. The main MIS 5 substages a-e can be identified, as well as Antarctic warm events AIM4 and A1-4 (at ~ 29, 39, 46, 53 and 59 ka; Fig. 3B).

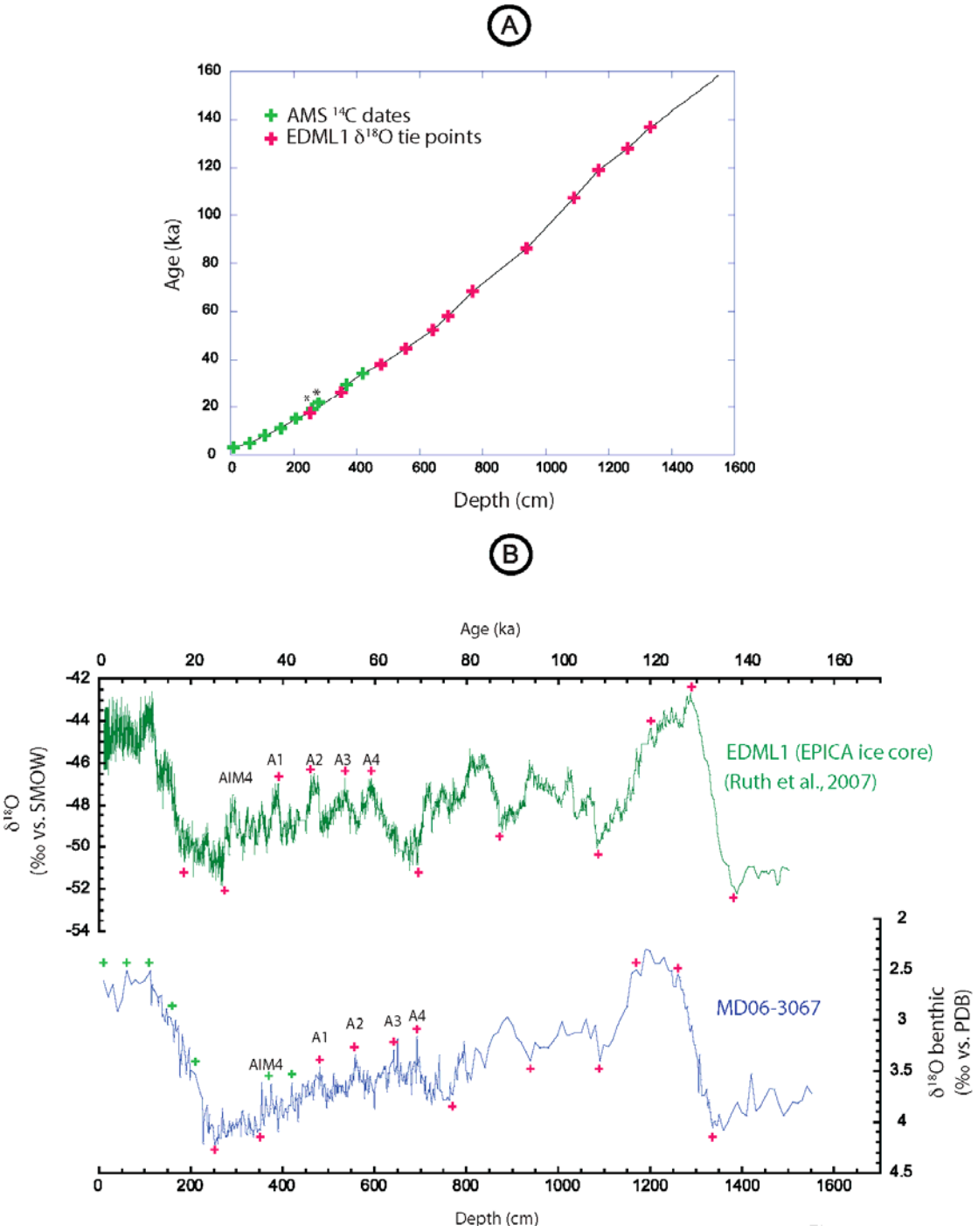

Figure 3. Age model based on seven accelerator mass spectrometry (AMS) ^{14}C dates and 12 $\delta^{18}O$ events for Core MD06-3067 (Table 1).

(a) Depth/age plot with AMS ^{14}C dates (green crosses) and $\delta^{18}O$ events (pink crosses). Asterisks mark AMS ^{14}C dates not used for age model.

(b) Comparison of MD06-3067 benthic $\delta^{18}O$ signal (bottom curve) with EDML1 $\delta^{18}O$ (top curve) (Ruth et al., 2007). Green crosses indicate AMS ^{14}C dates. Pink crosses indicate $\delta^{18}O$ events used as tie points. AIM4 and A1 to A4 refer to Antarctic Isotope Maxima or warm events.

Type	Depth (cm)	Calendar Age (years BP)	Description
AMS ^{14}C date	11 (section 1; 11–12 cm)	3390 ± 27	Species analyzed: *G. ruber, G. sacculifer*. ^{14}C conventional age: 3655 ± 30 years. Reservoir age correction: 480 years. Reference: KIA 33257.
AMS ^{14}C date	60 (section 1; 60–61 cm	4750 ± 70	Species analyzed: mixed surface dwelling planktonic foraminifers. ^{14}C conventional age: 4655 ± 30 years. Reservoir age correction: 480 years. Reference: KIA 33258.
AMS ^{14}C date	110 (section 1; 110–111 cm)	8205 ± 49	Species analyzed: *G. ruber*. ^{14}C conventional age: 7870 ± 40 years. Reservoir age correction: 480 years. Reference: KIA 33788.
AMS ^{14}C date	160 (section 2; 10–11 cm)	11,010 ± 125	Species analyzed: *G. ruber*. ^{14}C conventional age: 10100 ± 45 years. Reservoir age correction: 480 years. Reference: KIA 33789.
AMS ^{14}C date	210 (section 2; 60–61 cm)	15,250 ± 124	Species analyzed: *G. ruber, G. sacculifer*. ^{14}C conventional age: 13725 ± 65 years. Reservoir age correction: 630 years. Reference: KIA 33790.
δ^{18}O event	253 (section 2; 103–104 cm)	(18,400) 17400	Onset of Termination I
AMS ^{14}C date	260 (section 2; 110–111 cm)	19,460 ± 103	Species analyzed: *G. ruber*. ^{14}C conventional age: 16970 +90/–80 years. Reservoir age correction: 630 years. Reference: KIA 35211. Not used for generating age model.
AMS ^{14}C date	280 (section 2; 130–131 cm)	22,100 ± 131	Species analyzed: *G. ruber*. ^{14}C conventional age: 19110 ± 100 years. Reservoir age correction: 630 years. Reference: KIA 35212. Not used for generating age model.
δ^{18}O event	352 (section 3; 52–53 cm)	(27,300) 26,300	Benthic δ^{18}O increase at end of MIS 3
AMS ^{14}C date	370 (section 3; 70–71 cm)	29,690 ± 313	Species analyzed: *G. ruber*. ^{14}C conventional age: 25410 +190/–180 years. Reservoir age correction: 630 years. Reference: KIA 35214.
AMS ^{14}C date	420 (section 3; 120–121 cm)	34,470 ± 339	Species analyzed: *G. ruber*. ^{14}C conventional age: 29690 +300/–290 years. Reservoir age correction: 630 years. Reference: KIA 35215.
δ^{18}O event	480 (section 4; 30–31 cm)	(39,000) 38,000	Lowest δ^{18}O value at onset of A1 plateau
δ^{18}O event	557 (section 4; 107–108 cm)	(45,900) 44,900	End of A2 event
δ^{18}O event	642 (section 5; 42–43 cm)	(53,500) 52,500	Lowest δ^{18}O value of A3 plateau
δ^{18}O event	692 (section 5; 92–93 cm)	(59,200) 58,200	Lowest δ^{18}O value in center of A4 plateau
δ^{18}O event	769 (section 6; 19–20 cm)	(69,400) 68,400	Onset of MIS4
δ^{18}O event	939 (section 7; 39–40 cm)	(87,100) 86,100	End of MIS 5b
δ^{18}O event	1089 (section 8; 39–40 cm)	(108,500) 107,500	End of MIS 5d
δ^{18}O event	1169 (section 8; 119–120 cm)	(120,000) 119,000	End of MIS 5e plateau
δ^{18}O event	1260 (section 9; 60–61 cm)	(128,800) 127,800	Onset of MIS 5e plateau
δ^{18}O event	1335 (section 9; 135–136 cm)	(137,900) 136,900	Onset of Termination II

Table 1. Planktonic foraminiferal AMS ^{14}C dates and Benthic δ^{18}O Events used to derive the age model for Core MD06-3067. Calendar ages of δ^{18}O events in EDML1 (EPICA ice core) (Ruth et al., 2007) are given in parentheses. Ages of δ^{18}O events in Core MD06-3067 were shifted by 1000 years to accommodate signal propagation time from the Southern Ocean to the location of Core MD06-3067. For discussion, see text.

4.3 – Planktonic $\delta^{18}O$, Temperature and $\delta^{18}Osw$ reconstructions

4.3.1 – *G. ruber* and *P. obliquiloculata* $\delta^{18}O$

The surface and thermocline $\delta^{18}O$ records (Figs. 4 A and 5 A) from MIS 6 to the late Holocene exhibit well-defined main isotopic stages with overall higher variability in the thermocline than in the surface signal. The MIS 5e plateau at 118-127 ka is clearly defined in the *G. ruber* record, with values ranging from -2.5 to -2.6‰. The thermocline signal exhibits the highest depletion (-1.3 to -1.4 ‰) during MIS 5e (between 120 and 124 ka). The transition between MIS 5e to 5d corresponds to an enrichment of ~ 0.6 ‰ and ~ 0.9 ‰ in surface and thermocline $\delta^{18}O$ values, respectively. During the remainder of MIS 5, the $\delta^{18}O$ contrast between cold (5b and d) and warm (5a and c) phases is higher in the *P. obliquiloculata* thermocline record than in the surface record. The cold MIS 4 interval is marked by an enrichment of 0.6 ‰ in *G. ruber* $\delta^{18}O$ and 0.25 to 0.4 ‰ in *P. obliquiloculata* $\delta^{18}O$, whereas the transition between MIS 4 and 3 appears as a sudden depletion of 0.3 ‰ in both records. During MIS 2 and MIS 6, $\delta^{18}O$ values of surface and thermocline waters are similar as well as the amplitude of the decreases (~ 1.6 ‰) over Termination I (18.5-11 ka) and Termination II (137-127 ka). In the Holocene, average $\delta^{18}O$ values for both surface and upper thermocline waters are close to MIS 5e values.

4.3.2 – Sea surface and thermocline temperature

Temperature reconstructions based on Mg/Ca analysis of *G. ruber* and *P. obliquiloculata* in Core MD06-3067 indicate substantial glacial-interglacial temperature contrasts (Figs. 4B and 5B). The last deglaciation is marked by a warming of 5°C in both surface and thermocline waters, whereas the amplitude of warming during Termination II is larger in thermocline waters (5°C) than in surface waters (3.5°C). The higher amplitude of surface warming during Termination I results from the ~ 2°C colder SST during MIS 2 compared to MIS 6 (average of 24.5 °C for MIS 2 in contrast to 26.5 °C for MIS 6). The offset in SST between MIS 2 and MIS 6 is contrasted by surface $\delta^{18}O$ at MD06-3067 that is similar for MIS 2 and MIS 6, possibly indicating an influence of $\delta^{18}Osw$ and salinity.

During MIS 5e, the *P. obliquiloculata* temperature record exhibits a sharp maximum around 126 ka, which is contrasted by the broad plateau shown between 118 and 127 ka in the *G. ruber* record. The transition from MIS 5e to 5d (118-108 ka) also differs significantly in the surface and thermocline signals: *G. ruber* shows a 2°C cooling, whereas *P. obliquiloculata* exhibits a decrease of 6°C, leading to cool thermocline temperatures during MIS 5d (20-21 °C), which are only slightly warmer than during MIS 6 (21-22°C). Temperature fluctuations during MIS 5d-a are more marked in thermocline waters (23-20 °C) than in surface waters (28-26 °C). However, the MIS 5a to MIS 4 transition is better defined in the SST than in the thermocline record (28 to 25.5°C vs. 23 to 21.5°C, respectively). During MIS 3, SST values exhibit high amplitude variability (ranging from 28.5 to 24.5 °C), showing prominent cooling episodes at ~ 49.5-46.5 ka and ~ 37-30 ka and warming pulses during stadials/Antarctic warm periods (notably during the Heinrich H4/A1 events). Thermocline temperatures fluctuate markedly (24-20 °C) but show no distinct trend in contrast to SST, which clearly reflect stadials/Antarctic warm periods. Lowest SST (26-24 °C) occurs during MIS 2 (27.5-19 ka), when SST displays a characteristic double trough. The glacial decrease in temperature is less distinct in the *P. obliquiloculata* thermocline record with values fluctuating between 20 and 23°C.

Figure 4. Surface water hydrology over the last 160 kyr, based on analysis of *G. ruber* (white) in Core MD06-3067. Shading marks glacial marine isotope stages (MIS 2, 4, and 6).

(a) $\delta^{18}O$ record of *G. ruber* (white).

(b) SST derived from Mg/Ca of *G. ruber* (white). Anomalously cold SST during MIS 3 and MIS 2 indicate phases of intensified upwelling.

(c) Surface $\delta^{18}Osw$ uncorrected for sea level (thin black line). Solid red line indicates $\delta^{18}O$ sea level equivalent (from Waelbroeck et al., 2002).

(d) Surface $\delta^{18}Osw$ corrected for sea level. Dashed line indicates modern local $\delta^{18}Osw$ of surface water.

(e) Benthic $\delta^{18}O$ record measured mainly on *P. wuellerstorfi* and *C. mundulus*.

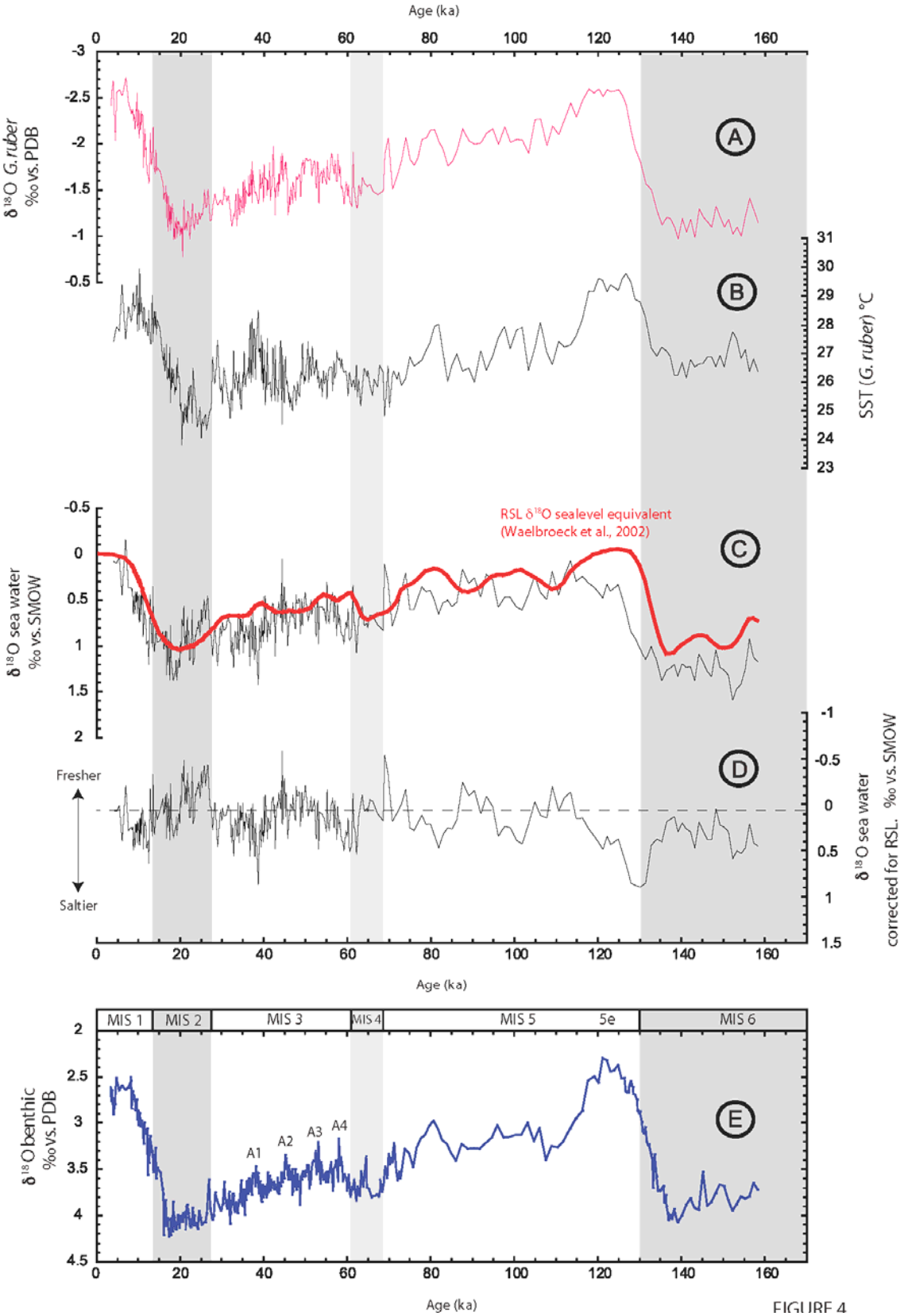
Age (ka)
δ18O G.ruber ‰ vs. PDB
A
B
SST (G.ruber) °C
RSL δ18O sealevel equivalent (Waelbroeck et al., 2002)
δ18O sea water ‰ vs. SMOW
C
D
Fresher
Saltier
δ18O sea water corrected for RSL. ‰ vs. SMOW
MIS 1
MIS 2
MIS 3
MIS 4
MIS 5
5e
MIS 6
δ18O benthic ‰ vs. PDB
A1
A2
A3
A4
E

FIGURE 4

4.3.3 – Surface and thermocline δ^{18}Osw (sea level corrected)

Sea level corrected surface δ^{18}Osw show ~ 1 ‰ variability during the last glacial cycle (Fig. 4C-D). This high amplitude variability partly stems from the 1.5 kyr temporal resolution of the δ^{18}O sea level equivalent curve used for correction (Waelbroeck et al., 2002), which is significantly lower than in our records (~ 200 yrs over the last glacial cycle). According to calibrations of δ^{18}Osw in terms of salinity in the tropics (0.3 ‰/psu; LeGrande and Schmidt, 2006; Oppo et al., 2007), these variations correspond to a salinity change of up to ~ 3 psu, which is more than the present day seasonal and regional variability (Locarnini et al., 2006). However off Mindanao, changes in the δ^{18}O of precipitation and runoff potentially influenced the amplitude of δ^{18}Osw fluctuations over the last glacial cycle. Transient increases in sea level corrected surface δ^{18}Osw occur during MIS 3 stadials, whereas values decrease markedly at ~ 45 ka and during the LGM (26-19 ka), when SST were unusually cool. Reconstructed sea level corrected thermocline δ^{18}Osw is generally slightly more enriched than today (~ 0.5 ‰), but does not show any significant glacial-interglacial trends (Fig. 5C-D). The enrichment in surface and thermocline sea level corrected δ^{18}Osw during Termination II apparently stems from age model inconsistencies between the sea level δ^{18}O equivalent (Waelbroeck et al., 2002) used for correction and the MD06-3067 record.

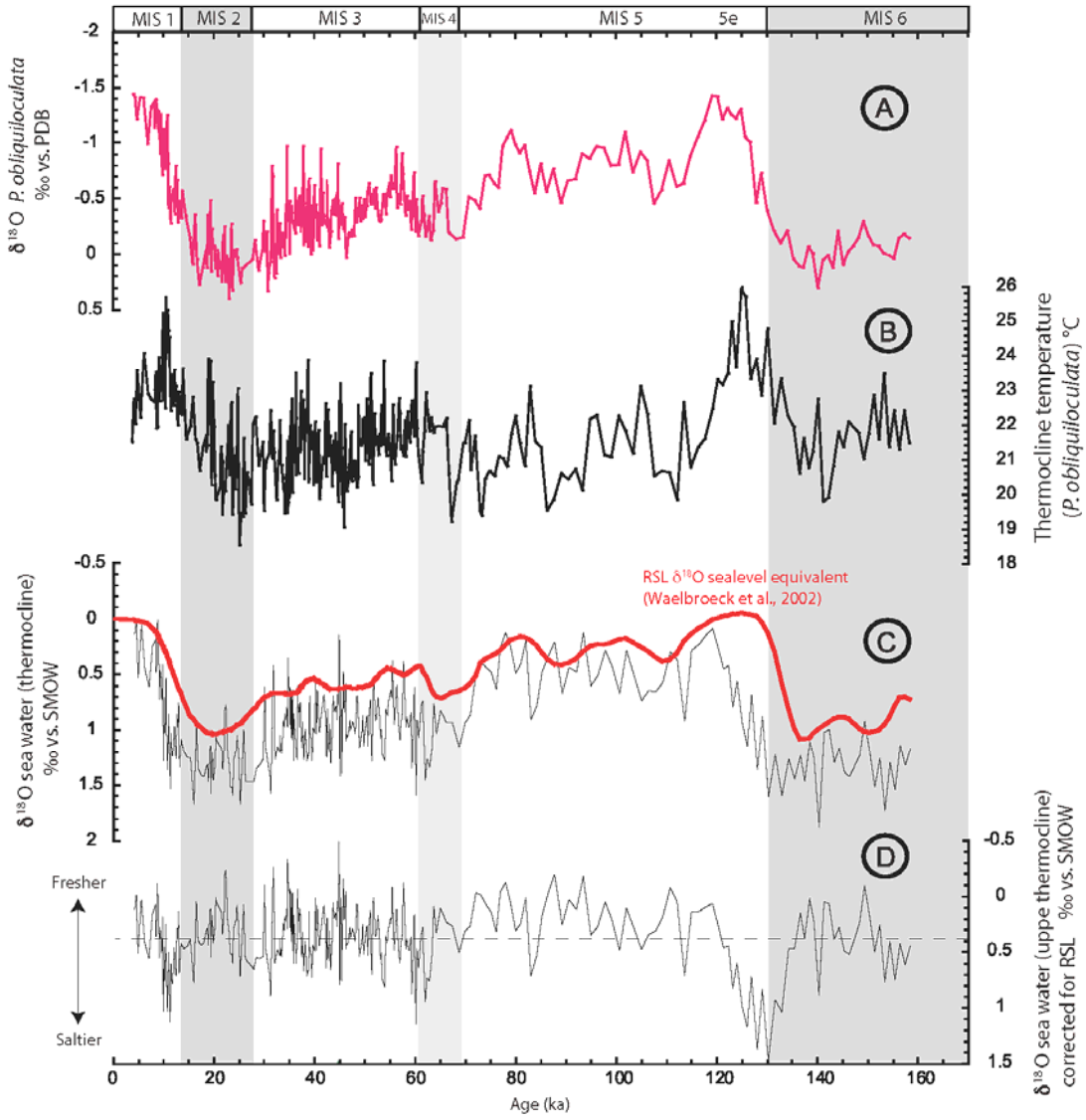

Figure 5. Upper thermocline hydrology over the last 160 kyr, based on analysis of *P. obliquiloculata* in Core MD06-3067. Note enhanced thermocline temperatures during MIS 5e and early Holocene. Shading marks glacial marine isotope stages (MIS 2, 4, and 6).

(a) $\delta^{18}O$ record of *P. obliquiloculata*.

(b) Temperature of the upper themocline derived from Mg/Ca of *P. obliquiloculata.*

(c) Thermocline $\delta^{18}O$ sw uncorrected for sea level (thin black line). Solid red line indicates $\delta^{18}O$ sea level equivalent (from Waelbroeck et al., 2002).

(d) Thermocline $\delta^{18}O$ sw corrected for sea level. Dashed line indicates modern local $\delta^{18}O$ sw of thermocline water.

4.4 – Floral and Faunal indicators of paleoproductivity

Emiliana huxleyi and *F. profunda* dominate the coccolith assemblage, representing more than 60 % of the six major species recognized by the automated recognition system SYRACO (Fig. 6A). A brief decrease of *F. profunda* to 45 % during MIS 5 (at ~ 100 ka) coincides with an increase in the relative abundance of *G. ericsonii* from 15 to 30 %. The two major species *F. profunda* and *E. huxleyi* show distinct long-term trends with *F. profunda* showing elevated abundances from MIS 6 to MIS 5c and in the Holocene, whereas *E. huxleyi* increases markedly in abundance from MIS 4 to the LGM. Since paleoproductivity is anticorrelated to the abundance of the deep dwelling species *F. profunda* (Beaufort et al., 1997), it broadly correlates with the abundance of the shallow dwelling species *E. huxleyi* in Core MD06-3067.

Highest productivity occurs during the LGM, MIS 3 and MIS 4 and lowest productivity during MIS 5e, whereas MIS 5d-5a and MIS 6 show intermediate values between these levels.

Benthic foraminiferal abundances are closely related to the availability of food at the sea floor, which is largely derived from the export flux of primary production in the photic zone (Loubere, 1994 and 1996). In Core MD06-3067, there is considerable difference in the temporal distribution of the four major paleoproductivity indicators (Fig. 6A-D). Globobuliminids, which occur abundantly in tropical upwelling areas, show peaks in abundance (>8 %) during MIS 2 and MIS 3 at ~ 18, 20, 24, 32-35, 45-50, 52 and 55 ka. During MIS 4 and MIS 6, globobuliminids vary between 3 and 8 %, whereas abundances decrease to 0-2 % during interglacials. Miliolids, typically reflecting mesotrophic conditions, exhibit a pronounced glacial-interglacial variability with abundances mostly >10 % during MIS 2-4 and MIS 6 and dropping below 10 % during interglacials. Globocassidulinids, which increase in numbers following seasonal phytodetritus pulses (Gooday, 1993), have their highest abundances during MIS 3 at ~ 37-41 ka (30 to >50 %) and Termination II, whereas abundances generally remain between 10 and 30 % in other intervals. *Bolivinita quadrilatera*, indicative of mesotrophic conditions, shows highest abundance during MIS 6 and the early part of Termination II (reaching >35 %), then fluctuating below 15 % from MIS 5e to the Holocene.

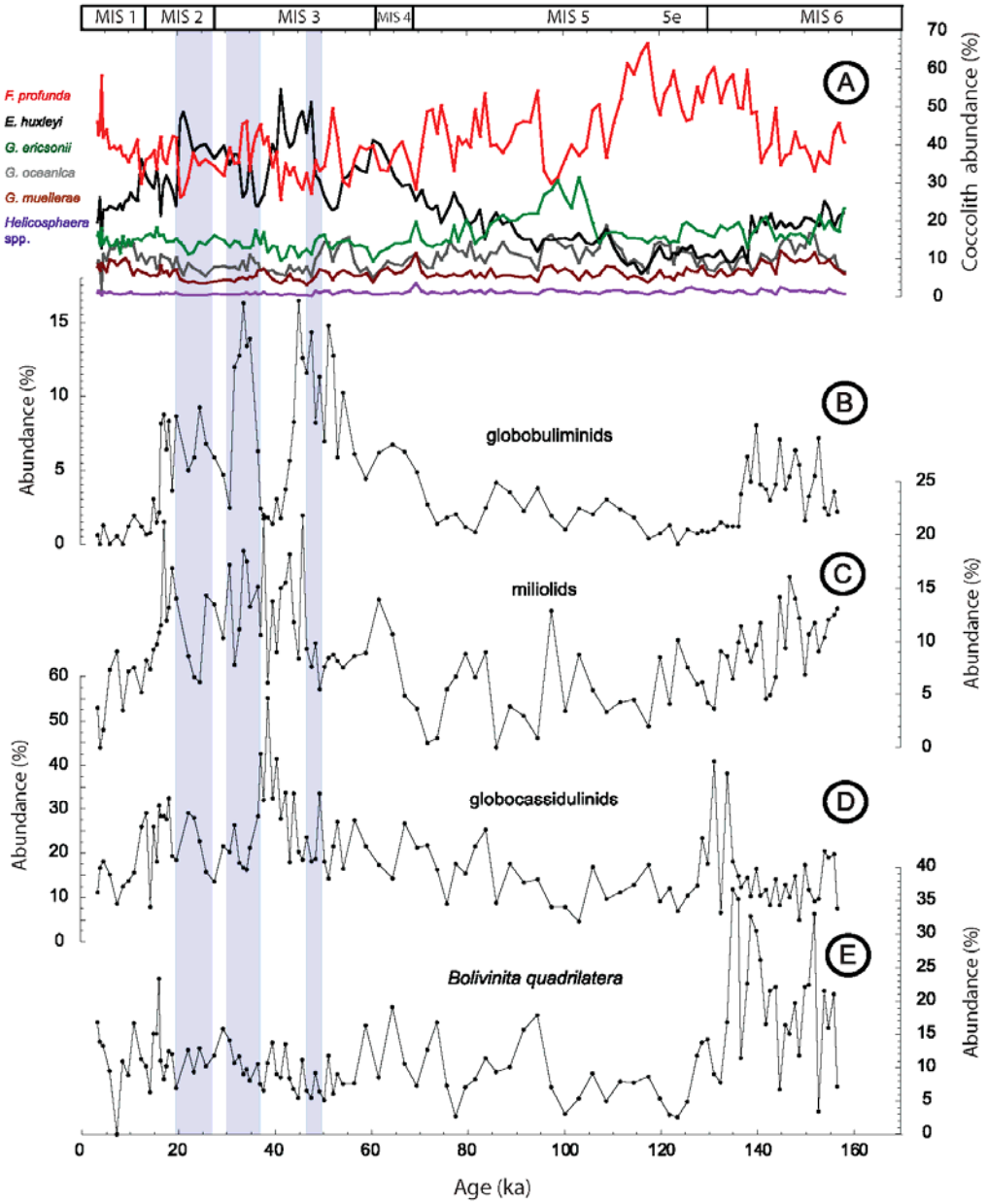

Figure 6. Relative percentage abundance of major coccolith and benthic foraminiferal high□productivity index taxa in Core MD0-3067. Blue bars indicate periods of intense surface and upper thermocline cooling, implying a reduced upper ocean temperature gradient.

(a) Percent abundance of six major taxa within coccolith assemblages (*F. profunda, E. huxleyi, G. ericsonii, G. oceanica, G. muellerae*, and *Helicosphaera* spp.).

(b) Percent abundance of globobuliminids.

(c) Percent abundance of miliolids.

(d) Percent abundance of globocassidulinids.

(e) Percent abundance of *Bolivinita quadrilatera*.

In summary, both floral and faunal indicators exhibit distinct glacial-interglacial distribution patterns with lower productivity characterizing warm stages (MIS 5,

Holocene) and increased productivity marking colder stages (MIS 6, MIS 4-2). Marked fluctuations in the composition of the coccolith and benthic foraminiferal assemblages suggest episodic increases during MIS 4-2, whereas productivity levels remained more stable and overall lower during MIS 6.

5 – Discussion

5.1 – Glacial-interglacial SST contrast

SST estimates based on Mg/Ca of G. ruber in Core MD06-3067 reveal a sharp glacial-interglacial contrast offshore eastern Mindanao over the last 160 kyr (Fig. 4B). SST shows an overall difference of ~ 3.5 °C over Termination II and ~ 5 °C over Termination I. In other areas of the WPWP, SST estimates exhibit consistent increases of ~ 3.5 °C over Terminations I and II (Lea et al., 2000 and 2003; Kienast et al., 2001; Stott et al., 2002 and 2007; Visser et al., 2003; Oppo and Sun, 2005; de Garidel-Thoron et al., 2007), except in the Sulu Sea, where lower values were estimated, based on foraminiferal counts and alkenones (2.2 °C and 1°C, respectively, de Garidel-Thoron et al., unpublished data). In Core MD06-3067, the higher SST contrast over Termination I is due to substantially cooler SST (by ~ 2 °C) during the LGM than during MIS 6. These LGM values are colder (by ~ 1.5 to 2 °C) than in other WPWP locations including the nearby Core MD98-2181 in the Davao Gulf, offshore southern Mindanao (Stott et al., 2002, Suppl. Fig. 1B).

Further discrepancies in SST are evident during MIS 3, when we compare the records from the Davao Gulf (Core MD98-2181, Saikku et al., 2009, Suppl. Fig. 1B) and offshore eastern Mindanao (Core MD06-3067). SST shows marked deviations (of 1-2 °C) at ~ 55-53, 49.5-46.5, 39-36.5 and 33-31 ka, suggesting different controls on SST, related to local oceanographic settings. Site MD06-3067 represents a more open western Pacific location, strongly affected by upwelling of cool intermediate water masses, whereas Site MD98-2181 is located at the distal end of the Davao Gulf, which is separated by a shallow sill from the open Pacific Ocean (Fig. 1). This sill extends over several hundred kms from South Mindanao to Miangas Island in water depths of just a few hundred meters (<800 m). We speculate that SST variability off eastern Mindanao during MIS 2 and MIS 3 is linked to changes in the intensity of the MC, which drives local upwelling. In contrast, SST variations in Core MD98-2181 appear related to millennial-scale atmospheric temperature variations in the northern hemisphere (Saikku et al., 2009), and show close resemblance to SST patterns in the Sulu Sea (Dannenman et al., 2003) and South China Sea (Kienast et al., 2001; Oppo and Sun, 2005).

5.2 – Mindanao Dome variability over the last 160 kyr.

5.2.1 – Long-term trends in upper ocean thermal structure

Today, the Mindanao Dome affects the stratification of the upper water column along the eastern coast of Mindanao by influencing the depth of the thermocline (Fig. 2). This deep upwelling system seasonally brings cold water up to 75 m water-depth, thus causing the thermocline to dome up without having much effect on SST (Udarbe-Walker and Villanoy, 2001; Tozuka et al., 2002). The gradient between surface *(G. ruber)* and thermocline *(P. obliquiloculata)* temperatures in Core MD06- 3067 provides a useful tool to reconstruct the degree of upward doming of the thermocline that is expressed in the thermal contrast within the upper water column over the last 160 kyr (Fig. 7C). We infer that an increasing thermal gradient between surface and thermocline waters (ΔT°C) indicates stronger upward doming of isopcynals, hence a shoaling of the thermocline. However, upwelling of cooler waters to the surface results in a thicker mixed layer and depressed ΔT°C, thus we need also to monitor surface and thermocline temperatures to evaluate changes in upper ocean stratification.

Two prominent episodes of thermocline warming occurred at ~ 11-9.5 ka and 130-126 ka, when thermocline temperatures reached 25-26 °C, compared to average temperatures of 23-20 °C (Fig. 5B). The ΔT°C also decreased during these intervals, suggesting that dome activity was substantially reduced and cool upwelling waters did not reach the thermocline. In the later part of the Holocene and MIS 5e and over most of MIS 5, the ΔT°C increased to ~ 6-5 °C, as thermocline temperature decreased, indicating renewed influence of the Mindanao Dome, at least comparable to the present day. In contrast to this view, Kienast et al., (2008) suggested a Holocene deepening of the nutricline/thermocline at the location of Core MD06- 3067, based on nitrogen isotope evidence. In our records the Holocene decrease in productivity would support the latter interpretation, and thermocline cooling may reflect a general cooling of western Pacific intermediate water rather than advection of nutrient-rich cool deeper water.

The MD06-3067 record reveals low thermocline temperatures (23-20 °C) and a depressed ΔT°C during glacial periods, in particular during MIS 4-2, when sharp episodic declines in ΔT°C occur (down to ~ 3 °C). We interpret these intervals as

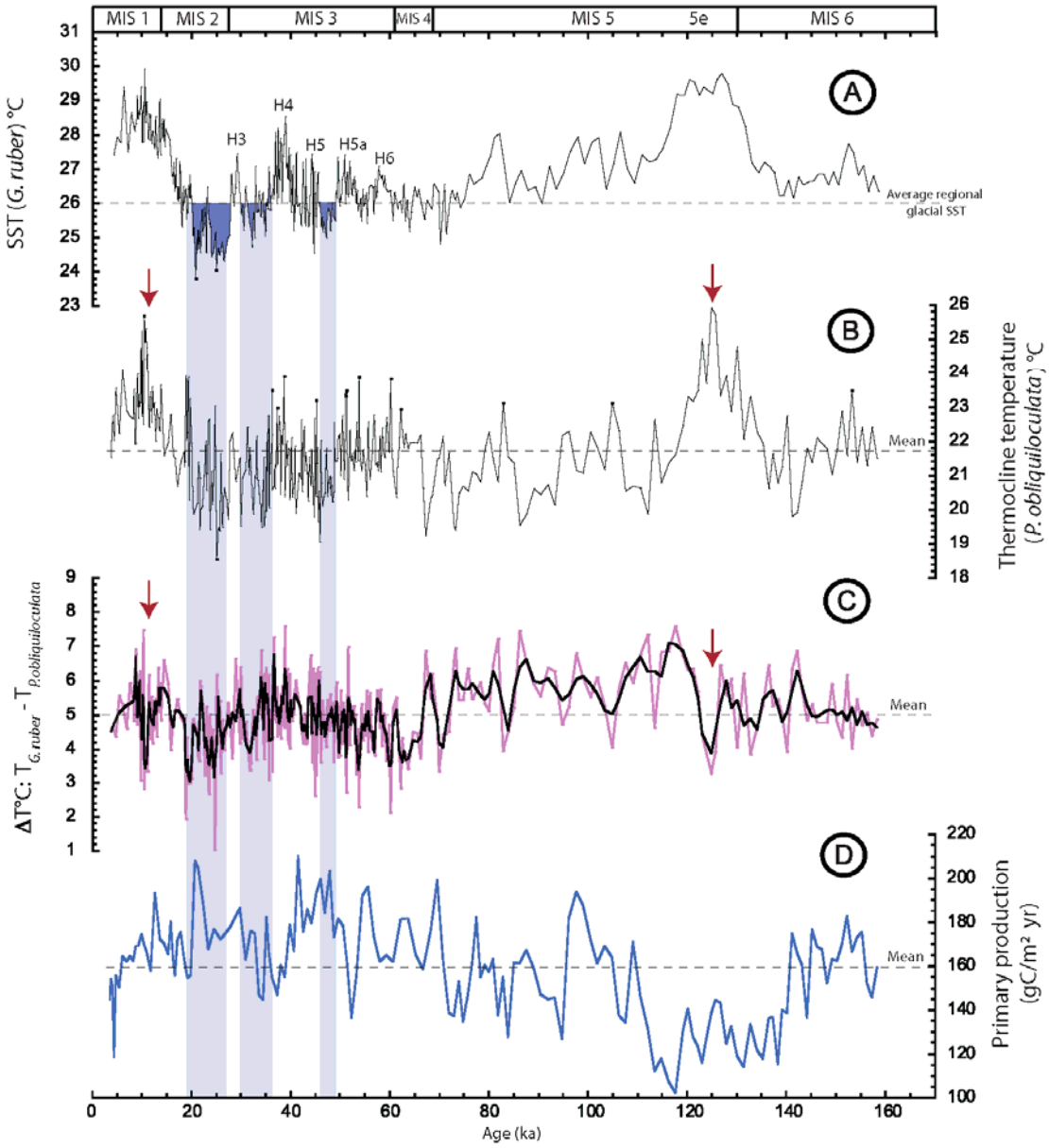

Figure 7. Records of surface-to-thermocline temperature contrast and primary productivity from Core MD06-3067. Blue bars indicate periods of intense surface and upper thermocline cooling, implying a reduced upper ocean temperature gradient. Red arrows mark prominent collapses of Mindanao Dome during MIS 5e and early Holocene.

(a) *G. ruber* (white) Mg/Ca–derived SST. Dashed line indicates average regional glacial SST.
(b) *P. obliquiloculata* Mg/Ca–derived thermocline water temperature. Dashed line indicates mean thermocline temperature over the last 160 kyr.
(c) Thermal gradient between surface and thermocline waters (DT°C = Tsurface − Tthermocline). The profile was computed as the difference between SST and thermocline temperature shown in Figures 4b and 5b. Dashed line indicates mean thermal gradient over the last 160 kyr.
(d) Primary production estimated from relative abundance of the coccolith species *F. profunda*. Dashed line indicates mean primary production over the last 160 kyr.

reflecting intense doming off Mindanao and vigorous upper ocean mixing. Enhanced activity of the Mindanao Dome during glacial times is supported by productivity proxies (coccoliths and benthic foraminifers; Fig. 6A-E), which indicate increased productivity during the LGM, most of MIS 3, MIS 4 and to a lesser extent during MIS 6. Globobuliminids, globocassidulinids and miliolids (Fig. 6B-C), typical of elevated carbon flux at the seafloor, increase significantly during these intervals.

High abundance of *B. quadrilatera* (Fig. 6E) during MIS 6 is also diagnostic of enhanced export, but may reflect a different source of food, related to changes in local current systems.

Nakatsuka et al., (1995) proposed that the dome became more active during glacials due to a strong East Asian winter monsoon. During glacial winters, enhanced high pressure over the Asian landmass plausibly intensified boreal winter monsoonal winds and strengthened the MC. In addition, the boreal winter monsoon season may have become prolonged by the southward shift of the ITCZ during glacial boreal summers. Terrestrial runoff proxy data from the same core indicate increased precipitation over Mindanao during MIS 2 and MIS 4 (Kissel et al., 2010), which supports the contention of a southward shift in the boreal summer position of the ITCZ and/or intensification of the tropical convection (Rosenthal et al., 2003; Partin et al., 2007). Dome activity appears to have been less intense during MIS 6 than during MIS 2, as shown by higher ΔT°C (~ 5-6 °C) and productivity indicators. The intensity of the East Asian winter monsoon during MIS 6 remains controversial, as some studies suggest a strong monsoon regime (Xiao et al., 1999; Chen et al., 2000), whereas others indicate weakening of the monsoon (Guo et al., 2009; Rousseau et al., 2009). Our results support a weaker winter monsoon during MIS 6 than during MIS 2, although considerably enhanced in comparison to interglacials.

5.2.2 – Millennial-scale variability during MIS 3 and MIS 2

Superimposed on the long-term trends are a number of significant millennial scale variations during MIS 4-2. Several transient intervals of highest productivity (carbon flux to the seafloor), marked by peak abundance in *Globobulimin*a spp. (>8 %; Fig. 6B), are evident between 17 and 55 ka. Most of these intervals are characterized by unusually sharp drops in SST (down to ~ 24-26°C at ~ 49.5-46.5, 37-30 and 27.5-19 ka, Fig. 7A) and by a depressed upper ocean thermal gradient (below 4°C within the upper ~ 100 m, Fig. 7C). Today, *Globobulimina* spp. Represent the most common

species in major upwelling areas such as the Arabian Sea and eastern Pacific (Jannink et al., 1998; Cannariato et al., 1999). The coincidence between high primary productivity and unusually low SST at this WPWP location suggests nutrient enrichment through upwelling of cooler mid-depth waters to the ocean surface. Enriched nutrient supply to the mixed layer is supported by elevated abundance of *E. huxleyi* (shallow photic zone producer) in the coccolith assemblages (Fig. 6A). Additional evidence of surface upwelling is provided by AMS ^{14}C dates derived from surface dwelling planktic foraminifers. AMS ^{14}C dates in two glacial samples (KIA 35211 and KIA 35212) indicate ages ~ 1800 and ~ 3000 years older than ages based on our age model (19.6 and 22.1 ka vs. 17.8 and 19.1 ka, respectively). These age offsets can be explained by upwelling of older, deeper water to the surface during periods of intensified dome activity. The SST record also provides evidence of sea surface warming during Heinrich Events H3, H4, H5, H5a and H6 (Fig. 7). This is in sharp contrast to most other records from the WPWP, which exhibit a northern hemisphere signal, characterized by surface cooling during stadials (Heinrich events) and warming during interstadials (Kienast et al., 2001; Dannenmann et al., 2003; Oppo and Sun, 2005; Saikku et al., 2009). Whereas these WPWP records appear to be mainly influenced by atmospheric teleconnections, episodes of sea surface warming at the location of Core MD06-3067 likely reflect periodic decreases in the intensity of the MC and concomitant decreases in upwelling and upper ocean mixing during Heinrich events. We suggest that millennial-scale variations in the Mindanao Dome upwelling during MIS 3 were linked to oscillations in the maximum displacement of the ITCZ and attendant changes in monsoonal wind and surface current circulation systems in response to high-latitude climate forcing.

5.3 – Significance of Mindanao Dome for regional climate and ocean dynamics

The Mindanao Dome is situated at a major tropical water mass crossroad, and it interacts with a number of climatic features, notably the East Asian winter monsoon, the meridional and zonal heat transfer linked to NEC variability and ENSO state and the inter-ocean heat, salt and nutrient transfer via the ITF. In their investigation of the Mindanao Dome's seasonal dynamics, Masumoto and Yamagata (1991) suggested that local upwelling intensified during the East Asian winter monsoon, when a positive wind stress curl (cyclonic circulation) increases in the region. Since the Mindanao dome is forced by strong northeasterly, coast parallel winds, the intensity

of the dome is directly related to the strength of the East Asian winter monsoon. ENSO influences the structure and intensity of the Mindanao Dome upwelling due to the strong coupling between the northeasterly wind regime (East Asian winter monsoon) and the El Niño phenomenon. Today, the mature phase of El Niño often occurs during boreal winter, and is usually accompanied by a weaker winter monsoon along the East Asian coast resulting in warmer and wetter winter conditions over SE Asia (Wang et al., 2000). Thus, the variability of the Mindanao Dome provides a direct indicator of the ENSO state, as upwelling intensifies when a strong cyclonic gyre becomes established during La Niña conditions, whereas strong El Niño events tend to suppress the cyclonic circulation, reducing Ekman transport.

During MIS 2, vigorous upwelling provides evidence of a strongly enhanced East Asian winter monsoon and prevailing La Niña conditions. Increased upper ocean mixing in the Sulu Sea (de Garidel-Thoron et al., 2001) and the South China Sea (Steinke et al., 2010) additionally supports strengthening of the East Asian winter monsoon during MIS 2. In contrast, local warming during stadials indicates reduced upwelling and prevalence of El Niño-like conditions during episodes of weaker meridional overturning circulation. These findings are in agreement with high resolution $d^{18}O$seawater records from the Davao Bay (Stott et al., 2002; Saikku et al., 2009) and the Sulu Sea (Dannenmann et al., 2003) and cave $\delta^{18}O$ records from Borneo (Partin et al., 2007), which were interpreted as reflecting more frequent El Niño events during stadials.

Changes in the intensity of the MC, which drives upwelling, have major repercussions in both the zonal and 648 meridional re-distribution of heat in the equatorial Pacific. The Mindanao Dome is situated within the ITF main inflow area from the Pacific, thus influencing the heat, salt and nutrient budget of ITF waters. Today, inflowing waters are characterized by a distinct salinity maximum within the upper thermocline. Intense vertical mixing along the ITF pathway as well as freshwater export from the Java Sea radically alter the stratification of the upper water column, resulting in an unusually fresh and cool subsurface outflow with a steep thermoclineand no distinct salinity stratification (Gordon, 2005). Opening of the freshwater portal through the Java Sea in the early Holocene (~ 9.5 ka) led to intensification of the ITF thermocline flow and reduction of the surface component downstream of the Makassar Strait (Xu et al., in press). Therefore since the early Holocene, the freshwater export from the South China Sea has exerted a more important control on the heat and salt export into the Indian Ocean than the primary composition of Pacific inflow waters. However

during the LGM, the ITF acted as a more direct conduit of Pacific surface and thermocline waters because the South China Sea was disconnected fromthe ITF. Increased upwelling of the Mindanao Dome promoted inflow of cooler, nutrient-enriched waters with reduced vertical stratification, and vigorous mixing within the narrower glacial passages further decreased stratification of ITF outflow waters (Xu et al., in press). Evidence for a glacial nutrient-enriched ITF is preserved in Eastern Indian Ocean productivity records such as the silicon-rich upwelling of ITF water masses at Ninetyeast Ridge (Broecker et al., 2000). Glacial productivity maxima were also reported from the ITF outflow within the Timor Sea (Müller and Opdyke, 2000; Holbourn et al., 2005; Kawamura et al., 2006), suggesting that the ITF provided a major channel for nutrient export from the Pacific to Indian Oceans, although it remains unclear to what extent nutrient enrichment within the Indonesian seas by mixing or runoff enhanced productivity in the eastern Indian Ocean. The northwestern edge of the Mindanao dome is also the place where the NEC bifurcates into the MC and Kuroshio Current, which form the main pathways for meridional heat transfer in the Pacific and exert major control on SE Asian and NW Pacific climate. SST records from the Okinawa Trough indicate weakening of the Kuroshio during Heinrich events, hence reduced heat transfer toward the high latitudes (Li et al., 2001; Xiang et al., 2007). On short timescales, there is evidence that the variability of the Kuroshio and Mindanao currents is linked to the ITCZ seasonal migration (Qu et al., 2008) and ENSO state (Yamagata et al., 1985), which strongly influence monsoonal winds. On longer timescales, the position and intensity of these currents appear to be mainly determined by changes in the interhemispheric temperature gradient, exposure or flooding of extensive tropical shelves related to sea level and prevalent radiative forcing. Taking these features and considerations together, the Mindanao Dome is an oceanographic feature within the WPWP with implications to the climatology of the wider region and beyond. This makes the dome a feature of particular interest, when attempting to unravel changes in western Pacific atmospheric and oceanographic circulation patterns and how they may be linked to far-field climatic influences from the high latitudes.

6 – Conclusion

Paleoproductivity indicators, SST and thermocline temperature reconstructions in Core MD06-3067 reveal considerable glacial-interglacial as well as sub-orbital variability in the activity of the Mindanao Dome over the last 160 kyr. Evidence for periodic glacial upwelling during MIS 2 and MIS 3 is provided by enhanced surface productivity, unusually low SST, low thermal gradient within the upper water column and remarkably old AMS ^{14}C ages of surface dwelling foraminifers that indicate a surface layer radiocarbon reservoir age between ~ 1800 and ~ 3000 yrs. Sea surface warming during Heinrich events mark periodic collapses of the Mindanao Dome upwelling during MIS 3. We attribute the successive surface warmings and coolings during MIS 2 and MIS 3 to changes in the ENSO state and associated latitudinal shifts in the ITCZ position that affected boreal winter monsoonal winds and upper ocean circulation patterns. Our results indicate that La Niña conditions prevailed during the LGM, whereas an El Niño-like mode dominated during Heinrich events. Dome activity differed substantially over the last two glacial cycles: intense Ekman transport led to episodic upwelling during MIS 2 and MIS 3, whereas the upper ocean remained more stratified during MIS 6. Since monsoonal winds strongly influence the intensity of the Mindanao Current (Masumoto and Yamagata, 1991) driving regional upwelling off eastern Mindanao, our records provide a proxy for the intensity of the East Asian winter monsoon.

Acknowledgements

We thank Yvon Balut, the crew of RV “Marion Dufresne” and the French Polar Institute (IPEV) for all their efforts and support during the MARCO POLO 2 Cruise (IMAGES program). We are grateful to Marcus Regenberg and Guillaume Leduc for helpful discussions, to Jian Xu for advice regarding Mg/Ca analysis and to Brigitte Salomon and Karin Kissling for technical assistance. We also thank Rainer Zahn, Helen Neil and one anonymous reviewer for insightful, constructive comments. This research was funded in Germany by the Deutsche Forschungsgemeinschaft (DFG grant Ku649/26-1), in France by the Commissariat à l’Energie Atomique (CEA) and the Centre National de la Recherche Scientifique (CNRS), and in Canada by the Natural Sciences and Engineering Research Council of Canada (NSERC) and the Canadian Institute for Advanced Research (CIFAR).

Supplementary material

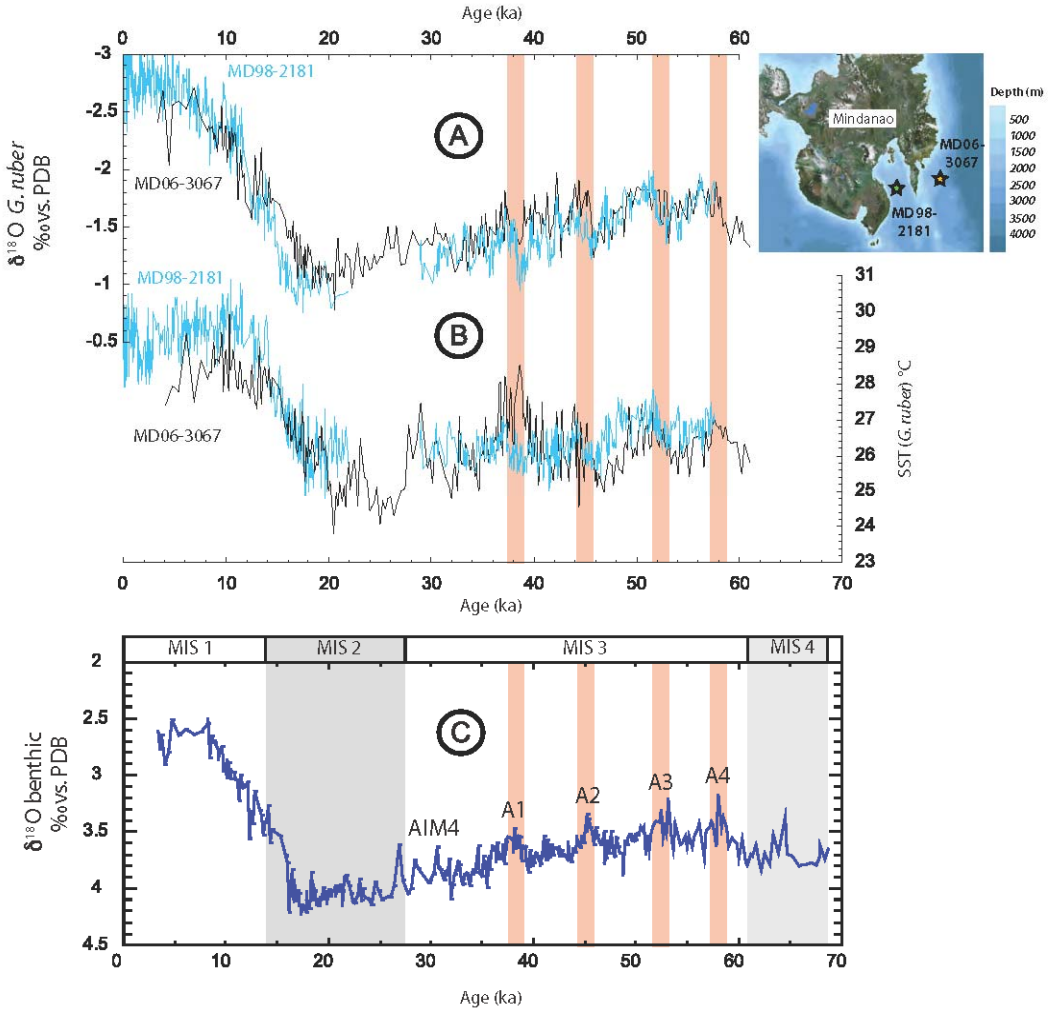

Supplementary Figure 1

Surface water hydrology over the last 60 kyr, based on analysis of G. ruber (white) in Core MD06-3067. AIM4 and A1 to A4 refer to Antarctic Isotope Maxima or warm events. Data from Core MD98-2181 from Stott et al., (2007) for Holocene and Termination I and from Saikku et al., (2009) for MIS 3.

A – *G. ruber* $\delta^{18}O$ in Cores MD06-3067 (black) and MD98-2181 (blue).

B – *G. ruber* (white) Mg/Ca derived SST in Cores MD06-3067 (black) and MD98-2181 (blue).

C – Benthic $\delta^{18}O$ in Core MD06-3067.

Mindanao Dome variability over the last 160 kyr: Episodic glacial cooling of the West Pacific Warm Pool

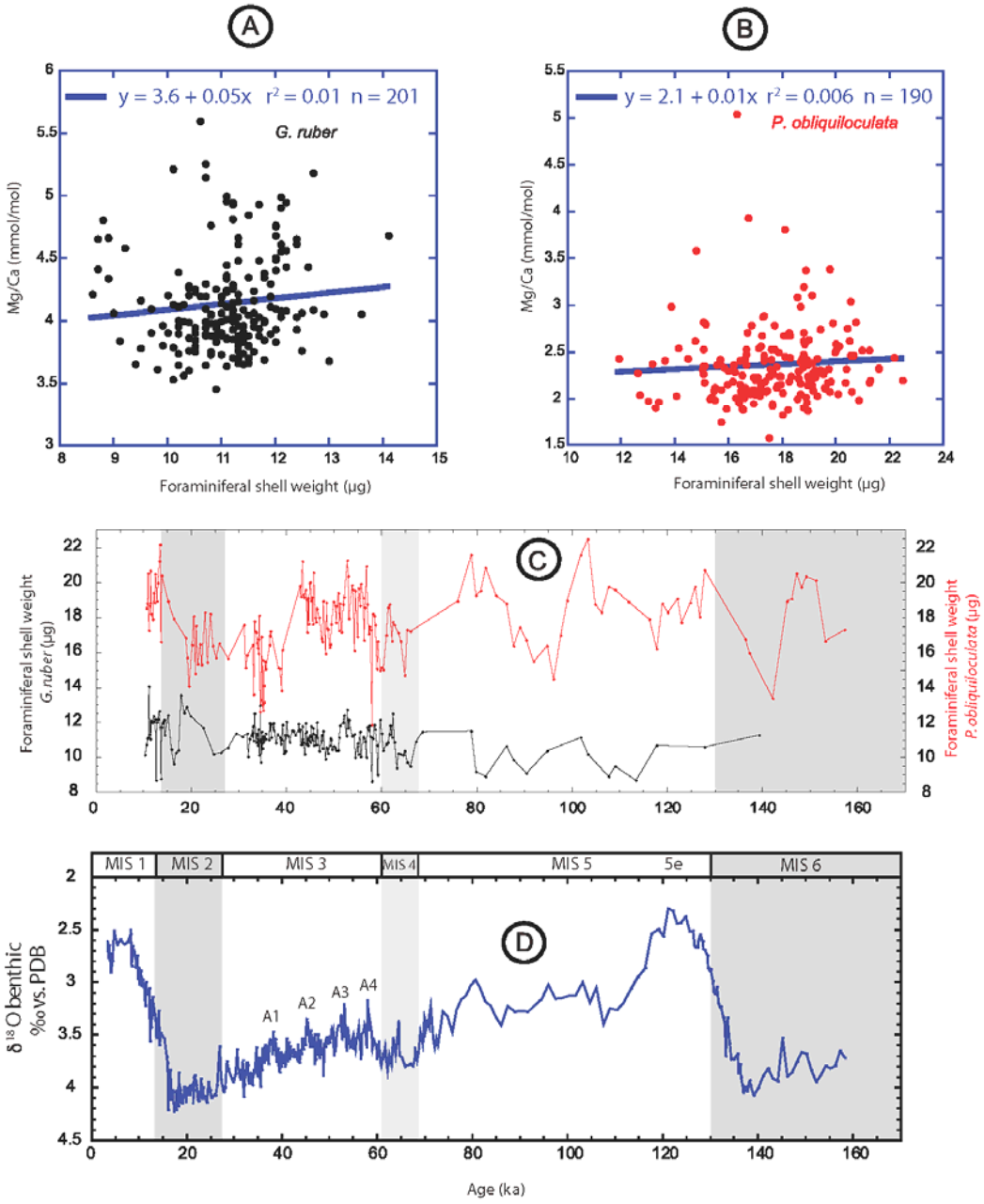

Supplementary Figure 2

A – Mg/Ca ratio of *G. ruber* plotted against foraminiferal shell weight in Core MD06-3067. Low r² correlation factor indicates no influence of dissolution on Mg/Ca.

B – Mg/Ca ratio of *P. obliquiloculata* plotted against foraminiferal shell weight in Core MD06-3067. Low r² correlation factor indicates no influence of dissolution on Mg/Ca.

C – Variations in *G. ruber* (black) and *P. obliquiloculata* (red) weights over the last 160 kyr in Core MD06-3067. No systematic offset occurs between glacial and interglacial periods.

D – Benthic $\delta^{18}O$ in Core MD06-3067.

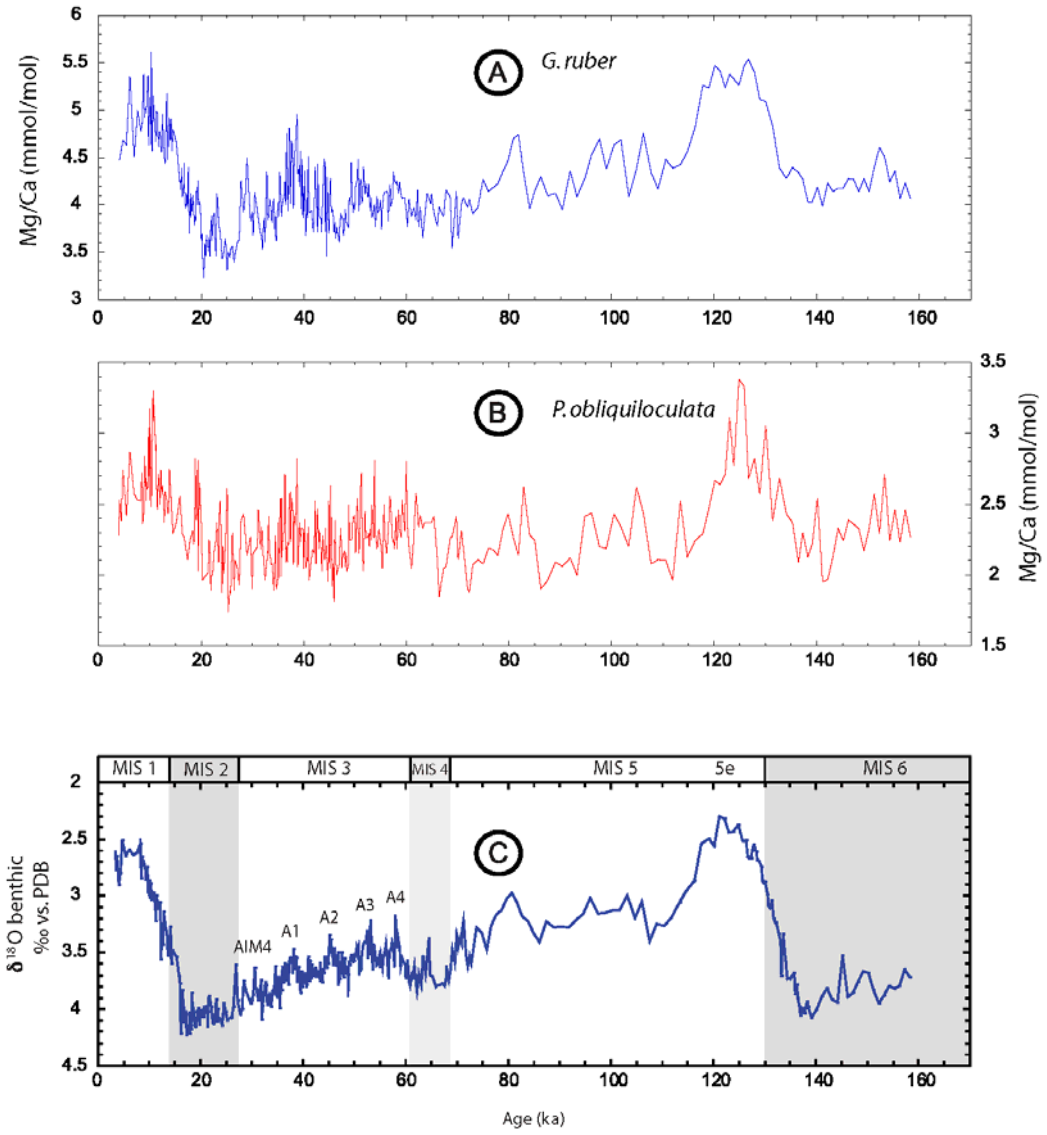

Supplementary Figure 3

A – Mg/Ca ratio of *G. ruber* in Core MD06-3067.

B – Mg/Ca ratio of *P. obliquiloculata* in Core MD06-3067.

C – Benthic $\delta^{18}O$ in Core MD06-3067.

Chapter III:
Deglacial re-organization of Pacific intermediate water masses during terminations I and II

Deglacial re-organization of Pacific intermediate water masses during terminations I and II

Abstract

Glacial production rates of Antarctic and North Pacific Intermediate Waters (AAIW and NPIW) are vigorously debated, as published records exhibit highly diverging results. In this study, we use benthic foraminiferal $\delta^{13}C$ and $\delta^{18}O$ in Cores MD06-3067 and MD06-3075 recovered off Mindanao Island (Philippines) to track the long-term evolution of intermediate waters in the western equatorial Pacific Ocean. The $\delta^{13}C$ record from Core MD06-3067 is characterized by two major, abrupt troughs during terminations I and II. Comparison with a high-resolution SW Pacific record (Pahnke and Zahn, 2005) reveals that these $\delta^{13}C$ troughs coincide with $\delta^{13}C$ high-level plateaus in the SW Pacific, previously interpreted as sudden increases in AAIW formation. We suggest that the deglacial $\delta^{13}C$ troughs in Core MD06-3067 indicate rapid intrusion of NPIW around Mindanao, linked to major re-organization in Pacific intermediate circulation during deglaciation. Comparison of benthic $\delta^{13}C$ records from Core MD06-3067 (1575 m) in the open western equatorial Pacific Ocean and Core MD06-3075 (1878 m) in the more isolated marginal Davao Gulf reveals a different evolution of intermediate water masses over termination 1. Lower benthic $\delta^{13}C$ values in Core MD06-3075, particularly during MIS2, reflect poorer ventilation and/or differences in carbon export flux at this more proximal location within the Davao Gulf.

1 – Introduction

The thermohaline circulation (THC, Defant, 1929) plays a major role in the regulation of Earth's climate (Manabe and Stouffer, 1994; Rahmstorf, 1996; Stocker and Schmittner, 1997; Rahmstorf and Ganapolski, 1999; Vellinga and Wood, 2007), as it controls the inter- and intra-ocean heat and salt balance (Gordon, 1986). For a long time, the formation of deep water in the North Atlantic has been perceived as the overriding driver of the THC with variations in deep water production considered responsible for abrupt climate changes (Bond et al., 1993; Rahmstorf et al., 1996). However during the last few years, there has been a growing interest in understanding the role of the Southern Ocean and North Pacific within the THC, as those two areas constitute sources of intermediate and deep water (McCartney, 1977 and 1982; Van Scoy et al., 1991; Freeland et al., 1998). Studies focusing on the influence of the Southern Ocean and North Pacific on the past and present variability of the thermohaline circulation highlighted the need of considering those two sources of intermediate and deep waters as major actors of the THC (Wright and Stocker, 1993; Mikolajewicz et al., 1997; Blunier et al., 1998; Vidal et al., 1999; Seidov et al., 2001; Schmittner et al., 2002; Spero and Lea, 2002; Knorr and Lohmann, 2003; Sijp and England, 2009). Recent work noticed a synchronicity between reduced formation of deep water in the North Atlantic and possible enhanced Antarctic Intermediate Water (AAIW) production in the Southern Ocean during terminations (Pahnke and Zahn, 2005), highlighting the presence of a North Atlantic/Southern Ocean circulation seesaw in the intermediate circulation during deglaciations. The sensitive response of AAIW production to glacial/interglacial cycles and rapid climatic changes such as Heinrich events and Dansgaard-Oeschger cycles (Ono et al., 2005) also suggests that the southern hemisphere circulation system has been a major actor in the past fluctuations of the global circulation. The role of the North Pacific in the THC is also eliciting increasing interest. An antiphase between North Atlantic and North Pacific deep or intermediate water formation was suggested by modelling studies (Wright and Stocker, 1993; Mikolajewicz et al., 1997; Schmittner et al., 2002) and sediment cores (van Geen et al., 1996) indicating a possible increase in North Pacific Intermediate Waters (NPIW) production following breakdown in the formation of north Atlantic deep and intermediate waters.

Glacial/interglacial variations in the production rate and the extent of Antarctic and North Pacific intermediate waters remain, however, a controversial issue. In fact,

several studies based on models and palaeoceanographic reconstructions concluded to reduced (Pahnke and Zahn, 2005; Bostock et al., 2004) or increased (Meissner et al., 2005; Liu et al., 2002; Muratli et al., 2009) AAIW production during the LGM. Similarly, some studies suggested low or absent formation of NPIW during the LGM (Keigwin, 1987; Weaver et al., 1998) while others argue to high glacial NPIW production rates (Duplessy et al., 1998; Lynch-Stieglitz and Fairbanks, 1994; Matsumoto et al., 2002; Meissner et al., 2005).

Today, deep and intermediate water from the Southern Ocean originate from the Weddell and the Ross Seas close to Antarctica (Kuhlbrodt et al., 2007). AAIW are generally found at a depth of 1000 to 2000 m, and prevail in the intermediate circulation of the southern and subtropical Pacific. The northern part of the Pacific basin is dominated by North Pacific Intermediate Water (NPIW), formed in the Bering Sea, the Sea of Okhotsk and in the Alaskan Gyre. The boundaries of AAIW and NPIW in the subtropical Pacific ocean are not fully clear, but oceanographic studies have shown the presence of an overlap of AAIW and NPIW in the western equatorial Pacific Ocean (Talley, 1999 and 2003; Bingham and Lukas, 1994).

This study is based on stable oxygen and carbon isotopes records of benthic foraminifera in Cores MD06-3067 and MD06-3075, recovered off Mindanao Island (South Philippines). The core sites are in the heart of the overlap between AAIW and NPIW, and are thus ideally located to monitor the past variability and extent of these two intermediate water masses. Thus, these records provide new insights into the glacial/interglacial evolution of the mid-depth circulation in the western equatorial Pacific Ocean as well as potential fluctuations in the production rates of AAIW and NPIW.

2 – Oceanographic settings

IMAGES Cores MD06-3067 (6°31 N, 126°30 E, 1575 m water depth, Fig 1) and MD06-3075 (6°29 N, 125°50 E; 1878 m water depth, Fig 1) were recovered with the Calypso Giant Corer on board R/V Marion-Dufresne during the Marco Polo 2 cruise in June 2006 (Laj et al., 2006). Core MD06-3067, located ~ 50km east off the eastern coast of Mindanao Island, represents an open West Pacific location, directly within the flow path of the Mindanao Current which forms the inflow part of the Indonesian

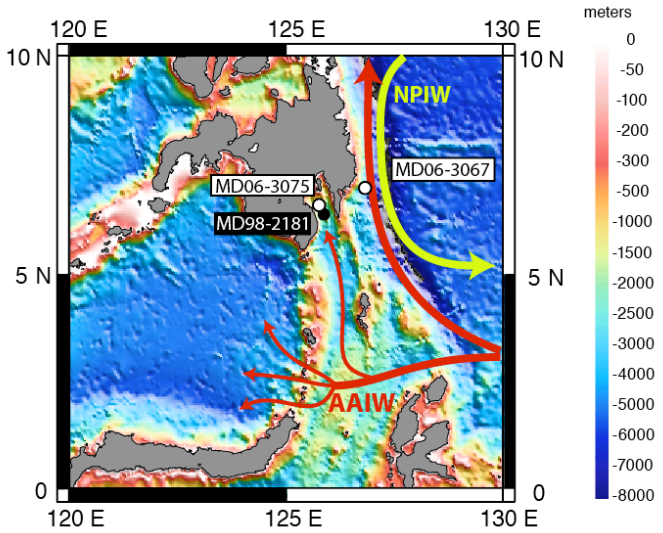

Fig. 1 – Location of cores MD06-3067 and MD06-3075 (this study) as well as MD98-2181 (Stott et al., 2007a). Note the relatively shallow sill extending south of Mindanao Island isolating the Davao Gulf from the open ocean. AAIW: Antarctic Intermediate Waters; NPIW: North Pacific Intermediate Waters. Map modified from Liu and Dittert (2010), generated from the ETOPO2 v.2 (NGDC) database.

Throughflow. This area is also influenced by the Mindanao Dome, and Core MD06-3067 thus provides a unique opportunity to monitor past changes in the climate and oceanography of this critical area. Multiproxy analysis from Core MD06-3067 has shown major modification in the structure of the upper water column over the last 160 Kyrs due to changes in the intensity of the Mindanao Dome (Bolliet et al., 2011). In this work, we focus on bottom waters, which according to the depth of the studied cores, correspond to the mid-depth circulation of the Pacific. According to Talley, (1999 and 2003), the Pacific intermediate circulation is dominated by AAIW between Antarctica and 10°N, whereas NPIW prevails at higher northern latitudes (Fig. 2). This scheme is observed over the almost entire Pacific basin. However, a southward incursion of NPIW in the western equatorial Pacific Ocean leads to an overlap of AAIW and NPIW in this region (Talley, 1999 and 2003). The two cores of this study are located in the heart of this overlapping zone, and thus constitute an essential archive of eventual changes in the influence of each of those two water masses in the Indo-Pacific region. This allows us to monitor the glacial/interglacial evolution of the latitudinal extent of Antarctic and North Pacific intermediate water masses, possibly related to fluctuations of their production rate, which remain vigorously debated.

The two cores are however representative of different circulation systems with Core MD06-3067 recording an open west Pacific signal whereas Core MD06-3075 located deeper in the Davao Gulf might be somewhat sheltered from the open Pacific Ocean

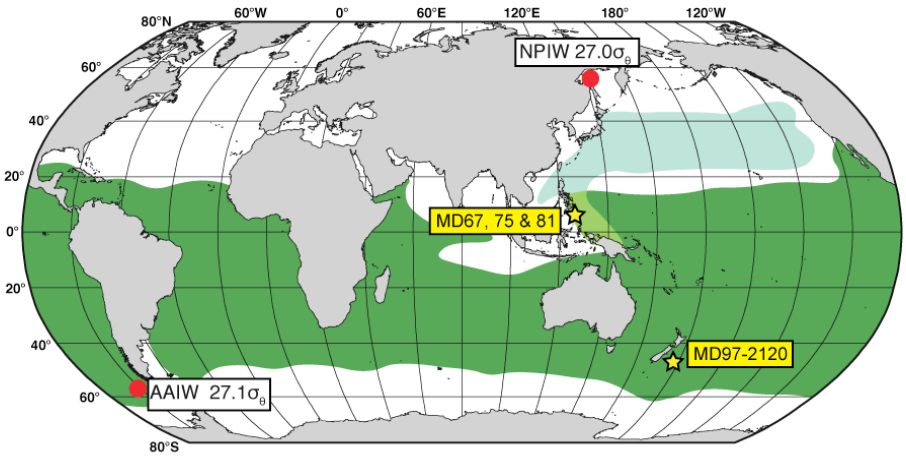

Fig. 2 – Locations of AAIW (dark green) and NPIW (light green) salinity minima in the world ocean (modified form Talley, 1999). Yellow stars indicate the position of cores MD06-3067, MD06-3075 (this study), MD98-2181 (Stott et al., 2007a) and MD97-2120 (Pahnke and Zahn, 2005). Red dots indicate the position of AAIW and NPIW production zones. Note the overlap of AAIW and NPIW in the western equatorial Pacific.

intermediate circulation, due to a shallow sill (<800 m) extending several hundred of kilometers south of Mindanao Island. Also, the water depth of MD06-3075 coresite (1878 m below sea level) corresponds to a depth different from the range of intermediate (generally 800-1500 m) and deep (>2000 m) water, as the boundaries of those watermasses differ in the litterature (Sverdrup 1942; Reid 1965; Talley and Joyce, 1992; Talley, 1993 and 1999). The study of eventual discrepancies between the signals from those cores located in a different oceanographic context may thus additionnally provide important information on a possible contrast in the local mid-depth circulation between the open Pacific Ocean and the somewhat marginal Davao Gulf.

3 – Material and Methods

Core MD06-3067 is 15.53 m long and is mainly composed of homogenous dark, olive gray silty clay. The upper two meters consist of brown to olive gray silty clay. A 2 cm thick ash layer is visible between 198 and 200 cm. Core MD06-3075 is 30.76 m long, and is also composed of dark, olive gray silty clay, with finely dispersed black ash grains as well as seldom ash pockets. We also note the presence of a hole between 142 and 150 cm, as well as a large piece of core liner in the sediment between 192

and 208 cm and of several ash layers from 1 to 5 cm thick between 700 cm and the bottom of the core.

3.1 – Sampling strategy

Core MD06-3067 is 15.50 m long, spanning from the late Holocene down to MIS 6. Sampling for benthic isotopes analysis was performed at a 2 cm resolution over Termination 2 and from MIS 4 to the early Holocene. Other time intervals were sampled at a 10 cm resolution. A total of 462 samples of 1 cm thickness, equivalent to 40 cc were processed. The complete sampling strategy for Core MD06-3067 was detailed in Bolliet et al., (2011).

Core MD06-3075 was sampled at 10 cm resolution over the upper 10.5 meters spanning the last 25 Kyrs, with however a brief interruption due to the presence of a piece of core liner between 192 and 208 cm. A total of 104 samples were processed.

3.2 – Isotope analysis

MD06-3067 oxygen isotopes benthic record was presented in Bolliet et al., (2011). Isotopes analysis of samples from Core MD06-3075 were mainly performed on 1 to 5 specimens of the epifaunal benthic foraminifera *C. pachyderma* and *P. wuellerstorfi* (>250 µm) and on *Uvigerina proboscidea* (infaunal benthic foraminifera) in two samples. Those two samples were not included in the $\delta^{13}C$ curve due to the possible influence of pore water on the $\delta^{13}C$ signal recorded by *Uvigerina proboscidea* (McCorkle et al., 1990), whereas 0.64 ‰ was deducted from the $\delta^{18}O$ values from this species to take account of the departure from isotopic equilibrium (Shackleton and Opdyke, 1973).

All samples were gently crushed into large fagments, agitated in ethanol for 2-3 seconds in an ultrasonic bath, decanted, then dried at 40°C. Stable carbon and oxygen isotopes were measured with the Finnigan MAT 251 mass spectrometer at the Leibniz Laboratory, Kiel University. The system is coupled online to a Carbo-Kiel Device (Type I) for automated CO_2 preparation from carbonate samples for isotopic analysis. Samples were reacted by individual acid addition (99% H_3PO_4 at 73 °C).

Standard external error is better than ±0.07 ‰ and ±0.05 ‰ for $\delta^{18}O$ and $\delta^{13}C$, respectively. In Core MD06-3067 replicate measurements on 32 samples of benthic

foraminifera samples indicate mean reproducibility of ±0.07 ‰ for $\delta^{18}O$ (32 samples, epifaunal and infaunal species, after the 0.64 ‰ adjustement applied to *Uvigerina proboscidea;* Bolliet et al., 2011) and ±0.05 ‰ for $\delta^{13}C$ (23 samples, epifaunal species). Replicate measurements on 21 samples from core MD06-3075 show an average standard deviation of ±0.07 ‰ and ±0.10 ‰ for $\delta^{18}O$ (epifaunal and infaunal species) and $\delta^{13}C$ (epifaunal species), respectively.

3.3 – Accelerator Mass Spectrometry AMS ^{14}C dating

AMS ^{14}C dating was performed on three samples from Core MD06-3075, using well-preserved planktonic foraminifera. Two samples were composed of *G. ruber* and *G. sacculifer* (KIA 41030 and KIA 41031) and a third sample was composed of mixed planktonic foraminifera (KIA 41029). AMS ^{14}C dating was performed at the Leibniz laboratory, Kiel University, following the protocol described by Nadeau et al., (1997) and Schleicher et al., (1998).

For samples younger than 13 ka, a reservoir age of 480 yrs was substracted from the conventional ages before conversion to calendar ages. For older samples, we applied a reservoir age of 630 yrs following Saikku et al., (2009). Conventional ages were converted to calendar ages following the protocol established by Fairbanks et al., (2005). Details of AMS ^{14}C dating for Core MD06-3067 are given by Bolliet et al., (2011).

4 – Results

4.1 – Chronology

A detailed description of the chronology of Core MD06-3067 is given in Bolliet et al., (2011). The age model of Core MD06-3075 was generated, following the same approach as for Core MD06-3067. Three AMS ^{14}C dates were used to constrain the upper part of the core (from 6 to 770 cm, see Table 1) and, between 770 and 1800 cm, a correlation of benthic $\delta^{18}O$ events with the benthic $\delta^{18}O$ signal of Core MD06-3067. A Stineman function was used to interpolate between tie points and AMS ^{14}C dates.

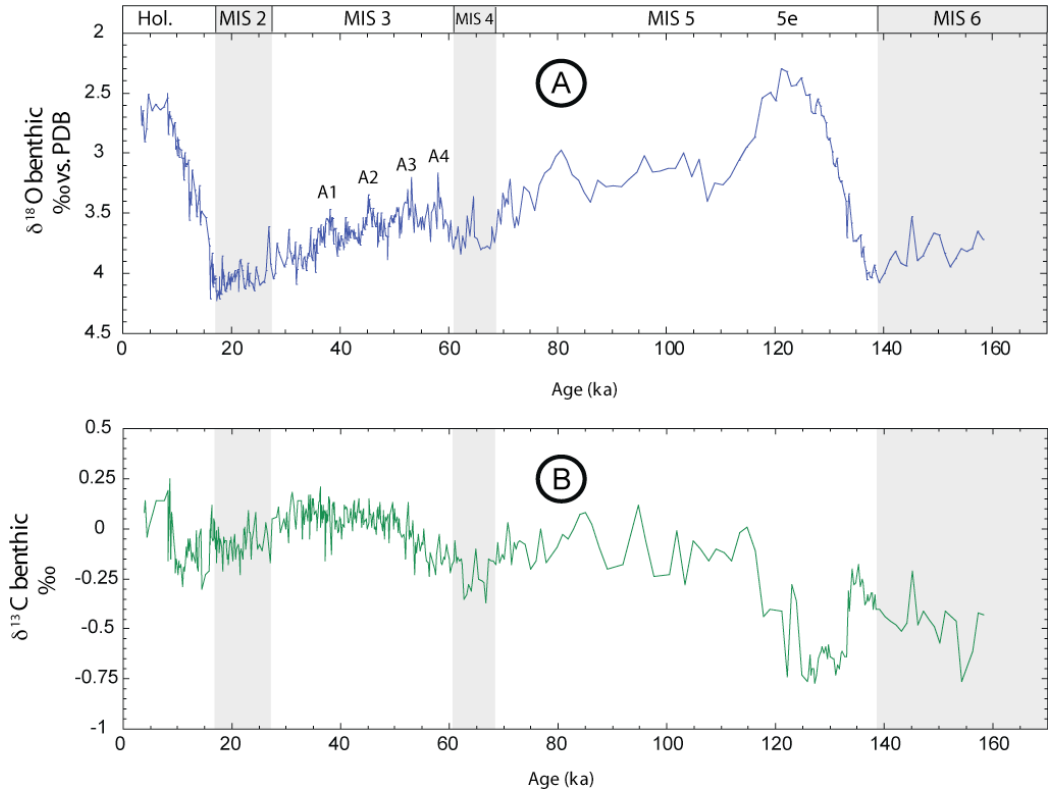

Fig. 3 – Benthic $\delta^{18}O$ (A; Bolliet et al., 2011) and $\delta^{13}C$ (B) signals from core MD06-3067. A1-4 on figure 3A refer to Antarctic events 1 to 4.

The output of this function has a geometric weight applied to the current point and ±10% of the data range, leading to a smoothed curve.

Our results from Core MD06-3075 cover the period from the LGM to the late Holocene, corresponding to the upper 10.5 meters of the core. Over this interval, Core MD06-3075 shows a higher sedimentation rate (ranging from 23 cm/kyr during the LGM up to 78 cm/kyr in the late Holocene) than Core MD06-3067 (~ 10 cm/kyr). The apparent increase in the sedimentation rate in Core MD06-3075 during the Holocene is due to the piston coring system, which creates an artificial elongation and oversampling in the upper part of the core (Széréméta et al., 2004).

4.2 – Benthic $\delta^{18}O$

The benthic $\delta^{18}O$ signal from Core MD06-3067 covers the last 160 ka with no interruption, spanning the interval from MIS6 to the Holocene (Fig. 3 A). For a detailed description of this record, see Bolliet et al., (2011).

The benthic $\delta^{18}O$ signal from Core MD06-3075 indicates a range of values over the last deglaciation (Fig. 4 A, red solid line) similar to values in Core MD06-3067, with an amplitude of 1.6‰, starting from glacial values of 4.2‰ and ending at around 2.6‰ at the beginning of the Holocene. The shape and duration of this termination are also similar in MD06-3067 and 3075 with a continuous and regular deglacial warming until the beginning of the Holocene recorded in both cores at ~ 8 ka.. MD06-3075 Holocene values are relatively stable, ranging from 2.5 to 2.7‰.

4.3 – Benthic $\delta^{13}C$

Carbon isotopes measurements on epibenthic foraminifers is commonly used as a tracer of past ocean circulation. Although important biases can appear particularly in areas, where high flux of fresh organic matter may induce seasonal phytodetritus layers at the sediment/water interface ("Mackensen effect", Mackensen et al., 1993), this method provides robust results in oligotrophic regions. Benthic $\delta^{13}C$ in Core MD06-3067 (Fig. 3 B) show a general increase from -0.4 to -0.6‰ during MIS 6, to 0 to 0.2‰ during the Holocene, following the characteristic long-term benthic $\delta^{13}C$ increase generally observed during the Pleistocene (Mix et al., 1995). This increase is however interrupted by troughs during MIS 4 and 2, consistent with the shift observed in the global ocean carbon isotopic composition (Labeyrie and Duplessy, 1985). Two major negative excursions in $\delta^{13}C$ occur during terminations II and I (negative shifts of 0.5‰ and 0.3‰, respectively), when lower $\delta^{13}C$ levels are reached than during the preceding glacial periods. Interestingly, these two troughs exhibit comparable shapes over the two terminations. At the beginning of terminations II and I (i.e. 139 and 17.4 ka), $\delta^{13}C$ values increase simultaneously with $\delta^{18}O$. However during both terminations, the rise in $\delta^{13}C$ is abruptly interrupted (at 134 and 16 ka, respectively) by troughs, whereas $\delta^{18}O$ continues to regularly decrease until the Holocene.

The $\delta^{13}C$ troughs have similar duration (8 kyrs), and are terminated by a sudden increase in values at the end of the deglaciation. This transition is particularly abrupt

during termination I, with values increasing by around 0.4‰ in less than 2 kyrs (10-8 ka).

The benthic $\delta^{13}C$ signal from Core MD06-3075 in the Davao Gulf (Fig. 4 B, red solid line) shows a trend over the last deglaciation drastically different from that in Core MD06-3067 in the open western Pacific Ocean off the eastern coast of Mindanao. In Core MD06-3075, the $\delta^{13}C$ record during termination I is marked by a regular and continuous increase of about 0.5‰ starting at 17.5 ka (-0.4‰) coinciding with the onset of the deglaciation, ending at 5 ka (0.1‰) and lagging the beginning of the Holocene by about 3 ka. After that, Holocene values show a remarkable stability, ranging between 0‰ and 0.2‰. It is also noticeable that prior to the beginning of termination I (17.5 ka), the MD06-3075 $\delta^{13}C$ signal exhibits highly variable values, whereas the signal becomes more consistent over the termination. In contrast, $\delta^{13}C$ record from Core MD06-3067 does not show such high variability over the last 25 ka (Fig. 4).

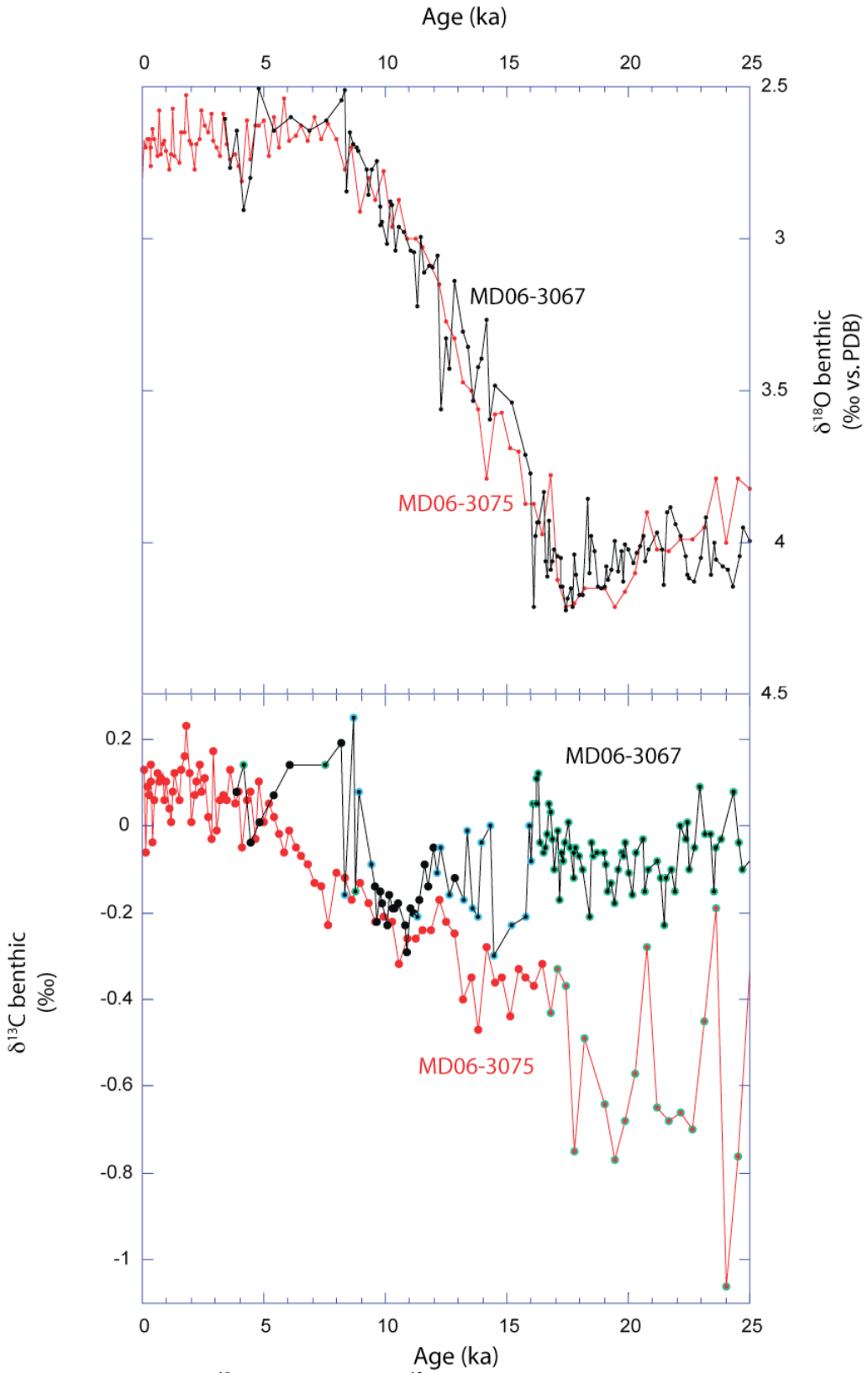

Fig. 4 – Benthic $\delta^{18}O$ (top figure) and $\delta^{13}C$ (bottom) signals from Cores MD06-3075 (red solid line) and MD06-3067 (black solid line) during the last termination. Measurements performed on *P. wuellerstorfi* (green circles), *C pachyderma* (red dots) *C. mundulus*, and mixed *P. wuellerstorfi/C. mundulus* (blue circles).

4.4 – Benthic foraminiferal assemblages.

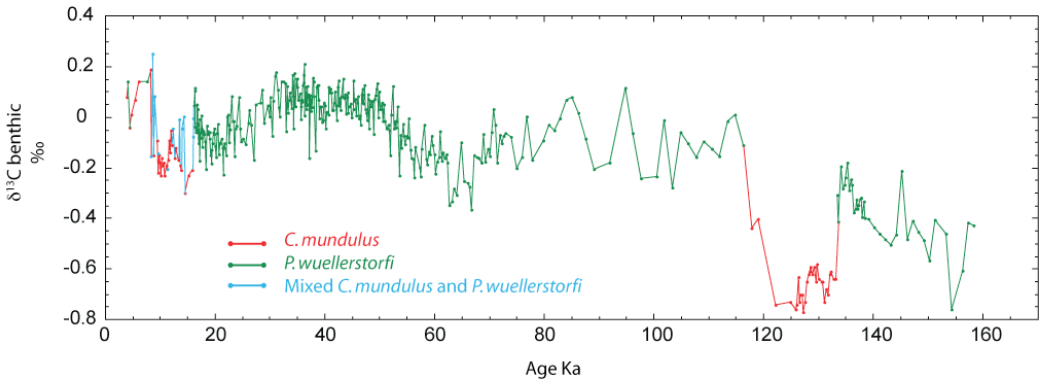

Fig. 5 – Benthic $\delta^{13}C$ from Core MD06-3067 and taxa of epibenthic foraminifera used for analysis.

The benthic $\delta^{13}C$ and $\delta^{18}O$ time series from Core MD06-3067 were constructed using different taxa of epibenthic species of foraminifera. Most of the isotopic measurements were performed on *P. wuellerstorfi*, but other epifaunal species were also measured, as important compositional changes in the benthic foraminiferal assemblages occurred during the terminations (Fig. 5). Within the 158-134 ka and 117-16 ka intervals *C. mundulus* was not found in the sediment, whereas *P. wuellerstorfi* is absent between 134 and 118 ka. Few specimens of *P. wuellerstorfi* were found in the sediment between 16 and 8 ka (average of 0.5 specimen of *P. wuellerstorfi* per sample within this time interval, vs. 2.8 between 16 and 117 ka, and 2.9 between 134 and 158 ka), whereas *C. mundulus* is relatively abundant during this interval. As a result, isotopes analysis is based on *C. mundulus* or a mixed *C. mundulus* and *P. wuellerstorfi* when this last species is present. However, replicate measurements indicate that the $\delta^{13}C$ values from *C. mundulus* and *P. wuellerstorfi* do not exhibit evident systematic offset (Holbourn et al., 2005).

The benthic isotopes time series from Core MD06-3075 are based on the epibenthic species *P. wuellerstorfi* (25 to 16.5 ka) and *C. pachyderma* (from 16.5 ka to the late Holocene) with additional measurement of *Uvigerina proboscidea* in two samples, only included in the $\delta^{18}O$ results.

5 – Discussion

5.1 – Long-term evolution of West Pacific mid-depth circulation.

5.1.1 – Meridional gradient in $\delta^{13}C$ in the Pacific.

Mid-depth $\delta^{13}C$ records spanning the two last glacial/interglacial cycles are relatively rare in the Pacific Ocean. Kissel et al., (2010) suggested a persistent influence of local bottom currents on sediments deposition at MD06-3067 core location over the last 160 kyr. A particularly interesting high-resolution, long-term $\delta^{13}C$ record from Core MD97-2120 located close to New Zealand was published by Pahnke and Zahn, (2005) and provides an essential archive of the intermediate circulation in the South Pacific. Comparison of benthic $\delta^{13}C$ from Cores MD97-2120 and MD06-3067 indicate a common long-term trend of increase during the last 160 ka characteristic of mid-depth Pacific water (Mix et al., 1995) (Fig. 6). The two signals exhibit a remarkably parallel trend from 40 ka up to the LGM, supporting a large-scale ocean-wide control on the $\delta^{13}C$ in the intermediate depth waters (Boyle, 1986; Mix et al., 1991). However, our $\delta^{13}C$ data are systematically lower than those from the South Pacific. Today, the northern Pacific exhibits a ^{13}C-depleted isotopic signature in comparison to the Southern Ocean, reflecting the meridional gradient of nutrient in this ocean (Kroopnick, 1985; Matsumoto et al., 2002; Talley et al., 2007; Fig. 7). Previous studies confirmed the possible presence of this gradient during the LGM at mid-depth (Matsumoto et al., 2002; Duplessy et al., 1998; Herguera, 1992; Lynch-Stieglitz, 1999). The systematic offset observed between the low-level $\delta^{13}C$ signal from Core MD06-3067 relative to the signal in Core MD97-2120 (Pahnke and Zahn, 2005) may reflect that the meridional gradient in $\delta^{13}C$ in the Pacific persisted over the last 160 ka.

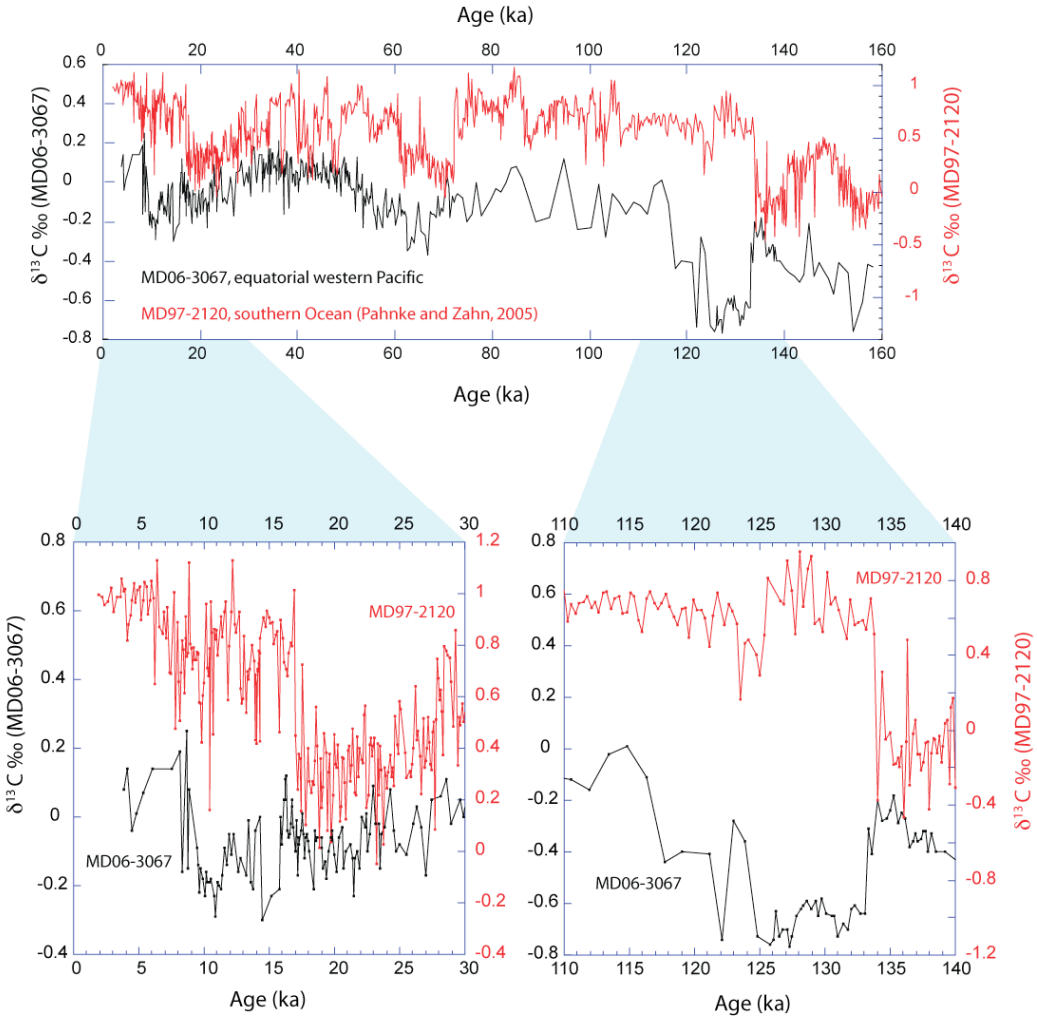

Fig 6 – Benthic $\delta^{13}C$ signals from Core MD06-3067 (black solid line) and MD97-2120 (red solid line; Pahnke and Zahn, 2005) over the last 160 kyrs (top). Bottom right and left figures are a zooming in on terminations II and I, respectively.

5.1.2 – Contrasted $\delta^{13}C$ in the Pacific during terminations.

Although the gradient between $\delta^{13}C$ from the southern and the western equatorial Pacific Ocean persisted over the last 160 kyr, those two sites exhibit major discrepancies in the $\delta^{13}C$ signal. In fact, Cores MD06-3067 and MD97-2120 show divergent abrupt $\delta^{13}C$ excursions during the two last deglaciations (Fig. 6), with increases of $\delta^{13}C$ in the South Pacific coinciding with sharp troughs in the western equatorial Pacific Ocean. Positive excursions of $\delta^{13}C$ in the South Pacific during terminations were also observed at lower latitudes by Bostock et al., (2004) in Core FR1/97 GC-12 along the eastern coast of Australia within the range of AAIW (990 m below sea level).

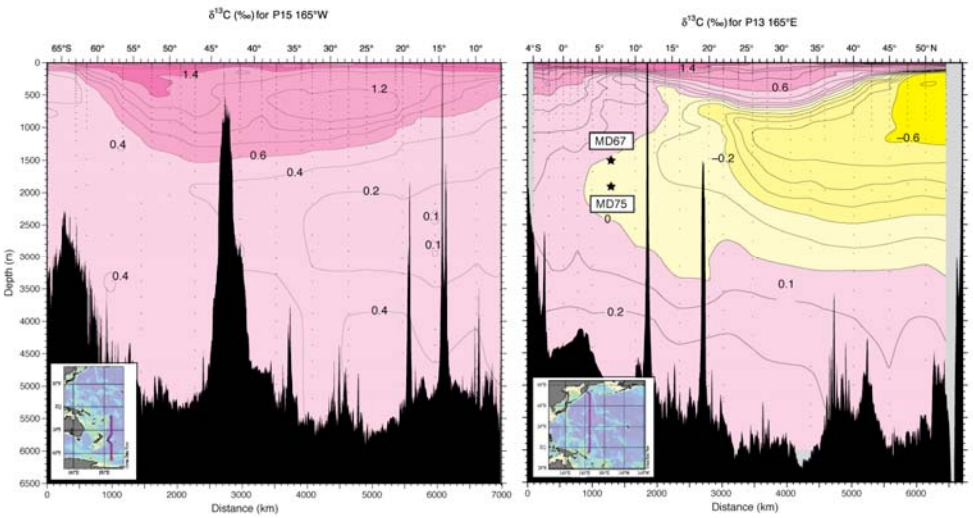

Fig. 7 – Latitudinal distribution of $\delta^{13}C$ vs depth in the Pacific Ocean with Cores MD06-3067 and MD06-3075 location. Section plots modified from WOCE Atlas Volume 2: Pacific Ocean; Sections P13 – 165°E (right) and P15 – 165° W (left), (Talley et al., 2007).

Such a divergence in $\delta^{13}C$ signals between the South Pacific and the western equatorial Pacific Ocean is not expected as mid-depth waters around Mindanao are supposed to mainly originate from the Southern Ocean (Qu et al., 1998, 1999 and 2004), even though modern observations also indicate the possible presence of NPIW in this zone (Talley, 1999 and 2003; Bingham and Lukas, 1994). The good agreement in the timing of the divergent excursions in $\delta^{13}C$ of the two cores suggests that the presumed increase in AAIW production recorded in the South Pacific may have been accompanied by major reorganization of the intermediate circulation in the western equatorial Pacific. The occurrence of these sudden $\delta^{13}C$ excursions shortly after the onset of both terminations and similarly lagging the deglacial warming (as recorded in $\delta^{18}O$) suggests that this reorganization in the mid depth circulation was linked to global climatic fluctuations and was engendered by similar mechanisms over the two last terminations. A close link between abrupt changes in the mid-depth circulation and glacial/interglacial climate variability is supported by results from Kissel et al., (2010) indicating a reduction of bottom water flow speed during glacials compared to warmer periods.

The sharp increases of $\delta^{13}C$ in the South Pacific during terminations I and II interpreted by Pahnke and Zahn (2005) as sudden increases of AAIW production and the corresponding abrupt troughs recorded in the $\delta^{13}C$ signal in Core MD06-3067 suggest that the western equatorial Pacific Oceanexperienced major changes in the origin of intermediate water-mass rather than changes in local productivity. This is

supported by productivity proxies (benthic foraminifers and coccoliths, Bolliet et al., 2011, Fig 6 A-E) indicating increased productivity during the LGM, most of MIS 3, MIS 4 and to a lower extent during MIS 6, and generally a decrease during terminations.

We propose that the negative excursions in Core MD06-3067 $\delta^{13}C$ signal during terminations I and II might be representative of sudden incursions of ^{13}C-depleted intermediate waters around Mindanao, originating from the North Pacific. This implies that NPIW would have replaced AAIW as the dominant mid-depth water-mass in the western equatorial Pacific after the beginning of the two last terminations, and switched back to a dominance of AAIW during the warm MIS 5e and Holocene. This scenario and the enhancement of AAIW formation in the South Pacific proposed by Pahnke and Zahn, (2005) would imply major reorganizations in the distribution of Antarctic and North Pacific water masses in the Pacific Ocean during the two last terminations. This reorganization of the intermediate circulation in the Pacific and the major intrusion of NPIW around Mindanao could reflect possible significant deglacial increases of NPIW production. The hypothesis of possible temporary deglacial incursions of NPIW in the western equatorial Pacific Ocean is corroborated by abrupt changes in the assemblages of benthic foraminifera, with *C. mundulus* replacing *P. wuellerstorfi* during the $\delta^{13}C$ negative excursions, reflecting possible abrupt switches in bottom currents and food supply at the MD06-3067 coresite.

We excluse that the abrupt offset in $\delta^{13}C$ may be due to a switch in the analyzed species, as the $\delta^{13}C$ signal of those two species have been intensively used for defining water mass geometry and geochemical properties. These species do not exhibit any major and systematic offset in their way of fractionating carbon isotopes (Ennyu and Arthur, 2004) and replicate $\delta^{13}C$ measurements from *P. wuellerstorfi* and *C. mundulus* do not show a significant offset (Ennyu and Arthur, 2004; Holbourn et al., 2005).

5.2 – Changes during glacial terminations

5.2.1 – Timing of benthic $\delta^{13}C$ deglacial changes in the Pacific.

Comparison of the benthic $\delta^{13}C$ records from Cores MD97-2120 (Pahnke and Zahn, 2005) and Core MD06-3067 over termination I reveals that the deglacial $\delta^{13}C$ excursion is recorded in Core MD97-2120 at ~ 17 ka and 1 kyr later in MD06-3067. This delay is also marked during termination II although the relatively limited precision of age models over this period may be partly responsible for this phasing. When considering that both age models are compatible, this feature suggests that the abrupt reorganization during terminations in the Pacific intermediate circulation would lag the beginning of the deglacial warming by at least 1000 yrs. Also the delay between $\delta^{13}C$ signals from Cores MD06-3067 and MD97-2120 indicates that this reorganization would have started in the Southern Ocean via a possible although still debated increase of AAIW production and would have then reached the tropics, around 1kyr later. This assumption is however limited by eventual discrepancies in the age models, especially concerning the precise dating of the starting point of termination I in Core MD97-2120. In fact, samples between 16 and 26 ka of this core are dated by linear regression, engendering a possible imprecision in the estimation of the starting date of the deglaciation.

5.2.2 – Comparison of the Davao Gulf and the open Pacific Ocean.

The comparison between Core MD06-3067 and MD06-3075 located in the Davao Gulf reveals large discrepancies in the evolution of the benthic $\delta^{13}C$ during the last termination (Fig. 4 B). In fact, Core MD06-3075 does not exhibit the major trough recorded in MD06-3067 between 16 and 8 ka. The deglaciation is characterized in MD06-3075 by a major and quite regular increase in benthic $\delta^{13}C$. The two records appear to converge with time, showing a contrast of about 0.6‰ during the LGM, and identical values during the mid-Holocene. This feature highlights the different evolution of the intermediate circulation at the two core sites, revealing the presence of water masses of highly contrasted isotopic signature at the LGM and progressively converging up to similar levels during the Holocene. Two factors may explain this contrasted evolution between the two cores distant of less than 150 km. Firstly, there is a significant difference in water depth between the two cores (1575 m for MD06-

3067 and 1878 m for MD06-3075). The depth of Core MD06-3075 is close to the usual range of Antarctic Deep Water (AADW; <2000 m; Talley et al., 1999) and may thus record the signature of a different water mass than the shallower Core MD06-3067. The depth of Core MD06-3075 also almost corresponds to the depth of the boundary in $\delta^{13}C$ observed in the glacial Pacific mid-depth waters at around 2000 m (Matsumoto et al., 2002), with particularly low $\delta^{13}C$ values below this limit. As the depth of this boundary might have fluctuated with time, deep ^{13}C-depleted waters may have reached the position of MD06-3075. The rise in $\delta^{13}C$ recorded in this core during the deglaciation as well as the substitution of *C. wuellerstorfi* by *C. pachyderma* in the benthic foraminiferal assemblages at 16.5 ka could thus reflect a decrease in the influence of this boundary, whereas the shallower Core MD06-3067 would not have been affected by those deep low $\delta^{13}C$ waters.

Core MD06-3075 is located in the Davao Gulf and may record a mid-depth circulation signal specific to this marginal basin, similarly to what is observed in other semi-enclosed seas of the Indo-Pacific region. In fact, the distal end of the Davao Gulf is separated by a relatively shallow sill from the open West Pacific. This sill extends over several hundred kms from South Mindanao to Miangas Island in water depths of just a few hundred meters (<800 m), possibly isolating the Davao Gulf from the mid depth circulation (1000-2000 m) of the open western Pacific Ocean. Lower benthic $\delta^{13}C$ values in Core MD06-3075 may reflect poorer ventilation and/or differences in carbon export flux at the more proximal location within the Davao Gulf during MIS 2 and Termination 1. The similarity in $\delta^{13}C$ values in the two cores during the Holocene suggests that hydrographic conditions may have been more similar at these two locations.

5.2.3 – Comparison of Cores MD06-3067 and MD98-2181.

Comparison (Fig. 8) between Core MD98-2181 (Stott et al., 2007a) and Core MD06-3067 (Bolliet et al., 2011) appears to support a local discrepancy between the sheltered Davao Gulf (MD98-2181 and MD06-3075) and the open West Pacific (MD06-3067). Unfortunately, epibenthic $\delta^{13}C$ data from MD98-2181 over termination I are scarce and do not exhibit a clear trend to allowing a robust comparison with our data. However, comparison of the benthic $\delta^{18}O$ signals from

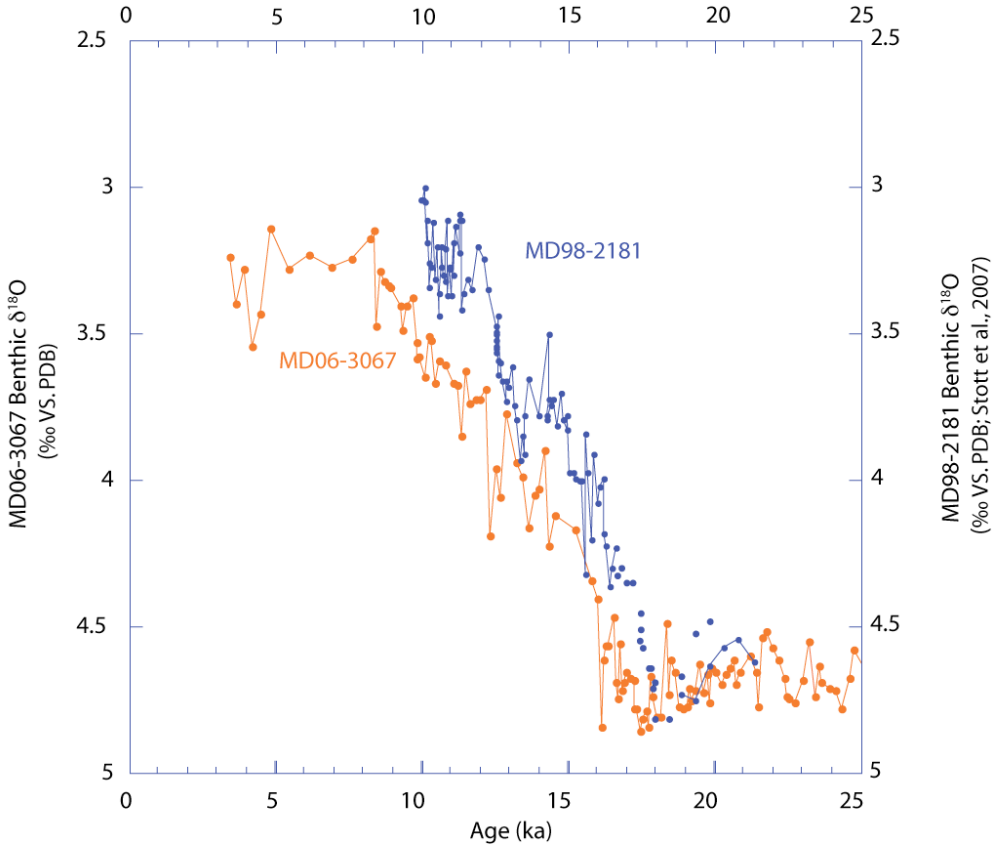

Fig. 8 – Benthic $\delta^{18}O$ signals over the last termination from Cores MD06-3067 (Orange curve; Bolliet et al., 2011) and MD98-2181 (Stott et al., 2007a).

our two cores and Core MD98-2181 shows a similar glacial/interglacial amplitude (1.6‰) with nevertheless apparent discrepancies in the timing of the last deglaciation. In fact, Core MD98-2181 shows a lead of 500 yrs in the starting point of the termination compared to MD06-3067 (17.9 vs 17.4 ka).

This temporal offset is amplified during the deglaciation, reaching ~ 2 kyrs at the beginning of the Holocene (10.5 ka in Core MD98-2181 vs 8.4 ka in Core MD06-3067). The age model of Core MD98-2181 used for this comparison differs from the one published by Stott et al., (2007a). In fact, 18 AMS ^{14}C dates based on planktonic foraminifera from Stott, (2007b; see Appendix) were used to constrain the ages of this core, using the reservoir ages indicated by Saikku et al., (2009), with although no additional 1000 yr shift of the benthic signal. The 500 yrs temporal offset between the two cores for the triggering of the deglaciation may be explained by different dating methods for this critical point (AMS ^{14}C dating for Core MD98-2181 and correlation of benthic $\delta^{18}O$ signal from MD06-3067 with the $\delta^{18}O$ record of EDML ice core from Ruth et al., 2007). On the contrary, benthic $\delta^{18}O$ signals from Cores MD06-3067 and 3075 reveal a remarkably similar timing and indicate a synchronous deglaciation

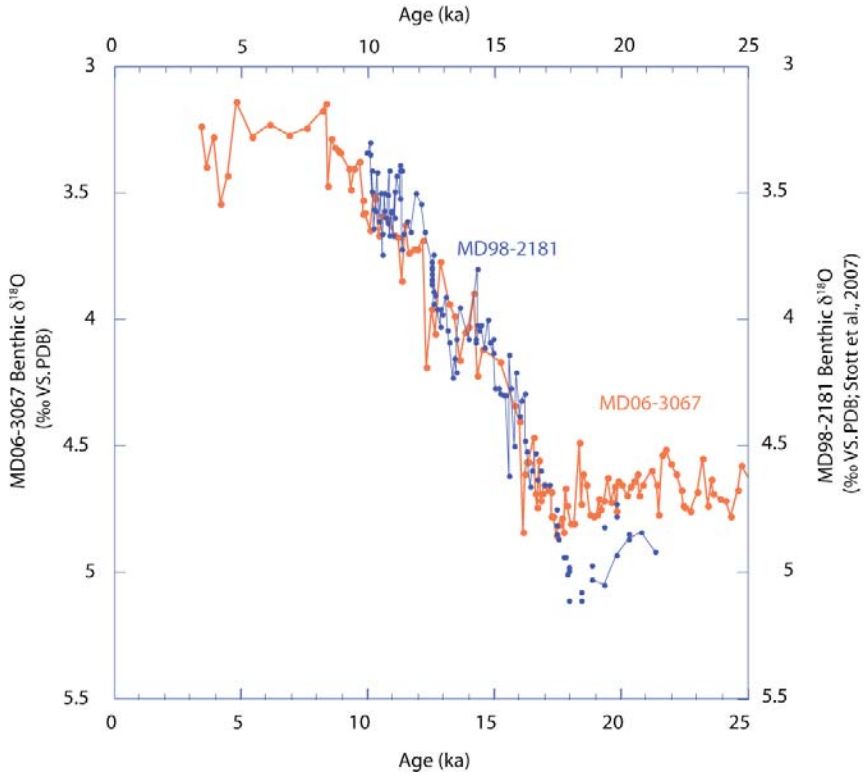

Fig. 9 – Benthic $\delta^{18}O$ signals over the last termination from Cores MD06-3067 (Orange curve; Bolliet et al., 2011) and MD98-2181 (Stott et al., 2007a) with a +0.3‰ correction applied to values from Core MD98-2181.

between the Davao gulf and the open western equatorial Pacific Ocean. Interestingly, when adding 0.3‰ to the benthic $\delta^{18}O$ values from Stott et al., (2007a) the deglacial phasing between MD06-3075 and MD98-2181 is reduced and both signals exhibit a similar timing and values during the deglaciation (Fig. 9).

This is particularly visible between 13 and 11.5 ka as both signals show a synchronous abrupt and major (0.5‰) decrease of benthic $\delta^{18}O$. The agreement between the deglacial benthic $\delta^{18}O$ signals engendered by the addition of this 0.3‰ correction to the data from Stott et al., (2007a) indicates that there might be finally no significant discrepancy between the two age models. However, this correction also creates a significant offset (0.3‰) in the glacial benthic $\delta^{18}O$ between the two cores. It indicates that glacial water-masses present at 2114m would have been around 1°C colder than the shallower water masses present at 1878 m (MD06-3075) and 1575 m (MD06-3067), and that this contrast disappeared at 17 ka. This contrast between our results and the data from Stott et al., (2007a) during the LGM abruptly reduced at the beginning of the deglaciation remains difficult to explain, and may result from different preparation techniques, with eventual discrepancies in the cleaning methods of benthic foraminifera

Conclusion

This study provides new insights into the poorly known past evolution of the intermediate circulation in the equatorial western Pacific Ocean. The $\delta^{13}C$ record from Core MD06-3067 indicates major changes in the isotopic signature of mid-depth waters around Mindanao during terminations I and II. Prominent troughs in $\delta^{13}C$ following the initial warming during deglaciation, suggest substantial changes in mid-depth circulation of the western equatorial Pacific Ocean during terminations. This pattern matches well the opposite trend recorded in the South Pacific and interpreted as an increase in AAIW production (Pahnke and Zahn, 2005).. These coeval changes imply a major reorganisation of intermediate water masses, as intrusion of NPIW extended to Mindanao, replacing AAIW during termination I and II. These abrupt major incursions of NPIW probably reflect temporary increases in intermediate and deep waters formation in the North Pacific.

Comparison of the benthic oxygen and carbon isotopes records from Core MD06-3067 and Cores MD06-3075 and MD98-2181 located in the proximate Davao Gulf reveals that MD06-3067 and MD06-3075 exhibit highly contrasted $\delta^{13}C$ signals during the LGM and over termination I. The offset between the signals is progressively reduced during the deglaciation, until similar values are reached during the mid Holocene. This may reflect a contrast in the nature of the bottom water at the two sites, as Core MD06-3075 may have been influenced by a more ^{13}C-depleted deep water-mass as suggested by Matsumoto et al., (2002). The topography of the region may also have played a role, as the Davao Gulf may have been partially isolated from the Pacific Ocean due to the relatively shallow sill separating the gulf from the open West Pacific, which may have led to poorer ventilation and/or differences in carbon export flux within the Davao Gulf during MIS2 and Termination 1.

MD06-3067 and MD98-2181 (Stott et al., 2007a) benthic $\delta^{18}O$ signals exhibit contrasted timing of the last deglaciation. A 0.3‰ correction applied to the data from Stott et al., (2007a) however suggests a good agreement of data and age models from the two cores, whereas glacial values appear to be significantly different. This contrast suggests a possible 1°C difference in bottom water temperature during the LGM between the two cores whereas deglacial benthic $\delta^{18}O$ are similar. A further investigation of eventual discrepancies in the protocol used in samples preparation would however be required.

Conclusion

Additional records from the western Pacific are needed to provide a more comprehensive overview and reliable reconstruction of the local intermediate circulation and in particular to determine the relative influence of AAIW and NPIW in this region. Additional long-term mid-depth $\delta^{13}C$ records in the Pacific would also be valuable to confirm the suggested deglacial reorganizations in the intermediate circulation, and to elucidate diverging results concerning the glacial AAIW and NPIW production rates.

Appendix

Depth (cm)	^{14}C Conventional Age (yr)	1σ std dev	Reservoir Age (yr)	Cal. age (yr B.P.)	1σ std. dev.
711	6950	50	480	7395	46
755	7360	50	480	7701	47
861	9480	65	480	10180	69
920	10450	120	480	11433	219
940	11050	310	480	12427	408
986	11050	75	480	12523	87
1000	11150	80	480	12614	74
1036	12100	80	480	13484	90
1047	12400	210	480	13749	195
1049	12650	80	480	13959	96
1054	12900	45	480	14307	120
1061	12850	80	480	14222	157
1086	13400	55	630	14880	103
1086	13450	75	630	14937	120
1211	15550	65	630	17945	191
1286	16800	95	630	19297	116
1486	20300	260	630	23476	358
1711	24800	130	630	28924	191

Position of AMS ^{14}C dates measured in planktonic foraminifers used to derive age model in Core MD98-2181. Data from Stott, (2007b).

Chapter IV: Monsoon variability and deep oceanic circulation in the western equatorial Pacific over the last climatic cycle: insights from sedimentary magnetic properties and sortable silt

Monsoon variability and deep oceanic circulation in the western equatorial Pacific over the last climatic cycle: insights from sedimentary magnetic properties and sortable silt

Catherine Kissel[1], Carlo Laj[1], Markus Kienast[2], Timothé Bolliet[3], Ann Holbourn[3], Paul Hill[2], Wolfgang Kuhnt[3], Pascale Braconnot[1]

1 : Laboratoire des Sciences du Climat et de l'Environnement/IPSL, CEA-CNRS-UVSQ,Avenue de la Terrasse, 91198 Gif-sur-Yvette cedex.

2 : Department of Oceanography, Dalhousie University, Halifax, Nova Scotia, Canada.

3 : Institut für Geowissenschaften, Christian-Albrechts-Universität, 24118 Kiel, Germany.

Paleoceanography, doi:10.1029/2010PA001980, accepted 8 June 2010.

Abstract

Magnetic and grain size properties of a sediment core located in the western equatorial Pacific, off the southeastern tip of the Philippine island of Mindanao, are presented in an effort to reconstruct past changes in the East Asian Monsoon and deep ocean circulation during the last 160 kyrs. The sedimentary concentration of magnetic particles, interpreted to reflect past changes in run-off from Mindanao, varies almost in antiphase with northern hemisphere insolation. This suggests that precipitation was lower in the western equatorial Pacific region during boreal insolation maxima, and thus corroborates model results showing opposing trends in precipitation between land and the marine realm there. Variations in the grain size distribution of the inorganic sediment fraction, as recorded by both the sortable silt mean size and the magnetic grain size, provide a monitor of changes in sediment reworking by bottom currents. The close correlation of this proxy of bottom current strength and the benthic $\delta^{18}O$ record from the same site implies a tight coupling between deep-water flow, most likely Antarctic Intermediate Water (AAIW), and global climate.

1 – Introduction

The western equatorial Pacific is a key area for understanding past climate variability and interactions between high and low latitudes. This region is affected by seasonal climate variations dominated by fluctuations in precipitation due to the migration of the Intertropical Convergence Zone (ITCZ) resulting in the seasonal march of the monsoon and interannual changes in precipitation patterns associated with the El Niño/Southern Oscillation (ENSO) phenomenon. Moisture and latent heat from these areas are distributed throughout the globe via large-scale atmospheric circulation. Their role in the global oceanic circulation and in particular the thermohaline circulation is fundamental, due to the salinity gradient with respect to high latitudes. Therefore, the western equatorial Pacific is a critical area for assessing the role of the oceanic circulation in the transfer between high and low latitudes climatic changes and in the heat and moisture transport and distribution.

We report here on a detailed study of the magnetic and grain size in a core (IMAGES core MD06-3067) taken at the southeastern tip of Mindanao (Laj et al., 2006). This area appears particularly relevant because it is affected by the East Asian Monsoon, the position of the ITCZ, and it is also a critical area for understanding past changes in the dynamics and in the pathways of the main oceanic water masses (Fig. 1). Whilst the present day patterns of surface and subsurface currents are relatively well documented, very little is known for deeper currents. It may be hypothesized, however, that water masses formed at high southern latitudes reach this region and thus directly transmit some high latitude fluctuations to low latitudes. This was recently suggested by Saikku et al., (2009) in a submillennial scale study of marine isotopic stage 3 in IMAGES core MD98-2181, located within the Davao Bay. Our core, located in the open West Pacific, is well suited for reaching our objectives which are: 1) monitoring changes in the monsoon activity *via* precipitation on land and the resultant sedimentary discharge and 2) investigating past variations in bottom current flow and their relationship with high latitude circulation patterns.

2 – Oceanographic and climatic setting

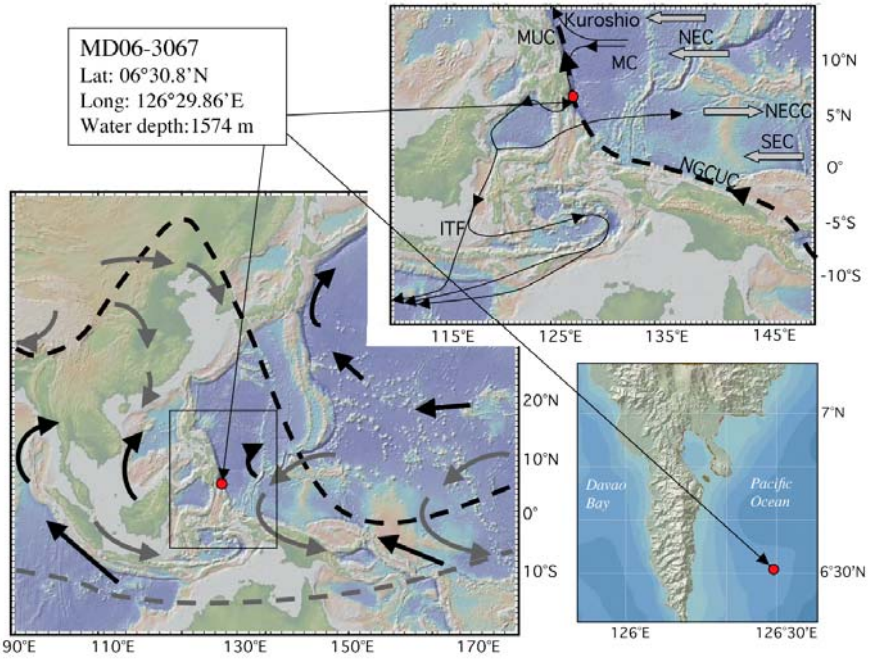

Fig. 1: Maps showing the location of core MD06-3067. Left: summer (dashed black line) and winter (dashed grey line) positions of the ITCZ and associated directions of tradewinds. Up right: main oceanic water masses (MC: Mindanao Current; MUC: Mindanao Under-Current; NGCUC: New Guinea Coastal Under-Current; ITF: Indonesian Throughflow; NEC: North Equatorial Current; NECC: North Equatorial Counter-Current; SEC: South Equatorial Current). Bottom right: more precise location of the core with respect to the southern tip of Mindanao and the Davao Bay. The maps are constructed using GeoMapApp software.

From an oceanographic point of view, the southern Mindanao area is called the "water mass cross roads" (Fine et al., 1994), because several water masses from the northern and southern hemispheres meet there (Fig. 1). The southward flowing Mindanao surface current (MC) originates from the North Equatorial Current at about 15°N. It has a near-surface speed 3 at present of about 1m/s on the average and experiences a vertical shear in the upper 300 m with a net transport increasing from north to south to attain a maximum of about 33Sv at the latitude of south Mindanao (Toole et al., 1990; Lukas et al., 1991). South of Mindanao, part of this current flows into the Celebes Sea and passes through a complex array of passages within the Indonesian archipelago to arrive in the Indian Ocean (the Indonesian Throughflow, ITF). The other part turns eastward and contributes to the North Equatorial Counter-Current. It probably also gives rise to the Mindanao Eddy.

At intermediate depth below the MC (i.e. depths > 400-600 meters), the Mindanao Under- Current (MUC) is connected to the strong northwestward flowing deep layer of the New Guinea Coastal Under Current (NGCUC) (Fig. 1). The latter, originating from the Northeastern coast of Australia (Lindstrom et al., 1987), merges with the southern-sourced Antarctic Intermediate Water (AAIW) and the deep part of the South Pacific Tropical Water and flows along the New Guinea northern coast from the Solomon Sea (Tsuchiya, 1991). At present, the retroflection flow of the MC from the Celebes Sea prevents the upper part of the NGCUC to flow northward (Kashino et al., 1996) while its deep part is free to pass. Tsuchiya (1991) demonstrated the role played by the NGCUC as the pathway of the AAIW into North Pacific. The CTD profile we obtained at the location of core MD06-3067 is very similar to the one reported by Lukas et al.,. (1991, Fig. 10) with very uniform temperature and salinity properties between 600 and 1500 m, with the salinity reaching about 34.6 psu at 1500 m. In the nearby WOCE E-W (P04) and N-S (P08) profiles all the chemical properties (temperature, salinity, silica, oxygen) are also very uniform at these depths (Talley, 2007). Broecker et al., 1986) showed nearly unchanged oxygen concentrations between 1360 and 1790 m water depth in a water column profile to the south of our coring site (5°S/128°E). Taken together, these scarce water column profiles and interpretations available to date suggest a homogenous water mass between 600 and 1800 m off Mindanao, most likely reflective of northward flowing AAIW.

The climate of the southern Mindanao region is strongly influenced by the East Asian monsoon induced by seasonal changes in the pressure gradient and resulting from the different potential heating between the ocean and the Asian continent (Fig. 1). Presently, heating of the Asian continent during boreal summer gives rise to a strong inflow of air from ocean to land. These strong winds result from the low pressure cell over the Asian continent, and cause rainfalls over southern Asia (i.e. the summer monsoon). The East Asian summer monsoon is associated with a very significant northward migration of the rain belt up to 45°N. In boreal winter, the situation is reversed with more arid conditions on the continent and 4 displacement of the ITCZ to about 10-15°S. The strength of the monsoon has undergone large changes in the past and it is widely recognized that they were largely forced by insolation (Wang et al., 2005). However, the debate is still active, depending on the region studied and the oceanic or continental proxies used, whether only precession or both precession and obliquity control the monsoon regime. As noted by Wang (2009), « the specific sea-

land settings of the regions may bring about different monsoon responses to the same orbital forcing ». This results from the fact that the monsoon is a large-scale phenomenon and therefore, shifts in the monsoon system lead to increase in precipitation rate in some areas and to decrease in others.

3 – Core site and sample material

Core MD06-3067 was recovered during the IMAGES XIV-MD155-Marco Polo 2 cruise on board the R. V. *Marion Dufresne* of the French Polar Institute (IPEV) (*Laj et al.,* 2006). The core site is located at 06°30.86'N and 126°29.86'E, 1574 m water depth, in the open western equatorial Pacific at the southeastern tip of the Philippines, off the island of Mindanao (Fig. 1). The 15.53 m long CALYPSO core is composed of medium olive gray silty clay with some pumice pebbles (up to 1 cm). An ash layer is present at 198-200 cm.b.s.f.

Directly on board, a fiducial line was drawn along the plastic tube containing the sediment before cutting the core into 1.5 m segments. So, although the core was not azimuthally oriented, the relative orientation of the different segments was preserved to within about 5°. These segments were then split longitudinally into two halves, taking care to cut along the fiducial line.

The archive half of the core was scanned for major element intensities using the Avaatech XRF core-scanner (Richter et al., 2006) at Bremen University. The working half was entirely sliced into 1 cm thick samples for the analysis of foraminifera at the University of Kiel. Two types of samples were taken for magnetic analyses. First, the archive half of the core was sampled continuously using 2x2x150 cm u-channels (see e.g. Weeks et al., 1993). In addition, standard 2x2x2 cm plastic cubic boxes were used to obtain samples for the study of the anisotropy of the susceptibility. Finally, small amounts (ca. 0.2 g) of sediments were also taken every 10 cm for the magnetic hysteresis measurements and first order reversal curves (FORC) analyses. Following the magnetic analyses at LSCE, the u-channels were shipped to Dalhousie University, where subsamples taken every 10 cm were used for determination of the disaggregated inorganic grain size composition.

4 – Results

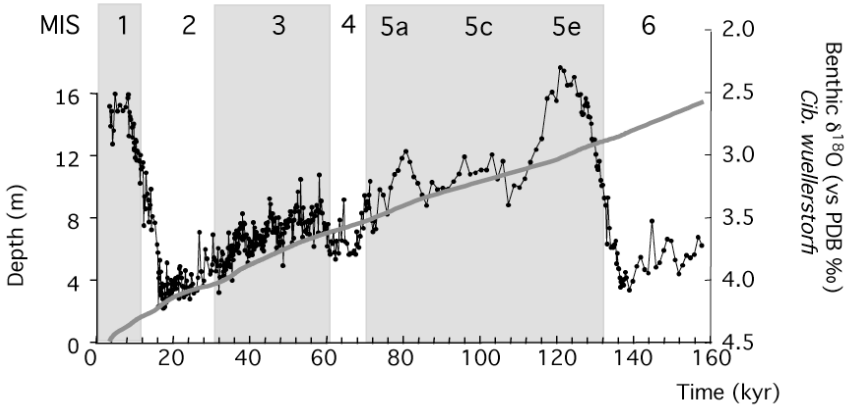

Fig. 2: Benthic oxygen isotope record and age-depth relationship (grey line) in core MD06-3067. MIS stands for Marine Isotopic Stages.

The age model of core MD06-3067, presented in detail in Bolliet et al (2011), is based on seven AMS ^{14}C dates for the upper 420 cm (ca. 34 kyr) of the core and on correlation of the benthic oxygen isotope record obtained from the epifaunal benthic foraminifera *P. wuellerstorfi* (see Fig. 2) with the EDML reference $\delta^{18}O$ record (Ruth et al., 2007). An age adjustment of 1000 years (sensu Stott et al., 2007a) is made for benthic age tiepoints to compensate for the travel time of the benthic oxygen isotope signal from the Southern Ocean to the Mindanao site. A detailed description of the methods used to characterize the magnetic properties and the disaggregated inorganic grain size composition is given in the Appendix. We focus here on the meaning of the used parameters in terms of nature, grain size and concentration of the magnetic particles and sortable silt mean size. We shall then discuss the variations observed in these parameters in terms of climatic and oceanic circulation changes in this region.

4.1 – Magnetic assemblage and major elements

The nature of the magnetic particles has been investigated using different parameters and properties (see Appendix). First, the coercivity parameters, S-ratio$_{-0.3T}$, Hmd_{ARM} and Hmd_{IRM} are very uniform all along the core with values around 0.98, 23 mT and 12 mT respectively, indicating that only low coercivity magnetic minerals are present in the core (Fig. 3a).Thermomagnetic experiments on samples at different depths all reveal a progressive decay of the saturation magnetization upon heating until a

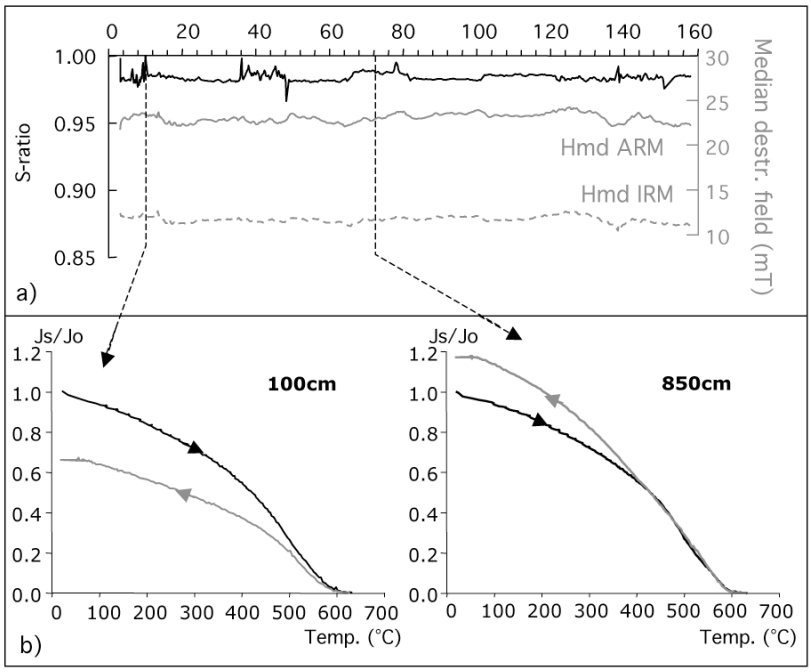

Fig. 3: Magnetic parameters defining the magnetic mineralogy in Core MD06-3067. a) Sratio-0.3T (black line) and median destructive fields of ARM and IRM (HmdIRM in dashed grey line and HmdARM in continuous grey line); b) two representative thermomagnetic curves obtained from different horizons with the heating curve in black and the cooling curve in grey. All indicate that the main carrier is low Ti-content magnetite.

complete loss of magnetization around 580-600°C (Fig. 3b). The subsequent cooling curve has the same shape, sometimes slightly below the heating curve, indicating a small degree of oxidation during heating. Both the Curie point at 580-600°C and the reversibility of the curves indicate that the preponderant low coercivity magnetic mineral is magnetite.

As magnetite is the largely dominant magnetic mineral in the sediment, we have used anhysteretic susceptibility (κARM, see Appendix) versus volume susceptibility (κ) and ARM versus IRM ratios to estimate the magnetic grain size (King et al., 1982). These ratios, plotted versus time as in Fig. 4, largely covary indicating a negligible paramagnetic contribution to κ .They both indicate that the bottom of the core is characterized by the coarsest magnetic grains and a sharp decrease of the magnetic grain size is observed around 130-140 kyr (at termination II). There is then a progressive coarsening trend up to marine isotopic stage 2 MIS2) with superimposed significant fluctuations. Termination I is also characterized by a sharp decrease in the grain size, which remains then relatively constant at the top of the sequence. When the hysteresis parameters are reported as magnetization ratio (Mrs/Ms) versus

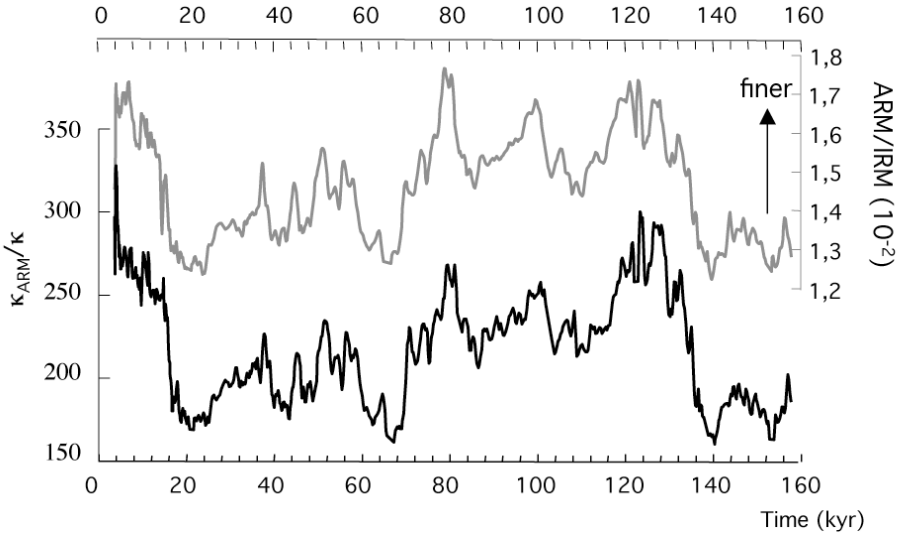

Fig. 4: Magnetic grain size in Core MD06-3067 expressed by the ratios ARM/IRM (in grey) and κARM/κ (in black). Both show the same variations versus time.

coercitive forces ratio (Hcr/Hc) (Day et al., 1977), they confirm the variability of the grain size of magnetite.

They also show that, in a general way, the mean sizes of these grains are relatively large,ranging between pseudosingle domain and multidomain areas (Fig. 5a). For magnetites, this corresponds to average grain sizes of about 10µm. FORC diagrams obtained from different horizons look very similar. However, the coercivity profiles horizontal profile across the Hu=0 line) of coarser intervals are clearly shifted toward lower ceorcivities than the finer intervals (Fig. 5b). The latter are therefore constituted of a large spectrum of magnetic grain sizes with a large majority of multidomain grains.

Among the three bulk magnetic parameters (Fig. 6), IRM and κ largely covary. Relative changes in the amplitude ARM are slightly different, again illustrating changes in magnetic grain sizes as discussed above. These magnetic parameters vary rather regularly within a stable envelope. The $CaCO_3$ content in this core is relatively low, ranging between 14% and 24%. Although CaCO3 is anticorrelated with the magnetic content, when susceptibility is corrected for this possible dilution effect (Pouthiers and Gonthier, 1978), the record still clearly documents the same variations as those observed in the uncorrected record (Fig. 6). Except for a small difference around 30 kyr, the down-core patterns of Fe and Ti intensities normalized by Ca intensity and expressed as log-ratios (Weltje and Tjallingii, 2008) are also very similar to the magnetic concentration (Fig. 6). Therefore, the magnetic grains, Fe and

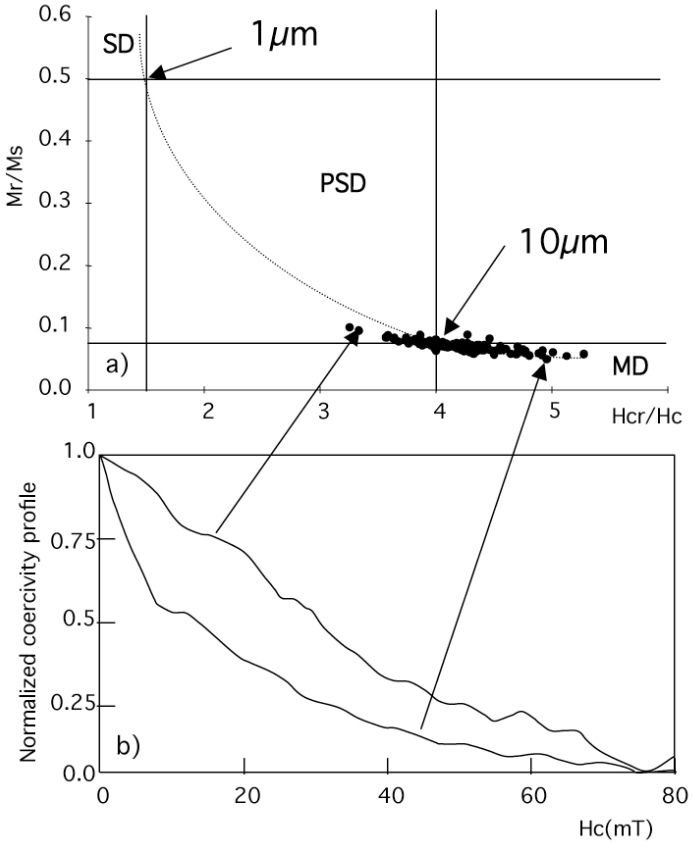

Fig. 5: Magnetic hysteresis parameters in Core MD06-3067 reported in a) as Mr/Ms versus Hcr/Hc ratios (Day et al., 1977) with the hyperbole (dashed line) corresponding to magnetite grain size distribution between SD (single domains), PSD (pseudo-single domains) and MD (multi-domains). b) two coercivity profiles from FORC diagrams (profiles along Hu=0) showing the different distribution of coercivities in samples characterized by the mean finest grains (grey) and coarsest grains (black).

Ti all trace the same terrigenous assemblage, the concentration of which varies in time independently from any carbonate dilution effect.

4.2 – Anisotropy of the low field magnetic susceptibility

The crystalline anisotropy of magnetite, the main magnetic mineral in Core MD06-3067, is very weak and shape anisotropy is dominant with the maximum susceptibility aligned with the long axis of the grain. In Core MD06-3067, the analysis of the 'magnetic fabric' thus provides information about the preferential alignment of the elongated magnetite grains in the sediment. Only the uppermost 1.5 m of Core MD06-3067 exhibits an elongated magnetic fabric aligned with the core axis. This illustrates perturbation due to the piston during the coring process.

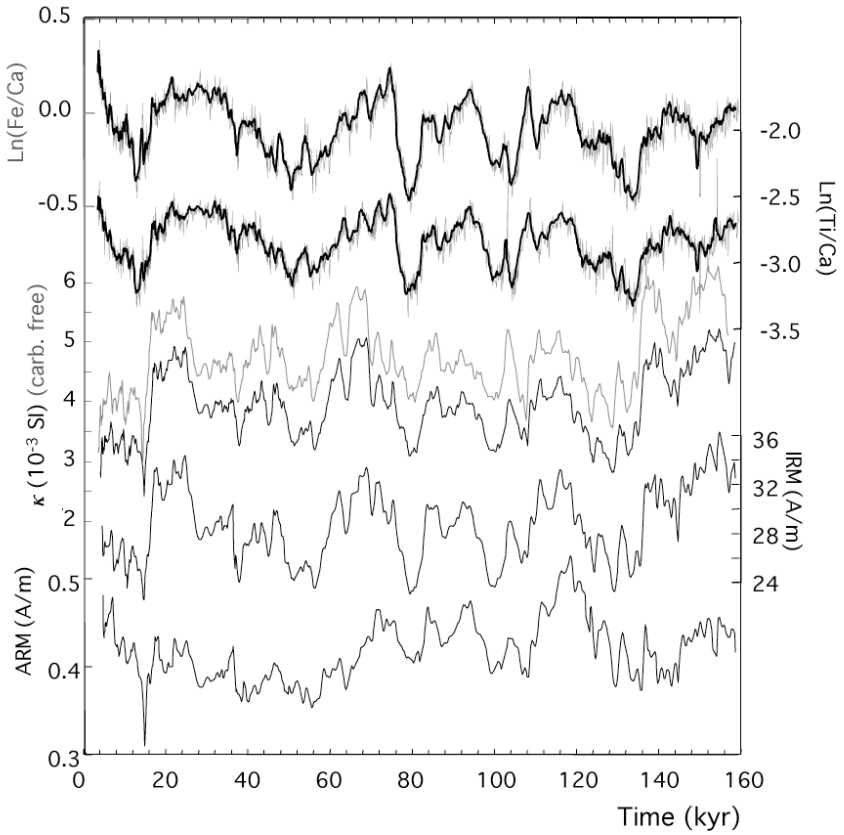

Fig. 6: Ti/Ca and Fe/Ca log-ratio (and a 7 points-running average) and bulk magnetic parameters (κ, IRM and ARM) curves versus time in Core MD06-3067. The magnetic susceptibility calculated on a carbonate-free basis is also reported on the same vertical scale as κ by the grey curve.

The rest of the core is entirely characterized by an oblate anisotropy ellipsoid with minimum axes K_{min} close to the vertical, i.e. perpendicular to the bedding plane (I_{mean} = 85°) Fig. 7). This is typical for a sedimentary magnetic fabric acquired during deposition and possible subsequent compaction. Within the bedding plane, we observe that the maximum axes of the AMS ellipsoid (K_{max}) are rather well grouped, marking a magnetic lineation. In order to determine the real orientation of the magnetic lineation in geographical coordinates, i.e. the orientation of the core in the horizontal plane, we used the average direction of the stable component of the NRM (Characteristic Remanent magnetization ChRM), which is precisely determined after stepwise demagnetization with a mean angular deviation (MAD) angle never exceeding 5°. After reorientation of Core MD06-3067, aligning the mean declination at 0°, the anisotropy lineation varies between 58° and 178° (80% of the data are between 80° and 133°) with an average direction around 113°. The directions of the principal axes K_{max} in geographical coordinates are reported in Fig. 7.

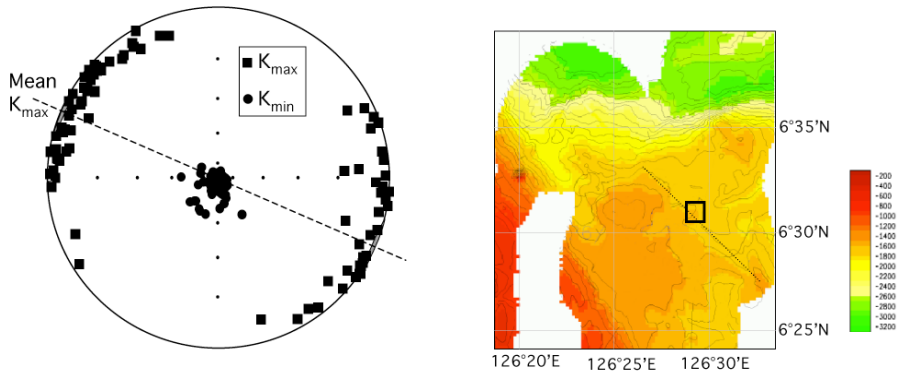

Fig. 7: Left: distribution of the principal axes of anisotropy (in geographic coordinates, see text): Kmin (black circles) and Kmax (black squares). The dashed line and the grey area illustrate the mean direction and associated ellipse of confidence for Kmax. Right: bathymetric map obtained around the site (square) during the survey on board the R.V. *Marion Dufresne* using the multibeam echosounder Thomson Seafalcon 11 and processed with Caraibes software (Laj et al., 2006).

4.3 – Grain size measurements

As an independent tool for deciphering changes in the bottom-current flow speed, the sortable silt mean size was examined (see Appendix). In Core MD06-3067, the down-core record of sortable silt mean size shown in Fig. 8 exhibits variations from about 22 µm to 29µm. As for the magnetic grain size, the coarsest grains are observed at the bottom of the core close to 20 kyr and the finest grains at the top of the core close to 120-130 kyr. The interpretation of the sortable silt mean diameter as a proxy of bottom current flow is corroborated by the disaggregated grain size distributions exemplified in Fig. 8.In general, the shape of these distributions is determined by source material, boundary shear stress and the extent of flocculation (McCave et al., 1995; Curran et al., 2004). The maximum grain size increases with boundary shear stress, suggesting that near-bed energy was higher in the glacial sample (II-130) compared to the interglacial sample (I-60), in line with the coarser sortable silt size and inferred stronger bottom current during this time interval. The slope of the fine portion (source slope) of the glacial and interglacial grain size distributions is similar Fig. 8) implying that the material originates from a single source throughout the time interval explored here.

5 – Discussion and Conclusion

5.1 – Orbitally controlled sedimentary discharge

As basaltic rocks are very rich in magnetites, the latter are abundant in oceanic sediments in the vicinity of basaltic sequences (Kissel et al., 1999; 2009; Mazaud et al., 2002). Both titanium and iron are also present in large amounts in many different minerals constituting basaltic rocks. Consequently, a terrigenous fraction rich in magnetites, Ti and Fe often characterizes oceanic sediments partly fed by nearby basaltic sources (Lavrov et al., 1973; Kissel et al., 2009). In core MD06-3067, magnetite concentration, Ti and Fe contents closely co-vary, thus indicating that they originate from nearby basaltic rocks. Both the magnetic grain size and the mean sortable silt size are significantly coarser than in open ocean environments distant from sediment source regions (e.g. Bianchi and McCave, 1999; Hall et al., 2001;2004; Kissel et al., 2009). This indicates that this basaltic source is very proximal to the coring site. Given the geology of the islands in this region and the location of the core, we infer that the detrital fraction originates from the basaltic rocks forming the large majority of the volcanic island of Mindanao (Sajona et al., 1997). The strong (33 Sv) southward directed surface (upper) Mindanao current causes the particles eroded from Mindanao to be largely transported southward. A canyon located north of our site could possibly receive part of the run-off sediments from Mindanao, but does not appear to be an impassable obstacle for the sediments to reach the coring site. In addition, the shelf in this area is very narrow, due to the presence of the very deep Philippine trench bordering the islands, thus making a significant contribution from re-suspension of sediment from the shelf during sea-level lowstands very unlikely.

Down-core variations in the abundance of magnetites are thus interpreted to directly reflect delivery of sediments from Mindanao Island, which, in turn, is used as a proxy for precipitation in the hinterland. The direct comparison of the total summer (June 1st - August 30th) insolation curve at 30°N with the magnetite concentration curves indicates a clear relationship (Fig. 9a). To better scrutinize this relationship, we performed a Blackman- Tukey spectral analysis using the Analyseries 2.0.3 software (Paillard et al., 1996) on the records of κ and IRM. The spectra shown in Fig. 9b indicate a broad and very significant maximum covering the obliquity and precession bands at 40 (obliquity) and 23 kyr precession) respectively.

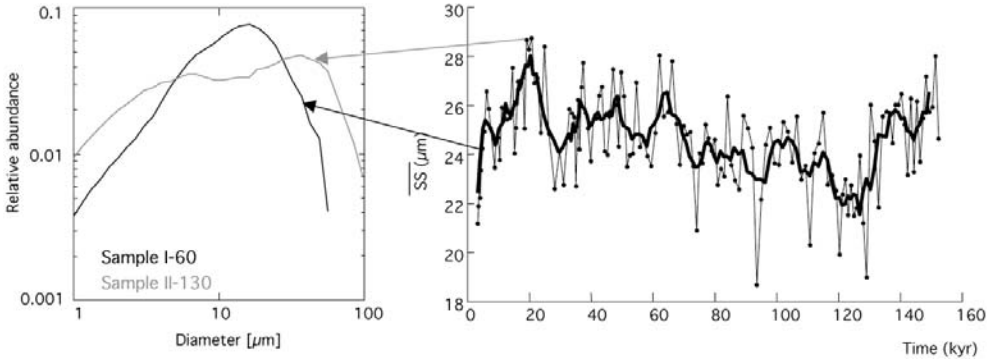

Fig. 8: Inorganic mean grain size in Core MD06-3067. Right hand side: Sortable silt mean size (thin black curve) and running average curve (thick line) versus time. Left hand side: examples of two spectra obtained for fine (black curve) and coarse (grey curve).

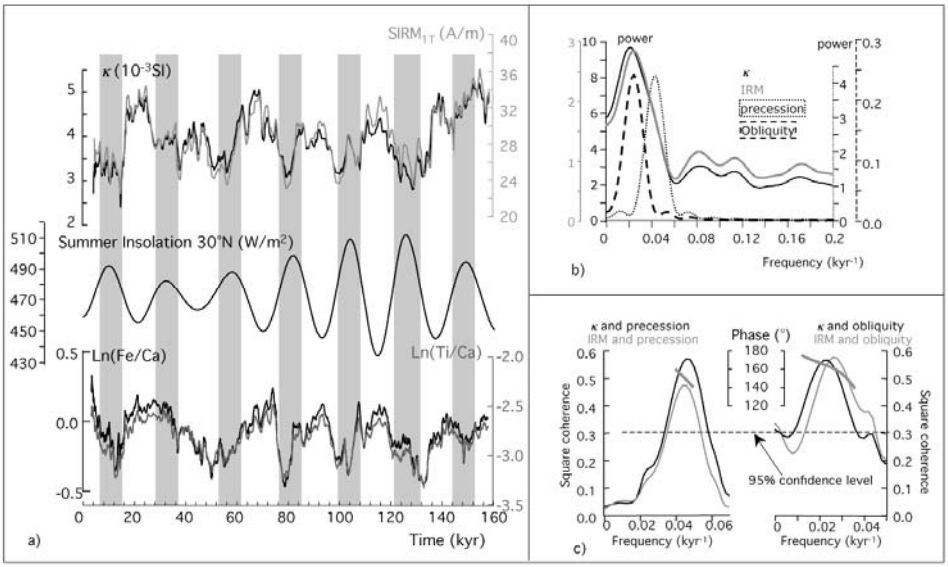

Fig. 9: Relationship between magnetic concentration in Core MD06-3067 and insolation. a) comparison between IRM, κ, Ln(Fe/Ca), Ln(Ti/Ca) (both reported as 7-points running average curves) and the summer (June, 1st to August 31th) mean insolation curve calculated at 30°N using Laskar et al., (2004) solution; b) Blackman-Tukey spectrum analysis calculated using Analyseries software (*Paillard et al.,* 1996) for κ (black), IRM (grey), and the insolation shown in a) after filtering at 23 kyr (named "precession", dotted line) and 40 kyr (named "obliquity", dashed line); c) squared coherence between κ (black), IRM (grey), and the 23 kyr-filtered insolation curve on the left and between κ, IRM, 40 kyr-filtered periodicity on the right. The phases between the magnetic parameters and the insolation ones are reported in degrees for the time domain in which the curves are significantly correlated.

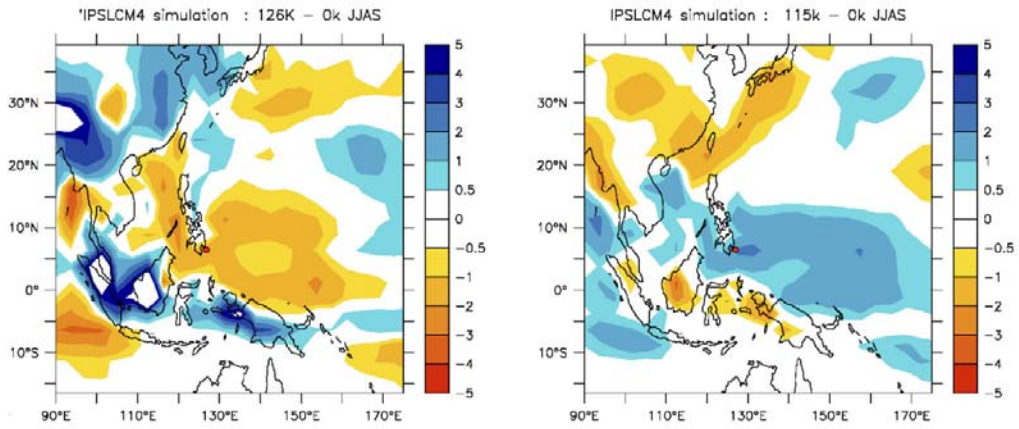

Fig. 10: Differences with 0 ka precipitation over the area (mm/d) for two characteristic periods: 126 ka on the left (maximum northern summer insolation) and 115 ka (minimum northern summer insolation). These simulations were made using the IPSL_CM4 ocean atmosphere coupled models (Braconnot et al., 2008).

These two cycles together control the fluctuations of the magnetic content off Mindanao i.e. changes in the East Asian summer monsoon intensity in this region. The other minor peaks in the curves at shorter periodicities are most likely not significant.

The coherence and the phasing of the orbital parameters with the proxy records, were inferred from cross-correlation between the different series. The precession and obliquity curves were obtained by filtering the insolation at 30°N shown in Fig. 9a using 23 kyr and 40 kyr filters respectively and they were cross-correlated with κ on one side and IRM on the other side.

In all cases, a significant coherence (>95% confidence limit) is observed for each periodicity between the orbital curves and each proxy, thus confirming the influence of both precession and obliquity. A significant coherence peak is associated with a phase shift of about 160° and 170° in the precession and the obliquity bands respectively. This implies that the run-off from Mindanao is almost anti-correlated with northern hemisphere insolation, i.e. maximum precipitation on this island roughly coincides with precession and obliquity minima calculated at 30°N. The small time shift of about 1-2 kyr between the two is short compared to the uncertainties of the age model and may not be significant. Therefore no firm conclusion can be drawn about it at the moment. This clear anticorrelation may appear inconsistent with the common association of strong boreal summer insolation with increased monsoon precipitation. However, Braconnot et al., (2008), have

inferred from GCM runs that precipitation in the area of Mindanao was lower during the insolation maximum at 126 kyr BP and stronger during the insolation minimum at 115 ka, while the situation was reverse on the Asian continent (Fig. 10). Models therefore suggest that in southeast Asia and in the western equatorial Pacific, there is a contrast between precipitation rates on land and in the marine realm.

In summary, the results from Core MD06-3067 support the suggestion of a control of the Asian summer monsoon by insolation in the western equatorial Pacific. In addition, this record from the open ocean offers a first experimental observation of lower precipitation regime on the ocean side than on the continent during boreal insolation maxima, corroborating GCM model results (Braconnot et al., 2008). This would illustrate a change of the rain belt position during summer. Other proxies from the same site show that during the same periods, the winter wind stress was also intensified, giving rise to enhanced upwelling off Mindanao (Bolliet et al., 2011). The seasonality contrast with longer winter seasons and a relative southward shift of the ITCZ during summer months can account for both effects. As emphasized by Wang (2009), each record is influenced by both global and regional components, the latter originating from regional sea-land thermal contrasts. Obviously more records are needed to improve our understanding of the system and to better constrain models.

5.2 – Near bottom current strength

Sediment particles larger than 10 μm, on average, behave non-cohesively and are size sorted by hydrodynamic processes (McCave et al., 1995). The mean size of this "sortable silt" fraction thus reflects the degree to which deep-sea sediments have been reworked by currents and is widely used as a proxy of bottom current strength (McCave and Hall, 2006 and references therein). In Core MD06-3067, the down-core record of sortable silt mean size parallels tightly the magnetic grain size record described above, and both show a clear glacial interglacial variability with coarser grains (stronger mean flow speeds) during glacial periods and finer grains (weaker flow) during interglacials. The close match between SS, magnetic grain sizes and benthic $\delta^{18}O$ holds beyond these mere glacial-interglacial contrasts, implying a close coupling between deep water flow at this site and global climate.

The presence of bottom current acting during the deposition of the particles can also be assessed by the study of the anisotropy of magnetic susceptibility (Rees, 1961;

1965; Hamilton and Rees, 1970; Ellwood and Ledbetter, 1977; Kissel et al., 1997). Because bottom currents, when they exist, statistically align the elongated magnetic particles during deposition, preferential alignment of the long axes of the anisotropy ellipsoids indicates the orientation of the bottom currents. In core MD06-3067, as we described above, the magnetic lineation observed in the deposition plane is oriented around 113° with a dispersion consistent with the local topography (about 130-135°) as surveyed with the multibeam of the R. V. *Marion Dufresne* during the Marco Polo 2 cruise (Fig. 7) (Laj et al., 2006). Since bottom flow is strongly dependent on the sea floor topography, this alignment between topography and magnetic particles confirms that deposition occurred under the influence of bottom currents. The statistical alignment of the particles throughout the entire length of the core suggests that a bottom current was continuously present during the last 160 kyrs. This, in turn, also implies that changes in the mean grain size are a more faithful recorder of variations in bottom current intensity than changes in the anisotropy parameters.

None of these methods yields a *quantitative* record of bottom current strength. However, as observed in Fig. 11, the magnetic and grain size proxies of bottom current flow bothclearly indicate relative changes in the strength of the bottom currents with invigorated glacial bottom currents at 1574 m off the SE Philippines, compared to weaker interglacial flow. Because the actual direction of flow cannot be determined using these methods, we follow here two lines of evidence to argue that most, if not all, bottom current variability observed in Core MD06-3067 is due to changes in the northward flow of circum Antarctica-sourced waters. First, studies of the present-day oceanography suggest that the deeper part of the NGCUC flows across the equator (where it becomes the MUC) transporting AAIW (Tsuchiya 1991; Fine et al., 1994; Qu and Lindstrom 2004), and possibly the upper layer of Pacific Deep Water (Saikku et al., 2009) into the North Pacific along the Mindanao coast. This is also consistent with the interpretation of regional subsurface hydrography proposed by Stott et al., (2007a). Second, based on sortable silt flow speed and benthic $\delta^{13}C$ water mass property records in a core sampling the deep western boundary current (3290 m water depth east of New Zealand), Hall et al., (2001) reconstructed greater Pacific ventilation during Pleistocene glacial periods.

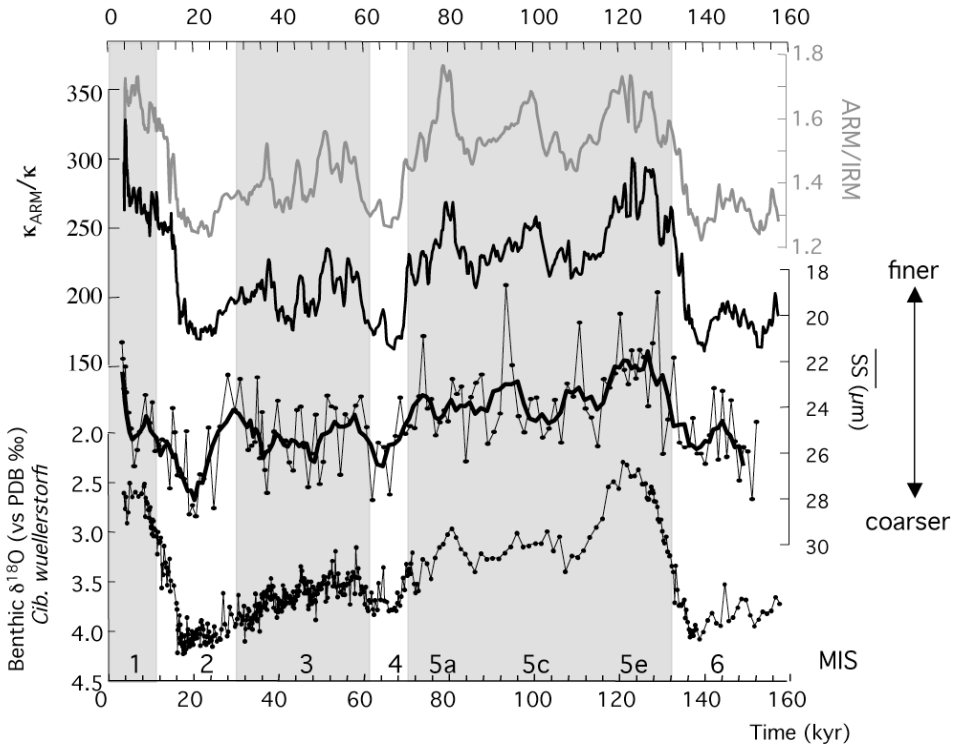

Fig. 11: comparison of temporal variations in the mean size of sortable silt and magnetic fraction with the benthic $\delta^{18}O$ curve in Core MD06-3067. The vertical scale for sortable silt has been inverted to report the finer grains upward and the coarser ones downward.

We note however, that McCave et al., (2008) inferred near-constant glacial-interglacial water mass structure and vigor of inflow from depth profiles (1200 to 4800 m water depth) of benthic $\delta^{13}C$ and sortable silt size on North Chatham Rise.

While the precise origin of bottom currents off Mindanao is somewhat ill-constrained (see above), the close match between benthic $\delta^{18}O$ and records of bottom flow speed yields evidence for a close coupling between global climate and deep circulation in the western equatorial Pacific on at least orbital timescales. The records and interpretation presented here are consistent with some, but not all reconstructions of Deep Western Boundary Current ventilation and flow speed. Efforts are underway to better constrain the chemical properties, and thus the origin of the near bottom water masses off Mindanao.

In summary, two main conclusions are drawn from this investigation of the long-term changes in the sedimentary parameters of core MD06-3067. First, significant changes in the run-off from Mindanao island as documented by variations in the concentration of the magnetic fraction are clearly linked to a combined effect of precession and obliquity. This implies that the summer monsoon intensity in this region is controlled by both orbital cycles. The antiphase between orbital and proxy records constitutes the first experimental evidence that this area is subject to a shift of the rain belt with lower precipitation rates during northern summer insolation maxima. This is consistent with the results obtained from GCM simulations. Second, records of sortable silt mean size and magnetic grain sizes provide valuable information about the strength of bottom currents on an orbital scale. Both proxies indicate stronger glacial deepwater flow compared to interglacial times, typical of a southern source type signal.

Acknowledgments

We are very grateful to the crew of the R.V. *Marion Dufresne,* who helped us a lot during the cruise under the command of Captain J. P. Hedrich. We also thank all the team from the French Polar Institute (IPEV). This cruise is part of the IMAGES program. We are grateful to Camille Wandres (LSCE) who helped with the measurements of the magnetic properties and to Aurélie Van Toer (LSCE) for her participation to the sortable silt measurements. A. Hill and A. Roy (Dalhousie Univ.) helped with the grain size analyses. U. Röhl and colleagues at Marum (Bremen University) gave valuable advice for using their Avaatech XRF scanner. Ph.Robion (Univ. Cergy) helped with the statistical treatment of the magnetic anisotropy data. We are grateful to L. Vigliotti and an anonymous reviewer for their advices to improve the manuscript. Funds for laboratory analyses in France were provided by the French Atomic Energy Commission and the Centre National de la Recherche Scientifique. Analytical work at Dalhousie was funded by NSERC Canada and the Canadian Institute for Advanced Research CIFAR). In Germany, analyses were funded by the German Research Foundation (DFG) through the grant number Ku649/26-1. This is LSCE Contribution 4201.

Appendix

The low field susceptibility was systematically measured on all the cores on board the V. *Marion Dufresne* during the MD155-Marco Polo2 cruise. The measurements were made with a Bartington point sensor, sensitive to the very first millimeter at the surface of the sediment. In order to get more representative data, although at lower resolution, we measured again the low field magnetic susceptibility in the laboratory at LSCE on u-channels with a 45-mm diameter MS2-C Bartington coil. The data were generated every 2 cm with a resolution close to 4 cm and they were normalized by the volume to get the volume susceptibility (κ).

The natural remanent magnetization (NRM) was measured using a 755-R 2G cryogenic pass-through magnetometer, equipped with a high resolution set of coils and placed in the μ-metal shielded room of LSCE. An in-line alternating field (AF) demagnetization unit was used for the stepwise demagnetization at 5, 10, 15, 20, 25, 30, 35, 40, 50, 60 and 80 mT. After demagnetization at 80 mT, about 97% of the initial magnetization was removed. Measurements were made every 2 cm with a resolution of about 4 cm. The direction of the Characteristic Remanent Magnetization (ChRM) was determined using principal component analysis through the results obtained from the demagnetization process (Kirschvink, 1980; Mazaud, 2005). For this calculation, we used 10 steps of demagnetization except at very few horizons where we used 9 steps. MAD angles very rarely exceed 5° (with a maximum at 8°) showing that the direction of magnetization is very stable upon demagnetization.

The Anhysteretic Remanent (ARM) and Isothermal Remanent (IRM) magnetizations were acquired and demagnetized also on u-channels using the same method and instruments. ARM was acquired along the vertical geographic axis in a peak alternating field of 100 mT and a steady bias field of 50 μT. During acquisition, the sampled were translated through the coils at a speed of about 1 cm/s, following Brachfeld et al., (2004). After acquisition, the ARM was then progressively demagnetized using 10 steps at 10, 15, 20, 25, 30, 35, 40, 50, 60, and mT. Saturated IRM (SIRM) was then acquired, also along the vertical geographical axis in six steps (0.05, 0.1, 0.2, 0.3, 0.5 and 1 T) using a 2G 1.6 m long pulsed solenoid. Backfield to 0.3 T was applied after saturation in order to calculate the S-ratio ($S_{-0.3T}$ = abs($IRM_{-0.3T}$/IRM_{1T})). SIRM was stepwise demagnetized using 10 steps (5, 10, 20, 25, 30, 35, 40, 50, 60, 80 mT). During the demagnetization of NRM, ARM and IRM, the u-

channels were translated at a speed of about 4 cm/s through the demagnetization coils. All the data were acquired using softwares developed at LSCE, which allow to considerably reduce the translation speed during the measurements, while the u-channel passes through the pick-up coil. This is particularly adapted to the measurements of very high magnetizations because the reduced translation speed allows to reliably count the flux jumps.

From the ARM and IRM stepwise demagnetizations, we could calculate the median destructive fields of these two remanent magnetizations. They are labeled Hmd_{ARM} and Hmd_{IRM}. Together with the S-ratio, they both give information about the coercivity spectrum of the magnetic particles included in the sediment.

ARM, κ and IRM were used to estimate changes in the average magnetic grain size. To calculate the ratio ARM/κ ratio, the ARM data are presented as an anhysteretic susceptibility (κ_{ARM}) by normalizing ARM by the DC biasing field.

Small chips were also taken at the surface of the sediment, at 10 cm intervals. After drying, they were used for the measurements of the hysteresis parameters using an AGM 2900 from Princeton Measurements Corporation. The hysteresis loops were made between +1 and –1 T. After adjustment of the high field slope, giving access to the high field magnetic susceptibility, the saturation magnetization (Ms), the remanent saturation magnetization (Mrs), the coercitive field (Hc) were calculated. Ms and Mrs were normalized by the mass of the sample. The remanent coercitive field (Hcr) was then determined by a remanent curve starting by a saturation at 1T followed by a stepwise decreasing field, opposed to the saturating one.

AMS is described by a symmetric tensor of second rank which in turn may be visualized as an ellipsoid with principal axes K_{max}, K_{int}, K_{min} ($K_{max}>K_{int}>K_{min}$). Depending on the magnetic minerals, AMS reflect the orientation of elongated particles or crystal lattices. Magnetites have a weak crystalline anisotropy and their shape anisotropy is dominant with the maximum susceptibility aligned with the long axis of the grain. The analysis of the magnetic fabric thus provides information about the preferential alignment of the elongated magnetite grains in the sediment. AMS measurements were made in Core MD06-3067 using cubic samples with a KLY-3 Agico anisotropy spinner magnetometer. We have carefully checked that there is no relation between the lineation and the direction along which the samples were pushed into the sediment, so the observed lineation is not related to our sampling technique.

The mean orientation of the principal axes of anisotropy was calculated using the method reported by Jelinek (1978).

All these parameters give access to the magnetic content of the sediments in terms of nature of the magnetic minerals, their grain size and their concentration (see text). Disaggregated inorganic grain size distributions (DIGS) were determined on the organic matter and carbonate-free (quantitatively removed by H_2O_2 and HCl, respectively) terrigenous sediment fraction using a Coulter Multisizer IIe electroresistance particle size analyzer. This Coulter Counter at Dalhousie University is equipped with 30, 140 and 400 um aperture tubes. Details of the analytical method are given in Curran et al., (2004). As per McCave et al., 1995), the sortable silt mean size (SS) presented here is defined as the mean of the 10-63 μm grain size range.

Chapter V: A mid-Holocene transition in the nitrogen dynamics of the western equatorial Pacific: Evidence of a deepening thermocline?

A mid-Holocene transition in the nitrogen dynamics of the western equatorial Pacific: Evidence of a deepening thermocline?

M. Kienast,[1] M. F. Lehmann,[2,3] A. Timmermann,[4] E. Galbraith,[5] T. Bolliet,[6] A. Holbourn,[6] C. Normandeau,[1] and C. Laj[7]

[1]Department of Oceanography, Dalhousie University, Halifax, Nova Scotia, Canada.

[2]GEOTOP, Universite«du Que«bec a` Montre«al, Montreal, Quebec, Canada.

[3]Now at Institute for Environmental Geoscience, Universität Basel, Basel, Switzerland.

[4]International Pacific Research Center, School of Ocean and Earth Science Technology, University of Hawai'i at Manoa, Honolulu, Hawaii, USA.

[5]Atmospheric and Oceanic Sciences, Princeton University, Princeton, New Jersey, USA.

[6]Institut für Geowissenschaften, CAU Universität, Kiel, Germany.

[7]Laboratoire des Sciences du Climat et de l'Environnement, CNRS, Gif-sur-Yvette, France.

Geophysical Research Letters, VOL. 35, L23610, 5 PP., 2008
doi:10.1029/2008GL035464 accepted 23 October 2008.

Abstract

Sedimentary $\delta^{15}N$ records from the oligotrophic western equatorial Pacific (WEP) off Mindanao show that late Holocene sedimentary $\delta^{15}N$ is substantially lower than that of the early Holocene, following a gradual >3 ‰ decrease that occurred between 7 and 3 kyrs ago. Analyses of modern day nitrate isotope profiles from the same region indicate the sensitivity of the WEP N pools towards (1) the advection of $\delta^{15}N$ -enriched nitrate from the Eastern Equatorial Pacific (EEP) by the North Equatorial Current (NEC) and the Mindanao Current in subsurface waters and, (2) at shallow depths, the input of new and ^{15}N-depleted nitrate through N_2 fixation. We suggest that the Holocene decrease in sedimentary $\delta^{15}N$ reflects a diminished relative input of ^{15}N-enriched nitrate to the surface biota, either through an increase of regional nitrogen fixation, a change in nitrate consumption along the advective path of nitrate supply, or a decrease in the vertical supply of ^{15}N-enriched nitrate from the NEC. The latter mechanism is consistent with a Holocene deepening of the WEP nitracline/thermocline.

1 – Introduction

The equatorial Pacific is fundamental to Earth's climate system, and has been purported to be instigator, amplifier and mediator of past global climate change on timescales ranging from inter-annual to orbital. Today, the El Niño Southern Oscillation (ENSO) dominates the inter-annual variability of the tropical Pacific, with teleconnections affecting climate conditions worldwide, and it has thus been proposed that past global climate change on centennial to orbital time-scales could have been modulated by "ENSO-like" variations in the mean state of the tropical Pacific. However, many reconstructions of past ENSO variability rely exclusively on sea surface temperature (SST) or sea surface salinity (SSS) reconstructions in the eastern and western equatorial Pacific. This is problematic due to the inherent uncertainty of SSS reconstructions, multiple causes of SST variability, and, not least, to the potential non-stationarity of ENSO-related climatic teleconnections (Bush, 2007).

The western equatorial Pacific (WEP) is considered to be an oligotrophic part of the ocean, where much of the nitrate is advected laterally from the eastern equatorial Pacific (EEP) (Peña et al., 1994; Turk et al., 2001), and interannual changes in vertical nitrate supply to the WEP euphotic zone are determined by the depth of the nitracline/thermocline, which itself is intimately linked with ENSO (Turk et al., 2001). Reconstructions of temporal variations in nitrate availability and supply in the WEP could thus provide a means of elucidating past variations in WEP thermocline depth and equatorial circulation, critical descriptors of the mean state of the tropical Pacific Ocean. Here we use modern water column profiles of the nitrogen and oxygen isotopic composition of nitrate in the WEP to provide calibration of the biogeochemical processes that drive N-transformations in the WEP today. High-resolution sedimentary $\delta^{15}N$ records from the WEP off Mindanao are presented in an attempt to elucidate Holocene variations in the WEP water column structure and circulation.

2 – Materials and Methods

Sediment cores MD98-2181 (6°18′N/125°49′E, 2114 m water depth), MD06-3067 (6°31′N/126°30′E, 1574 m water depth), and MD06-3075 (6°29′N/125°52′E, 1878 m water depth) were recovered during IMAGES expeditions aboard the Marion

Dufresne in 1998 and 2006, respectively, at three different sites in the WEP off Mindanao, SE Philippines (see Fig. S1 of the auxiliary material). Sites 81 and 75 are located inside the Bay of Davao, whereas site 67 is more open oceanic. The water column samples were retrieved close to the two core sites (station 1, outside the bay at 6°28′N/126°28′E, and station 2, inside the bay at 6°28′N/125°52′E) by hydrocast during the 2006 expedition. Water samples were immediately filtered (0.2 μm) and frozen at −80° C on board.

Natural abundance nitrate N and O isotope ratio measurements (denoted as $\delta^{15}N$ and $\delta^{18}O$, with $\delta = [(R_{sample}/R_{standard})-1) \times 1000$, where R represents the ratio of ^{15}N to ^{14}N or ^{18}O to ^{16}O, respectively) were performed using the "denitrifier method" (Casciotti et al., 2002; Sigman et al., 2001) (see auxiliary material for details). N and O isotope ratios are reported in ‰ relative to atmospheric N_2 for N and V-SMOW for O isotopes, respectively. The reproducibility of the method (based on duplicate measurements of standards and samples) is generally better than ±0.2‰ for $\delta^{15}N$ and ±0.5‰ for $\delta^{18}O$.

Sedimentary $\delta^{15}N$ was analyzed on dried, homogenized bulk sediment samples on an elemental analyzer coupled to a Finnigan Delta plus mass spectrometer at the Pacific Centre for Isotopic and Geochemical Research, UBC Vancouver, following standard procedures. Analytical precision of this method is better than ±0.2‰.

The age model for core MD98-2181 is adopted from Stott et al., (2004). For cores MD06-3067 and MD06-3075, the age models are based on aligning the planktonic foraminiferal oxygen isotope records (Bolliet et al., 2011) with the record from site 81, independently corroborated by ^{14}C dates. For site 67, the thus derived age model reveals that the top-most 3.5–4 kyrs were not recovered during coring operation. According to these age models, average sedimentation rates during the last 10 kyrs are ca. 14 cm/kyr at site 67, ca. 65 cm/kyr at site 75, and ca. 85 cm/kyr at site 81.

3 – Results and Discussion

3.1. – Water Column

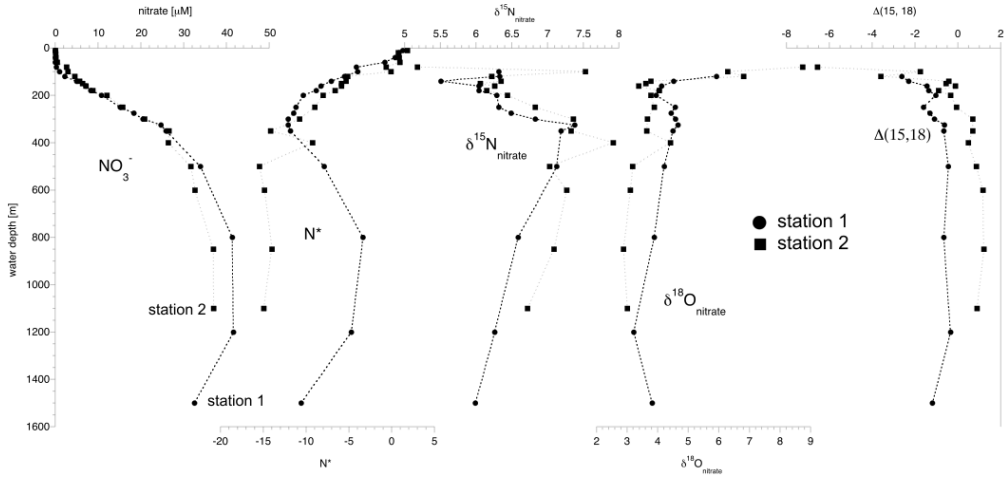

Fig. 1. Water column profiles of nitrate concentration, N* and the isotopic composition of nitrate (see text for definitions) at two sites off Mindanao. Station 1 (circle) is located close to site MD06-3067, station 2 (square) close to MD06-3075 inside the bay of Davao.

Both nitrate $\delta^{15}N$ and $\delta^{18}O$ below the mixed layer depth display values (Fig. 1; 6–8 ‰ for $\delta^{15}N$ and 3–5 ‰ $\delta^{18}O$) that are higher than the values for "mean" oceanic nitrate (5.5‰ and 2.5‰, respectively (e.g., Casciotti et al., 2002)) (see auxiliary materials for further details). The elevation above these mean oceanic nitrate isotope values, along with the comparatively low N* (N* = N−16 × P + 2.9 mmol m^{-3}; Fig. 1), can be explained by the advection of water masses that carry the geochemical signatures of water column denitrification, and originate in the Eastern Tropical Pacific (e.g., Sigman et al., 2005). This interpretation is consistent with previous studies suggesting import of ^{15}N enriched nitrate from the EEP to the WEP (Yoshikawa et al., 2006).

Consistent with a higher degree of partial denitrification (i.e., lower N* values), the ^{15}N-enrichment is more pronounced at Station 2 (Fig. 1). Towards the surface, in association with the decrease in nitrate to concentrations below the detection limit, nitrate $\delta^{18}O$ increases at both stations, in agreement with isotope fractionation (i.e., the preferential consumption of nitrate containing the lighter isotope ^{16}O) associated with nitrate uptake by phytoplankton (Casciotti et al., 2002). The $\delta^{15}N$, on the other hand, decreases as we approach nitrate-free surface waters. Based on previous studies (e.g., Casciotti et al., 2002; Lehmann et al., 2005), we would expect a parallel

evolution of nitrate $\delta^{15}N$ and $\delta^{18}O$ during algal nitrate uptake, with a ratio of ^{15}N to ^{18}O close to unity (see also auxiliary material). The decoupling of nitrate N and O isotope gradients (Fig.s 1 and S2) thus suggests the importance of additional N-transforming processes at the surface besides nitrate assimilation. The degree of the N-to O-isotope decoupling (i.e., the N-to-O isotope anomaly, or deviation from a 1:1 variation in $\delta^{15}N$ and $\delta^{18}O$) can be quantified using the approach of Sigman et al., (2005):

$$\Delta (15,18) = (\delta^{15}N - \delta^{15}N_m) - (\delta^{18}O - \delta^{18}O_m)$$

where $\delta^{15}Nm$ and $\delta^{18}Om$ are the mean $\delta^{15}N$ and $\delta^{18}O$ of deep water, respectively. We assigned values of 5.5 ‰ for $\delta^{15}Nm$ and 2.5 ‰ for $\delta^{18}Om$. A negative $\Delta(15,18)$ indicates a decrease (or lesser increase) in nitrate $\delta^{15}N$ relative to the $\delta^{18}O$. At both stations, surface waters are characterized by a clear negative nitrate isotope anomaly, with a decreasing trend in $\Delta(15,18)$ towards the ocean surface (Fig. 1).

Here we do not attempt a quantitative interpretation of the observed depth distribution of $\Delta(15,18)$ in the study area, because it would go beyond the scope of this paper. Several processes can theoretically lead to negative nitrate $\Delta(15,18)$ anomalies (e.g., nitrite re-oxidation (see Sigman et al., 2005; Casciotti and McIlvin, 2007)). Yet, details aside, the negative $\Delta(15,18)$ anomaly towards the surface is most consistent with the remineralization and accumulation of newly fixed nitrogen (see also auxiliary material). This regeneration of fixed N is expected to decrease the nitrate $\delta^{15}N$ while it does not significantly affect its $\delta^{18}O$ (relative to deep water nitrate) (Sigman et al., 2005; Bourbonnais et al., 2008). Following arguments made by Bourbonnais et al.,(2008), the discrepancy in magnitude of the surface nitrate isotope anomaly between Stations 1 and 2 may indicate spatial variations in the relative importance of N_2 fixation, with higher relative N_2 fixation rates at Station 2, where more negative $\Delta(15,18)$ values were measured. However, it needs to be noted that the interstation-variation in $\Delta(15,18)$ in the upper water column is partially due to the fact that the source waters from the thermocline already display different $\Delta(15,18)$. Thus, the spatial variation in the N_2 fixation rates may be less pronounced than is indicated by the upper water column $\Delta(15,18)$ at the two stations. The fact that we do not observe strongly positive N* values in the surface waters (as has been observed, for example, in the eastern subtropical N-Atlantic, e.g., Bourbonnais et al.,(2008)) does not a priori

argue against a strong contribution of N_2 fixation to total N export in the WEP, since the whole region is impacted by advective import of low-N* water masses from the EEP. Indeed, most probably, residual geochemical denitrification signatures imported from the east are partially offset by the input of newly fixed N. The $\delta^{15}N$ of the sedimentary organic matter reflects the relative contribution of either nitrate source (^{15}N-enriched nitrate from the thermocline versus ^{15}N-depleted N from N fixation).

3.2. – Sediment Record

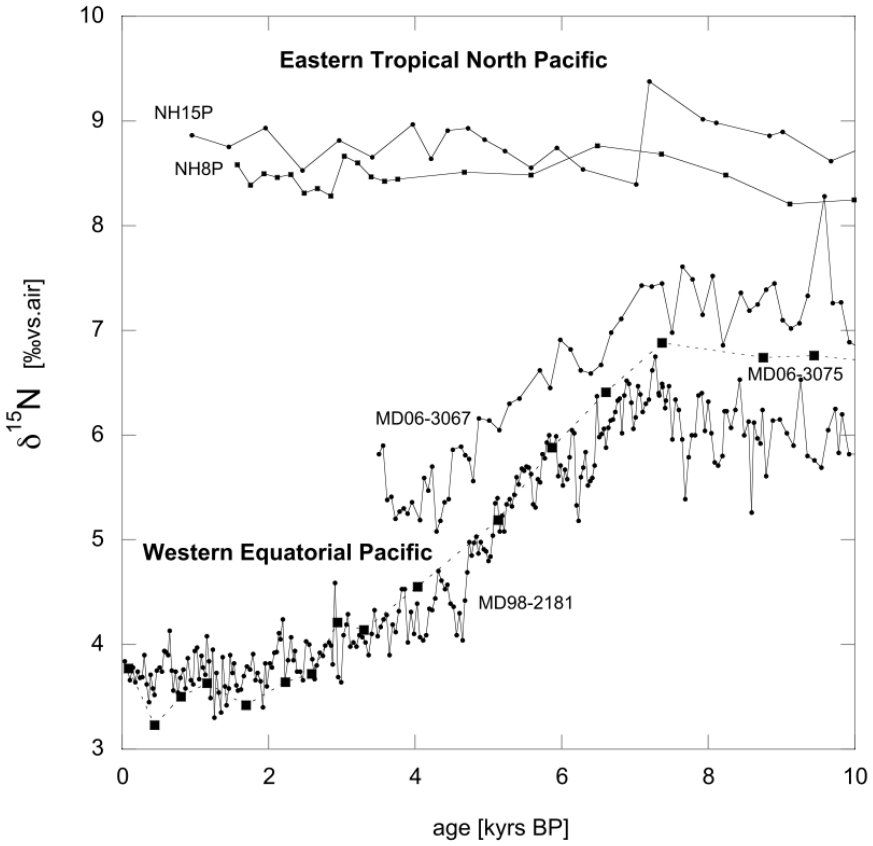

Fig. 2. Holocene $\delta^{15}N$ records from sites MD98-2181, MD06-3067, and MD06-3075 in the western equatorial Pacific compared to two records from the eastern equatorial Pacific off Mexico (NH8P and NH15P) (Ganeshram et al., 2000).

The bulk sedimentary $\delta^{15}N$ records from the western equatorial Pacific show stable values around 7 and 6 ‰, respectively, during the early Holocene (10-7 ka), followed by a > 3 ‰ decrease between 7 and 3 kyrs BP (Fig. 2). During the latest Holocene (not recovered at site 67, see above), $\delta^{15}N$ values are more or less constant around 3.5–4 ‰. Present-day N limitation (at comparatively low $\delta^{15}N$ values) suggests that

local N utilization has little impact on the bulk sedimentary $\delta^{15}N$ signal, and the lack of significant Holocene changes in chemical tracers of past productivity (TOC, biogenic opal, alkenone conc.; not shown) strongly suggests that variable local nitrate utilization is indeed an unlikely cause for the Holocene decrease. The similarity between the δ15N records at the three sites (Fig. 2) with very different sedimentation rates (see above) and proximity to terrigenous input also suggests that diagenetic overprint and/or variable inputs of organic or inorganic terrestrial N are not the prime cause of the Holocene decrease. The lower $\delta^{15}N$ values at sites 75 and 81 inside the bay are consistent with the dual nitrate isotopic signature suggesting a greater importance of N_2 fixation there (see above). Thus, sedimentary $\delta^{15}N$ in the study area is, indeed, reflective of the isotopic composition of the nitrate fueling phytoplankton production throughout the region.

Water column concentrations of O_2 today (e.g., Kashino et al., 1996) are well above the limit for local denitrification, and there is no evidence to indicate that this changed throughout the Holocene. While there are suggestions that the whole ocean nitrate $^{15}N/^{14}N$ may have reached a maximum value (1–2 ‰ greater than today) prior to 10 kyrs BP (e.g., Deutsch et al., 2004), this contrasts with the >3 ‰ decrease in sedimentary $\delta^{15}N$ off Mindanao that clearly occurs only after 7 kyrs BP. More importantly, sedimentary records from the Eastern Tropical North Pacific (ETNP), the most proximal water-column denitrification zone, are interpreted to reflect largely unchanged rates and extent of denitrification during the Holocene (cf. Ganeshram et al., 2000; Thunell and Kepple, 2004) (Fig. 2), which, in turn, implies a more or less constant N isotopic signature of the source of subsurface nitrate at the core sites in the WEP, in particular during the 7-3 kyrs interval. Four non-exclusive scenarios are entertained to explain the higher sedimentary $\delta^{15}N$ during the early Holocene: reduced rates of N_2 fixation; increased cumulative N utilization along the advective supply route of nitrate; intensified lateral advection of ^{15}N-enriched nitrate from the ETNP to the WEP; and increased vertical supply of ^{15}N-enriched nitrate to the photic zone. We elaborate upon, and evaluate, each of these hypotheses in turn.

1. Given the importance of N_2 fixation implied by the modern water column profiles (see above), higher $\delta^{15}N$ during the early Holocene could be indicative of reduced N_2 fixation rates then. Because there is presently no independent proxy to quantify past N_2 fixation rates, and forcing mechanisms of variations in N_2 fixation remain elusive, we cannot assess the importance of this factor in determining temporal variations in

sedimentary $\delta^{15}N$ off Mindanao. It is worth noting, however, that a reduced physical supply of nitrate to the photic zone between 7 and 3 kyrs BP, suggested by hypotheses (3) and (4), would have given N2-fixers an ecological advantage and may have shifted the balance of nitrogen nutrition towards newly fixed nitrogen.

2. The second scenario to explain the Holocene decrease in sedimentary $\delta^{15}N$ off Mindanao calls on a Holocene decrease in the "cumulative" N utilization along the advective nitrate supply route. The enrichment of $\delta^{18}O$-nitrate within near-surface waters shows that the nitrate supplied to phytoplankton here is a residuum of nitrate upwelled elsewhere, and circulated and partially consumed within the equatorial and subtropical circulation to some degree prior to delivery at the surface off Mindanao. Although the corresponding enrichment of $\delta^{15}N$-nitrate caused by this process is masked by modern N_2 fixation near the surface, past variations in the advective supply route could have modulated the cumulative N utilization component. A more pronounced utilization signature during the early Holocene could have been caused by variations in the ratio of macro- and micro-nutrients supplied to the photic zone, i.e., in the chemistry of the source waters (cf. Altabet, 2001), or by a change in the advective regime.

Assuming that the substantial Holocene decrease in $\delta^{15}N$ off Mindanao is not solely caused by these two biogeochemical factors, the higher early Holocene $\delta^{15}N$ values could be interpreted to reflect increased supply of ^{15}N-enriched NO_3^- from the EEP to the photic zone in the WEP, either laterally or vertically.

3. An increased lateral advection of 15N-enriched nitrate across the Pacific could be explained by a stronger North Equatorial Current (NEC) during the early Holocene, a change in the bifurcation of the NEC into the Mindanao Current (MC) and Kuroshio, or a deeper NEC in the EEP tapping into a zone of more intense denitrification there. While we have no means to assess the latter scenario, interannual variations observed today are used as analog to qualitatively discuss changes in the NEC transport and bifurcation and their effect on the MC transport. The NEC bifurcation latitude has only little effect on the MC transport (Kim et al., 2004), whereas the MC transport is highly correlated with NEC transport. The NEC transport, in turn, is driven in part by the northeasterly trade winds. To the extent that the easterly trade winds weaken with a more southerly position of the Intertropical Convergence Zone (ITCZ), the Holocene southward migration of the ITCZ (e.g., Haug et al., 2001) would thus point to a Holocene decrease in NEC, and thus MC, transport, in line with the Holocene

decrease in $\delta^{15}N$. This scenario is also consistent with the inferred Holocene decrease in sea surface salinities at site 81 (Stott et al., 2004) and in the WEP (de Garidel-Thoron et al., 2007). Reduced equatorial easterlies, however, would tend to shoal the WEP thermocline, which would increase the vertical supply of ^{15}N-enriched N (see below), and would thus counteract the effect of decreasing NEC transport.

4. Alternatively, the higher sedimentary $\delta^{15}N$ in the WEP during the early Holocene is reflective of an increase in the vertical supply of ^{15}N-enriched nitrate to the photic zone. This could have been caused by an overall shallower thermocline, an increase in upwelling associated with the Mindanao Dome (MD), or enhanced mixing through changes of the activity of westerly wind events and synoptic activity. Today, interannual variations in the strength of the Mindanao Dome appear to be caused by variations in the local upwelling due to positive curl associated with the Asian winter monsoon (Masumoto and Yamagata, 1991). Reconstructions of a Holocene increase in winter monsoon activity (e.g., Yancheva et al., 2007) thus render the latter cause of a Holocene decrease in the vertical supply of ^{15}N-enriched nitrate to the photic zone unlikely. We note, however, that ocean general circulation model analyses suggest a stronger MD upwelling associated with El Niño events (Christian et al., 2004). At the same time, the NEC transport also tends to intensify during El Niño (Qiu and Lukas, 1996), which would further increase the supply of ^{15}N-enriched N to the WEP photic zone (see above). A shallower early Holocene WEP thermocline as well as the link of the MD upwelling and NEC transport with ENSO events could thus be construed to reflect an intensification of the EEP cold tongue during the Holocene. A deeper late Holocene WEP thermocline inferred here is consistent with foraminiferal evidence from the WEP north of Papua New Guinea (de Garidel-Thoron et al., 2007) and with upper water column $\delta^{13}C$ and temperature gradients in core MD06-3067 (surface and thermocline dwelling foraminiferal stable isotope and Mg/Ca data (Bolliet et al., 2011). However, this scenario is incongruous with foraminiferal Mg/Ca SST reconstructions near the Galapagos Islands (Koutavas et al., 2002), and we note that analysis of present-day and mid-Holocene coupled general circulation model simulations conducted as part of the Paleomodel Intercomparison Project (Zheng et al., 2008) does neither reveal substantial changes of the mean thermocline in the Mindanao region, nor does it support the notion of a NEC weakening throughout the Holocene. It is tempting to speculate, however, that a Holocene deepening of the

WEP thermocline, suggested by the $\delta^{15}N$ records presented here, provided a necessary condition for ENSO variations to occur at all.

4 – Summary and Conclusion

Bulk sedimentary $\delta^{15}N$ records from the western equatorial Pacific display a >3 ‰ decrease between 7 and 3 kyrs BP, evidencing a significant decrease in the $\delta^{15}N$ of nitrate utilized during primary production. At the same time, water column nitrate isotope profiles at the coring sites show the presence of ^{15}N-enriched nitrate advected from the EEP at depth. While the data in hand do not provide conclusive evidence for the exact mechanisms responsible for the observed isotopic shift in the WEP, we argue here that they reflect variations in the balance between new production (N_2 fixation) and the production from advective and diffusive preformed nitrate sources. These two N-cycle processes may in turn be mechanistically linked in that a higher nitrate availability will attenuate N_2 fixation, generating positive feedbacks with regards to changes in the sedimentary $\delta^{15}N$. The Holocene decrease in sedimentary $\delta^{15}N$ off Mindanao could thus reflect an increased importance of local/regional N_2 fixation and/or a decrease in the cumulative impact of N utilization along the advective nitrate supply route. Alternatively, the sedimentary $\delta^{15}N$ records presented here could indicate a Holocene decrease in the vertical supply of ^{15}N-enriched nitrate to the photic zone, caused by a deepening of the thermocline in the WEP.

Acknowledgments

The samples used in this study were retrieved during IMAGES cruises of the R/V Marion Dufresne of the French Polar Institute (IPEV). We gratefully acknowledge L. Stott for providing sample material, A. Bourbonnais, B. Conard and K. Gordon for technical assistance, and two anonymous reviewers for constructive comments. This work was supported by IPEV, NSERC Canada, NSF (grant OCE00-81247), and a fellowship of the Canadian Institute for Advanced Research (CIFAR; M.K.).

General Conclusions

The climatic and oceanographic evolution of the western equatorial Pacific Ocean over the last 160 kyr was investigated through paleontological and geochemical analysis of calcareous microfossils and from two marine sedimentary cores, MD06-3067 and MD06-3075, recovered off Mindanao Island (Philippines).

The evolution of the upper water column structure within the inflow path of the Indonesian Throughflow was monitored using oxygen isotope analysis and paleotemperature reconstruction of surface and thermocline waters based on Mg/Ca analysis of the planktonic foraminifera *G. ruber* and *P. obliquiloculata* from Core MD06-3067. Results highlighted large amplitude variations in water masses temperature on glacial/interglacial and suborbital timescales, and the dominant influence of a regional upwelling system (Mindanao Dome) on the stratification of the upper water column. This study reveals major fluctuations in the thermal contrast between surface and thermocline water temperature during the last 160 kyrs, indicating particular a reduced contrast during MIS 4 and the LGM, in comparison to MIS 6, and unusually cool SSTs during the LGM, reflecting periods of intense activity of the Mindanao Dome. Enhanced activity of the dome during the LGM is corroborated by paleoproductivity records, based on benthic foraminiferal and coccolith assemblages, which provide evidence for higher surface productivity and substantially elevated carbon flux export to the seafloor.. The activity of the dome was however reduced during Antarctic war events A1-4, when high sea surface temperatures prevailed. The activity of the Mindanao Dome appears modulated by fluctuations in the latitudinal position of the ITCZ, in turn affecting monsoonal winds regimes and upper oceanic circulation in the Indo-Pacific region.

The geochemical properties of mid-depth water were reconstructed using stable isotopes of benthic foraminifera in Cores MD06-3067 and MD06-3075 over the last 160 and 25 kyrs, respectively. Benthic $\delta^{18}O$ results indicate similar amplitude and timing of the last deglaciation in the open Pacific Ocean (Core MD06-3067) and in the semi-enclosed Davao Gulf (MD06-3075). Benthic $\delta^{13}C$ data from Core MD06-3067, used as a tracer of past ocean circulation, indicate a long-term trend similar to

that exhibited in Core MD97-2120 from the Southern Ocean, reflecting the prevalent influence of AAIW in the western equatorial Pacific. However, this long-term trend was interrupted during terminations I and II by the occurrence of major troughs in benthic $\delta^{13}C$, which appear to reflect the abrupt incursions of ^{13}C-depleted mid-depth water originating from the North Pacific. These deglacial incursions of NPIW into the western equatorial Pacific suggest that a major re-organization in the latitudinal extent of mid-depth water masses occurred over the entire Pacific Ocean, possibly linked to significant fluctuations in the production rate of intermediate water during deglaciations. Comparison of benthic $\delta^{13}C$ data from Cores MD06-3067 and MD06-3075 indicate highly contrasted trends, indicating regional discrepancies between the intermediate circulation in the open Pacific Ocean and the relatively more isolated Davao Gulf separated from the open Pacific Ocean by a relatively shallow sill.

These results mark a step forward in understanding the evolution of the oceanic circulation in the Pacific Ocean during the late Pleistocene. However, futures studies, ideally comparing the co-evolution of the Indonesian Throughflow and the Kuroshio, are needed to provide further information on the evolution of the surface, intermediate and deep circulation in the western Pacific Ocean and on the long-term relationship between those two major current systems, originating from the North Equatorial Current. Investigation of the upper circulation in the Makassar Strait (mid-flow part of the ITF) and in the inflow part of the Mindanao Current would also provide essential information on the impact of the Mindanao Dome on the ITF inflow, although the recovery of high-quality cores is extremely challenging due to the complex seafloor topography and intricate interconnections between individual seas in the Australasian region. Additional studies focusing on the deeper circulation of the entire Pacific Ocean are also needed to more precisely monitor fluctuations in the production rates and latitudinal extent of intermediate and deep water over glacial/interglacial cycles, as results published during the last decade still remain highly divergent.

References

Altabet, M. A. (2001), Nitrogen isotopic evidence for micronutrient control of fractional NO_3^- utilization in the equatorial Pacific, *Limnol. Oceanogr., 46*, 368-380.

An, Z. S. (2000), The history and variability of the East Asian paleomonsoon climate, *Quaternary Sci. Rev.*, *19*(1-5), 171-187, doi:10.1016/S0277-3791(99)00060-8.

Anand, P., H. Elderfield, and M. H. Conte (2003), Calibration of Mg/Ca thermometry in planktonic foraminifera from a sediment trap time series, *Paleoceanography*, *18*(2), 1050, doi:10.1029/2002PA000846.

Antonov, J. I., R. A. Locarnini, T. P. Boyer, A. V. Mishonov, and H. E. Garcia (2006), World Ocean Atlas 2005, Volume 2: Salinity, in *NOAA Atlas NESDIS 61*, edited by S. Levitus, U.S. Government Printing Office, Washington, D.C., pp. 182.

Andruleit, H., and U. Rogalla (2002), Coccolithophores in surface sediments of the Arabian Sea in relation to environmental gradients in surface waters, *Mar. Geol.*, *186*(3-4), 505-526, doi:10.1016/S0025-3227(02)00312-2.

Arz, H. W., J. Patzold, and G. Wefer (1998), Correlated millennial-scale changes in surface hydrography and terrigenous sediment yield inferred from last-glacial marine deposits off northeastern Brazil, *Quaternary Res.*, *50*(2), 157-166, doi:10.1006/qres.1998.1992.

Barker, S., I. Cacho, H. Benway, and K. Tachikawa (2005), Planktonic foraminiferal Mg/Ca as a proxy for past oceanic temperatures: a methodological overview and data compilation for the Last Glacial Maximum, *Quaternary Sci. Rev.*, *24*(7-9), 821-834, doi:10.1016/j.quascirev.2004.07.016.

Beaufort, L., and D. Dollfus (2004), Automatic recognition of coccoliths by dynamical neural networks, *Mar. Micropaleontol.*, *51*(1-2), 57-73, doi:10.1016/j.marmicro.2003.09.003.

Beaufort, L., T. de Garidel-Thoron, A. C. Mix, and N. G. Pisias (2001), ENSO-like forcing on oceanic primary production during the Late Pleistocene, *Science*, *293*, 2440-2444, doi: 10.1126/science.293.5539.2440.

Beaufort, L., Y. Lancelot, P. Camberlin, O. Cayre, E. Vincent, F. Bassinot, and L. Labeyrie (1997), Insolation cycles as a major control equatorial Indian Ocean primary production, *Science*, *278*(5342), 1451-1454, doi:10.1126/science.278.5342.1451.

Bemis, B. E., H. J. Spero, J. Bijma, and D. W. Lea (1998), Reevaluation of the oxygen isotopic composition of planktonic foraminifera: Experimental results and revised paleotemperature equations, *Paleoceanography*, *13*(2), 150-160, doi:10.1029/98PA00070.

Bian, N., and P. A. Martin (2010), Investigating the fidelity of Mg/Ca and other elemental data from reductively cleaned planktonic foraminifera, *Paleoceanography*, *25*, PA2215, doi:10.1029/2009PA001796.

Bianchi, G. G., and I. N. McCave (1999), Holocene periodicity in North Atlantic climate and

deep-ocean flow south of Iceland, *Nature, 397*, 515-517, doi:10.1038/17362.

Bijma, J., W. W. Faber, and C. Hemleben (1990), Temperature and salinity limits for growth and survival of some planktonic foraminifers in laboratory cultures, *J. Foramin. Res.*, *20*(2), 95-116.

Bingham, F. M., and R. Lukas (1994), The southward intrusion of North Pacific intermediate water along the Mindanao Coast, *J. Phys. Oceanogr.*, *24*(1), 141-154.

Bjerknes, J. (1969), Atmospheric teleconnections from the equatorial Pacific, *Mon. Wea. Rev.* 97, 163-172.

Blunier, T., J. Chappellaz, J. Schwander, A. Dällenbach, B. Stauffer, T.F. Stocker, D. Raynaud, J. Jouzel, H. B. Clausen, C. U. Hammer, and S. J. Johnsen (1998), Asynchrony of Antarctic and Greenland climate change during the last glacial period, *Nature*, *394*(6695), 739-743, doi:10.1038/29447.

Bolliet, T., A. Holbourn, W. Kuhnt, C. Laj, C. Kissel, L. Beaufort, M. Kienast, N. Andersen, and D. Garbe-Schönberg (2011), Mindanao Dome variability over the last 160 kyr: Episodic glacial cooling of the West Pacific Warm Pool, *Paleoceanography*, 26, PA1208, doi:10.1029/2010PA001966.

Bond, G., W. Broecker, S. Johnsen, J. Mcmanus, L. Labeyrie, J. Jouzel, and G. Bonani (1993), Correlations between Climate Records from North-Atlantic Sediments and Greenland Ice, *Nature*, *365*(6442), 143-147, doi:10.1038/365143a0.

Bostock, H. C., B. N. Opdyke, M. K. Gagan, and L. K. Fifield (2004), Carbon isotope evidence for changes in Antarctic Intermediate Water circulation and ocean ventilation in the southwest Pacific during the last deglaciation, *Paleoceanography, 19,* PA4013, doi:10.1029/2004PA001047.

Boyle, E. A. (1986), Paired carbon isotope and cadmium data from benthic foraminifera: Implications for changes in oceanic phosphorous, oceanic circulation, and atmospheric carbon dioxide. *Geochim. Cosmochim. Acta, 50*, 265-276.

Bourbonnais, A., M. F. Lehmann, J. J. Waniek, and D. E. Schulz-Bull (2009), Nitrate isotope anomalies reflect N_2 fixation in the Azores Front region (subtropical NE Atlantic), *J. Geophys. Res., 114,* C03003, doi:10.1029/2007JC004617.

Brachfeld, S., C. Kissel, C. Laj, and A. Mazaud (2004), Viscous behavior of U-channels during acquisition and demagnetization of remanences: Implications for paleomagnetic and rock-magnetic investigations, *Phys. Earth Planet. Int., 145*, 1-8, doi:10.1016/j.pepi.2003.12.011.

Braconnot, P., C. Marzin, L. Gregoire, E. Mosquet, and O. Marti (2008), Monsoon response to changes in Earth's orbital parameters: comparisons between simulations of the Eemian and of the Holocene, *Clim. Past Discuss., 4*, 459-493, doi:10.5194/cpd-4-459-2008.

Broecker, W. S. (1982), Ocean Chemistry during Glacial Time, *Geochim. Cosmochim. Ac.*,

46(10), 1689-1705.

Broecker, W. S., W. C. Patzert, J. R. Toggweiler, and M. Stuiver (1986), Hydrography, chemistry and radioisotopes in the Southeast Asian Basins. *J. Geophys. Res., 91*, 14345-14354.

Broecker, W. S., E. Clark, J. Lynch-Stieglitz, W. Beck, L. D. Stott, I. Hajdas, and G. Bonani (2000), Late glacial diatom accumulation at 9°S in the Indian Ocean, *Paleoceanography*, *15*(3), 348-352, doi:10.1029/1999PA000439.

Bush, A. B. G. (2007), Extratropical influences on the El Niño-Southern Oscillation through the late Quaternary, *J. Clim., 20*, 788-800, DOI:10.1175/JCLI4048.1.

Cannariato, K. G., J. P. Kennett, and R. J. Behl (1999), Biotic response to late Quaternary rapid climate switches in Santa Barbara Basin: Ecological and evolutionary implications, *Geology*, *27*(1), 63-66, doi: 10.1130/0091-7613(1999)027<0063:BRTLQR>2.3.CO;2.

Casciotti, K. L., and M. R. McIlvin (2007), Isotopic analyses of nitrate and nitrite from reference mixtures and application to eastern tropical North Pacific waters, *Mar. Chem., 107*, 184-201, doi:10.1016/j.marchem.2007.06.021.

Casciotti, K. L., D. M. Sigman, M. Galanter Hastings, J. K. Böhlke, and A. Hilkert (2002), Measurement of the oxygen isotopic composition of nitrate in seawater and freshwater using the denitrifier method, *Anal. Chem., 74*, 4905-4912, doi: 10.1021/ac020113w.

Chen, F. H., Z. D. Feng, and J. W. Zhang (2000), Loess particle size data indicative of stable winter monsoons during the last interglacial in the western part of the Chinese Loess Plateau, *Catena, 39*(4), 233-244, doi:10.1016/S0341-8162(00)00083-7.

Christian, J. R., R. Murtugudde, J. Ballabrera-Poy, and C. R. McClain (2004), A ribbon of dark water: Phytoplankton blooms in the meanders of the Pacific North Equatorial Countercurrent, *Deep Sea Res., Part II, 51*, 209-228, doi:10.1016/j.dsr2.2003.06.002.

Clark, P. U., N. G. Pisias, T. F. Stocker, and A. J. Weaver (2002), The role of the thermohaline circulation in abrupt climate change, *Nature*, *415*(6874), 863-869, doi:10.1038/415863a.

Clement, A. C., M. A. Cane, and R. Seager (2001), An orbitally driven tropical source for abrupt climate change, *J. Climate*, *14*(11), 2369-2375, doi: 10.1175/1520-0442(2001)014<2369:AODTSF>2.0.CO;2.

Cléroux, C., E. Cortijo, J.-C. Duplessy, and R. Zahn (2007), Deep-dwelling foraminifera as thermocline temperature recorders, *Geochem. Geophys. Geosyst., 8*, Q04N11, doi:10.1029/2006GC001474.

CLIMAP (1976), Surface of Ice-Age Earth, *Science*, *191*(4232), 1131-1137.

Corliss, B. H. (1985), Microhabitats of benthic foraminifera within deep-sea sediments. *Nature, 314*, 435-438.

Curran, K. J., P. S. Hill, T. M. Schell, T. G. Milligan, and D. J. W. Piper (2004), Inferring the mass fraction of floc-deposited mud: Application to fine-grained turbidites. *Sedimentology, 51*, 927-944, doi: 10.1111/j.1365-3091.2004.00647.x.

Curry, W. B., J. -C. Duplessy, L. D. Labeyrie, and N. J. Shackleton (1988), Changes in the distribution of $\delta^{13}C$ of deep water ΣCO_2 between the last glaciation and the Holocene. *Paleoceanography, 3*, 317-341

Dannenmann, S., B. K. Linsley, D. W. Oppo, Y. Rosenthal, and L. Beaufort (2003), East Asian monsoon forcing of suborbital variability in the Sulu Sea during Marine Isotope Stage 3: Link to Northern Hemisphere climate, *Geochem. Geophys. Geosyst., 4*(1), 1001, doi:10.1029/2002GC000390.

Day, R., M. Fuller, and V. A. Schmidt (1977), Hysteresis properties of titano-magnetite: grain-size and compositional dependence. *Phys. Earth Planet. Int., 13*, 260-267.

Ellwood, B.B., and M.T. Ledbetter (1977), Antarctic bottom water fluctuations in the Vema Channel: effects of velocity changes on particle alignment and size, *Earth Planet. Sci. Lett.*, *35*, 189-198.

De Deckker, P., N. J. Tapper, and S. van der Kaars (2003), The status of the Indo-Pacific Warm Pool and adjacent land at the Last Glacial Maximum, *Global Planet. Change*, *35*(1-2), 25-35, doi:10.1016/S0921-8181(02)00089-9.

de Garidel-Thoron, T., L. Beaufort, B. K. Linsley, and S. Dannenmann (2001), Millennial-scale dynamics of the east Asian winter monsoon during the last 200,000 years, *Paleoceanography*, *16*(5), 491-502, doi:10.1029/2000PA000557.

de Garidel-Thoron, T., Y. Rosenthal, F. Bassinot, and L. Beaufort (2005), Stable sea surface temperatures in the western Pacific warm pool over the past 1.75 million years, *Nature*, *433*(7023), 294-298, doi:10.1038/nature03189.

de Garidel-Thoron, T., Y. Rosenthal, L. Beaufort, E. Bard, C. Sonzogni, and A. C. Mix (2007), A multiproxy assessment of the western equatorial Pacific hydrography during the last 30 kyr, *Paleoceanography, 22*(3), PA3204, doi:10.1029/2006PA001269.

de Villiers, S., M. Greaves, and H. Elderfield (2002), An intensity ratio calibration method for the accurate determination of Mg/Ca and Sr/Ca of marine carbonates by ICP-AES, *Geochem. Geophys. Geosyst.*, *3*(1), 1001, doi:10.1029/2001GC000169.

Defant, A. (1929), Dynamische Ozeanographie, *Springer, New York.* 222 pp.

Dekens, P. S., D. W. Lea, D. K. Pak, and H. J. Spero (2002), Core top calibration of Mg/Ca in tropical foraminifera: Refining paleotemperature estimation, *Geochem. Geophys. Geosyst., 3*(4), 1022-1051, doi:10.1029/2001GC000200.

Deutsch, C., D. M. Sigman, R. C. Thunell, A. N. Meckler, and G. H. Haug (2004), Isotopic constraints on glacial/interglacial changes in the oceanic nitrogen budget, *Global Biogeochem. Cycles, 18*, GB4012, doi:10.1029/2003GB002189.

Ding, X., F. Guichard, F. Bassinot, L. Labeyrie, and N. Q. Fang (2002), Evolution of heat transport pathways in the Indonesian Archipelago during last Deglaciation, *Chinese Science Bulletin 47* (22), 1912-1917, doi: 10.1360/02tb9418.

Dollfus, D., and L. Beaufort (1999), Fat neural network for recognition of position normalised objects, *Neural Networks*, *12*(3), 553-560, doi:10.1016/S0893-6080(99)00011-8.

Duplessy, J. -C., M. Arnold, E. Bard, E. Cortijo, L. Labeyrie, C. Laj, B. Lehman, A. Mazaud, M. Paterne, N. Tisnerat, and L. Vidal (1998), Le carbone 14 : progrès récents et limitations de la méthode de datation. In: Causse, C. and F. Gasse, Editors, 1998. *Hydrologie et Géochimie Isotopique, ORSTOM, Paris*, 229-250.

Duplessy, J. C., N. J. Shackleton, R. G. Fairbanks, L. Labeyrie, D. Oppo, and N. Kallel (1988), Deepwater source variations during the last climatic cycle and their impact on the global deepwater circulation, *Paleoceanography, 3*(3), 343-360, doi:10.1029/PA003i003p00343.

Duplessy, J. -C., N. J. Shackleton, R. K. Matthews, W. Prell, W. F. Ruddiman, M. Caralp, C. H. Hendy (1984), ^{13}C record of benthic foraminifera in the last interglacial ocean: implications for the carbon cycle and the global deep water circulation. *Quaternary Research, 21*, 225-243.

Dürkop, A., A. Holbourn, W. Kuhnt, R. Zuraida, N. Andersen, and P. M. Grootes (2008), Centennial-scale climate variability in the Timor Sea during Marine Isotope Stage 3, *Mar. Micropaleontol.*, *66*(3-4), 208-221, doi:10.1016/j.marmicro.2007.10.002.

Elderfield, H., and G. Ganssen (2000), Past temperature and delta ^{18}O of surface ocean waters inferred from foraminiferal Mg/Ca ratios, *Nature*, *405*(6785), 442-445, doi:10.1038/35013033.

Ennyu, A., and M. A. Arthur (2004), Early to middle Miocene paleoceanography in the southern high latitudes off Tasmania. In: Exon, N. F., J. P. Kennett, and M. J. Malone (eds.), The Cenozoic Southern Ocean: Tectonics, Sedimentation and Climate Change Between Australia and Antarctica, *Geophys. Monogr. Ser., 151*, 215-233.

Fairbanks, R. G., M. N. Evans, J. L. Rubenstone, K. Broad, M. D. Moore, C. D. Charles, (1997), Evaluating climate indices and their geochemical proxies measured in corals, *Coral Reefs, 16*, 93-100, doi: 10.1007/s003380050245.

Fairbanks, R. G., R. A. Mortlock, T. C. Chiu, L. Cao, A. Kaplan, T. P. Guilderson, T. W. Fairbanks, A. L. Bloom, P. M. Grootes, and M. J. Nadeau (2005), Radiocarbon calibration curve

spanning 0 to 50,000 years BP based on paired $^{230}Th/^{234}U/^{238}U$ and ^{14}C dates on pristine corals, *Quaternary Science Reviews, 24*(16-17), 1781-1796, doi:10.1016/j.quascirev.2005.04.007.

Farmer, E. C., A. Kaplan, P. B. de Menocal, and J. Lynch-Stieglitz (2007), Corroborating ecological depth preferences of planktonic foraminifera in the tropical Atlantic with the stable oxygen isotope ratios of core top specimens, *Paleoceanography*, *22*, PA3205, doi:10.1029/2006PA001361.

Fine, R. A., R. Lukas, F. M. Bingham, M. J. Warner, and R. H. Gammon (1994), The western equatorial Pacific: A water mass crossroads, *J. Geophys. Res.*, 99(C12), 25,063-25,080, doi:10.1029/94JC02277.

Firing, E., Y. Kashino, and P. Hacker (2005), Energetic subthermocline currents observed east of Mindanao, *Deep Sea Research Part II: Topical Studies in Oceanography*, *52*(3-4), 605-613, doi:10.1016/j.dsr2.2004.12.007.

Freeland, H. J., A. S. Bychkov, F. Whitney, C. Taylor, C. S. Wong, and G. I. Yurasov. (1998), WOCE section P1W in the Sea of Okhotsk. 1. Oceanographic data description. *J. Geophys. Res. 103*:(C8). 15613-15623.

Ganeshram, R. S., T. F. Pedersen, S. E. Calvert, G. W. McNeill, and M. R. Fontugne (2000), Glacial-interglacial variability in denitrification in the World's Oceans: Causes and consequences, *Paleoceanography*, 15(4), 361-376, doi:10.1029/1999PA000422.

Gingele, F. X., P. De Deckker, and C. D. Hillenbrand (2001), Clay mineral distribution in surface sediments between Indonesia and NW Australia - source and transport by ocean currents, *Mar. Geol.*, *179*(3-4), 135-146, doi:10.1016/S0025-3227(01)00194-3.

Godfrey, J. S. (1996), The effect of the Indonesian throughflow on ocean circulation and heat exchange with the atmosphere: A review, *J. Geophys. Res.-Oceans*, *101*(C5), 12217-12237.

Gooday, A. J. (1993), Deep-sea benthic foraminiferal species which exploit phytodetritus: Characteristic features and controls on distribution, *Mar. Micropaleontol., 22*, 187-205, doi:10.1016/0377-8398(93)90043-W.

Gordon, A. L., (1986), Inter-ocean exchange of thermocline water. *J. Geoph. Res.-Oceans, 91*(C4): 5037-5046.

Gordon, A. L., and J. L. McClean (1999), Thermohaline stratification of the Indonesian Seas: Model and observations, *J. Phys. Oceanogr., 29*(2), 198-216, doi:10.1175/1520-0485 (1999)029<0198:TSOTIS>2.0.CO;2.

Gordon, A. L., R. D. Susanto, and K. Vranes (2003), Cool Indonesian throughflow as a consequence of restricted surface layer flow, *Nature*, *425*(6960), 824-828, doi:10.1038/nature02038.

Gordon, A. L. (2001), Interocean Exchange. Chapter 4.7. In: Ocean Circulation and Climate, G. Siedler, J. Church, and J. Gould (Eds.), *International Geophysics, 77*, Academic Press, 303-314, doi:10.1016/S0074-6142(01)80125-X.

Gordon, A. L. (2005), The Indonesian Seas: Oceanography of the Indonesian Seas and their throughflow, *Oceanography, 18*(4), 14-27.

Graham, N. E., and T. P. Barnett (1995), ENSO and ENSO-related predictability. Part II: Northern Hemisphere 700-mb height predictions based on a hybrid coupled ENSO model. *J. Climate, 8*, 544-549.

Greaves, M., S. Barker, C. Daunt, and H. Elderfield (2005), Accuracy, standardization, and interlaboratory calibration standards for foraminiferal Mg/Ca thermometry, *Geochem. Geophys. Geosyst., 6,* Q02D13, doi:10.1029/2004GC000790.

Greaves, M., et al.,(2008), Interlaboratory comparison study of calibration standards for foraminiferal Mg/Ca thermometry, *Geochem. Geophys. Geosyst., 9*, Q08010, doi:10.1029/ 2008GC001974.

Guillou, H., B. S. Singer, C. Laj, C. Kissel, S. Scaillet, and B. R. Jicha (2004), On the age of the Laschamp geomagnetic excursion, *Earth Planet. Sci. Lett., 227*(3-4), 331-343, doi:10.1016/j.epsl.2004.09.018.

Guo, Z. T., A. Berger, Q. Z. Yin, and L. Qin (2009), Strong asymmetry of hemispheric climates during MIS-13 inferred from correlating China loess and Antarctica ice records, *Clim. Past, 5*(1), 21-31, doi:10.5194/cp-5-21-2009.

Hall, I. R., G. G. Bianchi, and J. R. Evans (2004), Centennial to millennial scale Holocene climate-deep water linkage in the North Atlantic, *Quart. Sci. Rev., 23*, 1529-1536, doi:10.1016/j.quascirev.2004.04.004.

Hall, I. R., I. N. McCave, N. J. Shackleton, G. P. Weedon, S. E. Harri (2001), Intensified deep Pacific inflow and ventilation in Pleistocene glacial times, *Nature, 412,* 809-811, doi:10.1038/35090552.

Hamilton, N. D. and A. I. Rees (1970), The use of magnetic fabric in paleocurrent estimation, in: S.K. Runcorn Ed., *Paleogeophysics, Academic, Orlando, Fla.*, 445-464.

Haug, G. H., K. A. Hughen, D. M. Sigman, L. C. Peterson, and U. Rohl (2001), Southward migration of the intertropical convergence zone through the Holocene, *Science, 293*, 1304-1308, doi: 10.1126/science.1059725.

Hemleben, C., M. Spindler, and O. R. Anderson (1989), Modern Planktonic Foraminifera, Springer, New York, pp. 363.

Herguera, J. C., E. Jansen, and W. H. Berger (1992), Evidence for a Bathyal Front at 2000-M Depth in the Glacial Pacific, Based on a Depth Transect on Ontong Java Plateau, *Paleoceanography, 7*(3), 273-288, doi:10.1029/92PA00869.

Heron, S. F., E. J. Metzger, and W. J. Skirving (2006), Seasonal variations of the ocean surface circulation in the vicinity of Palau, *J. Oceanogr.*, *62*(4), 413-426, doi: 10.1007/s10872-006-0065-3.

Hirst, A. C., and J. S. Godfrey (1993), The Role of Indonesian Throughflow in a Global Ocean Gcm, .*J Phys. Oceanogr.*, *23*(6), 1057-1086.

Holbourn, A., W. Kuhnt, H. Kawamura, Z. Jian, P. Grootes, H. Erlenkeuser, and J. Xu (2005), Orbitally paced paleoproductivity variations in the Timor Sea and Indonesian Throughflow variability during the last 460 kyr, *Paleoceanography, 20*, PA3002, doi:10.1029/2004PA001094.

Hu D., M. C. Cui, T. Qu, and Y. X. Li (1991), A Subsurface Northward Current off Mindanao Identified by Dynamic Calculation. In K. Takanao, editor, Oceanography of Asian Marginal Seas, Elsevier, New York, *Oceanography, 54*, 359-365.

Hu D., M. C. Cui (1989), The Western Boundary Current in the Far-Western Pacific Ocean. In: Progress of Western International Meeting and Workshop on TOGA CORAE, May 24-30, Picaut J., R. Lukas, T. Delcroix, eds, Noumea, New Caledonia. 123-134.

J. Lynch-Stieglitz, and R. G. Fairbanks (1994), A conservative tracer for glacial ocean circulation from carbon isotope and paleonutrient measurements in benthic foraminifera. *Nature 369*, 308-310.

Jannink, N. T., W. J. Zachariasse, and G. J. Van der Zwaan (1998), Living (Rose Bengal stained) benthic foraminifera from the Pakistan continental margin (northern Arabian Sea), *Deep Sea Res., Part I, 45*(9), 1483-1513, doi:10.1016/S0967-0637(98)00027-2.

Jansen, J. H. F., S. J. Van der Gaast , B. Kostner, and A. J. Vaars (1992). CORTEX, a XRF-Scanner for chemical analyses of sediment cores. *GEOMAR Reports J5/Berichte-Reports, Geol. Paläont. Inst. Kiel 57* (ICP IV, Program & Abstracts, 155).

Jansen, J. H. F., S: J. Van der Gaast, B. Koster, and A. J. Vaars (1998), CORTEX, a shipboard XRF-scanner for element analyses in split sediment cores. *Marine Geology, 151*, 143-153.

Jelinek, V. (1978), Statistical processing of anisotropy of magnetic susceptibility measured on groups of specimens. *Studia geoph. geod., 22*, 50-62.

Jorissen, F. J., H. C. de Stigter, and J. G. V. Widmark (1995), A conceptual model explaining benthic foraminiferal microhabitats. *Marine Micropaleontology 26*, 3-15.

Kalnay, E., et al.,(1996), The NCEP/NCAR 40 Year Reanalysis Project, *Bull. Am. Meteorol. Soc., 77*(3), 437-471, doi:10.1175/1520-0477 (1996)077<0437:TNYRP>2.0.CO;2.

Kashino, Y., A. Ishida, and Y. Kuroda (2005), Variability of the Mindanao Current: Mooring observation results, *Geophys. Res. Lett.*, *32*(18), doi:10.1029/2005GL023880.

Kashino, Y., M. Aoyama, T. Kawano, N. Hendiarti, Syaefudin, Y. Anantasena, K. Muneyama, and H. Watanabe (1996), The water masses between Mindanao and New Guinea, *J. Geophys. Res., 101*, 12391-12400.

Kawamura, H., A. Holbourn, and W. Kuhnt (2006), Climate variability and land-ocean interactions in the Indo Pacific Warm Pool: A 460-ka palynological and organic geochemical Record from the Timor Sea, *Mar. Micropaleontol., 59*, 1-14, doi:10.1016/j. marmicro.2005.09.001.

Keigwin, L. D., (1987), North Pacific deep water formation during the latest glaciation. *Nature, 330* (362-364). 401-427.

Kienast, M., M. F. Lehmann, A. Timmermann, E. Galbraith, T. Bolliet, A. Holbourn, C. Normandeau, and C. Laj (2008), A mid-Holocene transition in the nitrogen dynamics of the western equatorial Pacific: Evidence of a deepening thermocline?, *Geophys. Res. Lett., 35*, L23610, doi:10.1029/2008GL035464.

Kienast, M., S. Steinke, K. Stattegger, and S. E. Calvert (2001), Synchronous tropical South China Sea SST change and Greenland warming during deglaciation, *Science, 291*, 2132-2134, doi:10.1126/science.1057131.

Kim, Y. Y., T. Qu, T. Jensen, T. Miyama, H. Mitsudera, H.-W. Kang, and A. Ishida (2004), Seasonal and interannual variations of the North Equatorial Current bifurcation in a high-resolution OGCM, *J. Geophys. Res., 109*, C03040, doi:10.1029/2003JC002013.

King, J. W., S. K. Banerjee, J. Marvin and Ö. Özdemir (1982), A comparison of different magnetic methods for determining the relative grain size of magnetite in natural materials: some results from lake sediments. *Earth Planet. Sci. Lett., 59*, 404-419.

Kirschvink, J. L. (1980), The least-squares line and plane and the analysis of paleomagnetic data, *Geophys. J. Roy. Astron. Soc., 62,* 699-718

Kissel, C., C. Laj, B. Lehman, L. Labeyrie, V. Bout-Roumazeilles (1997), Changes in the strength of the Iceland-Scotland Overflow Water in the last 200,000 years: Evidence from magnetic anisotropy analysis of core SU90-33, *Earth Planet. Sci. Lett. 152*, 25-36.

Kissel, C., C. Laj, M. Kienast, T. Bolliet, A. Holbourn, P. Hill, W. Kuhnt, and P. Braconnot (2010), Monsoon variability and deep oceanic circulation in the western equatorial Pacific over the last climatic cycle: Insights from sedimentary magnetic properties and sortable silt, *Paleoceanography, 25*, PA3215, doi:10.1029/2010PA001980.

Kissel, C., C. Laj, T. Mulder, C. Wandres, M. Cremer (2009), The magnetic fraction: a tracer of

deep water circulation in the North Atlantic, *Earth Planet. Sci. Lett., 288 (*3-4), 444-454, doi:10.1016/j.epsl.2009.10.005.

Knorr, G., and G. Lohmann (2003), Southern Ocean Origin for the resumption of Atlantic Thermohaline Circulation during Deglaciation. *Nature, 424*, 532-536, doi:10.1038/nature01855.

Koutavas, A., J. Lynch-Stieglitz, T. M. Marchitto, and J. P. Sachs (2002), El Niño-like pattern in ice age tropical Pacific sea surface temperature, *Science*, *297*(5579), 226-230, doi: 10.1126/science.1072376.

Kroopnick, P. M. (1985), The distribution of $\delta^{13}C$ of CO_2 in the world oceans, *Deep-Sea Res., 32*, 57-84.

Kuhlbrodt, T., A. Griesel, M. Montoya, A. Levermann, M. Hofmann, and S. Rahmstorf (2007), On the driving processes of the Atlantic meridional overturning circulation, *Rev. Geophys., 45*, RG2001, doi:10.1029/2004RG000166.

Kuhnt, W., S. Hess, and Z. M. Jian (1999), Quantitative composition of benthic foraminiferal assemblages as a proxy indicator for organic carbon flux rates in the South China Sea, *Mar. Geol., 156*(1-4), 123-157, doi:10.1016/S0025-3227(98)00176-5.

Labeyrie, L., and J. C. Duplessy (1985), Changes in the oceanic $^{13}C/^{12}C$ ratio during the last 140,000 years: High latitude surface records: *Palaeogeography, Palaeoclimatology, Palaeoecology, 3*, 217-240.

Laj, C., et al., (2006), Les rapports de campagnes à la mer: MD155-Marco Polo 2, IMAGES XIV cruise report, 11 juin au 6 juillet 2006, *Publ. Inst. Polaire Fr. OCE/2006/06, Publ. de Inst. Polaire Fr*., Brest, France.

Laskar, J., P. Robutel, F. Joutel, M. Gastineau, A. C. M. Correia, and B. Levrard (2004), A long-term numerical solution for the insolation quantities of the Earth, *Astron. Astrophys., 428*, 261-285, doi: 10.1051/0004-6361:20041335.

Lavrov, V. M., V. K. Nikolayeva, and M. S. Barash (1973), Titanium in the quaternary deposits of the Atlantic Ocean, *Oceanology, 13*, 57-62.

Lea, D. W., D. K. Pak, and H. J. Spero (2000), Climate impact of late quaternary equatorial Pacific sea surface temperature variations, *Science, 289*, 1719-1724, doi:10.1126/science. 289.5485.1719.

Lea, D. W., D. K. Pak, L. C. Peterson, and K. A. Hughen (2003), Synchroneity of tropical and high-latitude Atlantic temperatures over the last glacial termination, *Science, 301*, 1361-1364, doi:10.1126/science.1088470.

Lea, D. W., T. A. Mashiotta, and H. J. Spero (1999), Controls on magnesium and strontium uptake in planktonic foraminifera determined by live culturing, *Geochim. Cosmochim. Ac.*, *63*(16), 2369-

2379, doi:10.1016/S0016-7037(99)00197-0.

Leduc, G., L. Vidal, K. Tachikawa, and E. Bard (2009a), ITCZ rather than ENSO signature for abrupt climate changes across the tropical Pacific?, *Quaternary Res.*, *72*(1), 123-131, doi:10.1016/j.yqres.2009.03.006.

Leduc, G., L. Vidal, O. Cartapanis, and E. Bard (2009b), Modes of eastern equatorial Pacific thermocline variability: Implications for ENSO dynamics over the last glacial period, *Paleoceanography, 24*, PA3202, doi:10.1029/2008PA001701.

Lee, T., I. Fukumori, D. Menemenlis, Z. F. Xing, and L. L. Fu (2002), Effects of the Indonesian Throughflow on the Pacific and Indian oceans, *J. Phys. Oceanogr.*, *32*(5), 1404-1429, doi: 10.1175/1520-0485(2002)032<1404:EOTITO>2.0.CO;2.

LeGrande, A. N., and G. A. Schmidt (2006), Global gridded data set of the oxygen isotopic composition in seawater, *Geophys. Res. Lett., 33*, L12604, doi:10.1029/2006GL026011.

Lehmann, M. F., D. M. Sigman, D. C. McCorkle, B. G. Brunelle, S. Hoffmann, M. Kienast, G. Cane, and J. Clement (2005), Origin of the deep Bering Sea nitrate deficit: Constraints from the nitrogen and oxygen isotopic composition of water column nitrate and benthic nitrate fluxes, *Global Biogeochem. Cycles, 19*, GB4005, doi:10.1029/2005GB002508.

Li, T., Z. Liu, M. A. Hall, S. Berne, Y. Saito, S. Cang, and Z. Cheng (2001), Heinrich event imprints in the Okinawa Trough: Evidence from oxygen isotope and planktonic foraminifera, *Palaeogeogr. Palaeoclimatol. Palaeoecol., 176*, 133-146, doi:10.1016/S0031-0182(01)00332-7.

Lin, H. L., and H. Y. Hsieh (2007), Seasonal variations of modern planktonic foraminifera in the South China Sea*, Deep Sea Res., Part II, 54*, 1634-1644, doi:10.1016/j.dsr2.2007.05.007.

Lin, H. L., W. C. Wang, and G. W. Hung (2004), Seasonal variation of planktonic foraminiferal isotopic composition from sediment traps in the South China Sea, *Mar. Micropaleontol., 53*, 447-460, doi:10.1016/j.marmicro.2004.08.004.

Lindstrom , E., R. Lukas, R. Fine, E. Firing, S. Godfrey, G. Meyers, M. Tsuchiya (1987), The Western Equatorial Pacific Ocean circulation study, *Nature, 330,* 533-537.

Lindstrom, E., J. Butt, R. Lukas, and S. Godfrey (1990), The flow through Vitiaz Strait and St. George's Channel, Papua, New Guinea, The Physical Oceanography of Sea Straits, edited by Pratt, L., *Kluwer Academic, Norwell, Mass*. 171-189

Liu, K.-K., and N. Dittert (2010) Web-based electronic supplements, Appendix C. In: Liu, K.-K., L. Atkinson, R. A. Quinones, L. Talaue-McManus, (eds) *Carbon and nutrient fluxes in continental margins. Springer, Berlin*.

Liu, Z., S.-I. Shin, B. Otto-Bliesner, J. E. Kutzbach, E. C. Brady, and D. Lee (2002), Tropical cooling at the last glacial maximum and extratropical ocean ventilation , *Geophys. Res. Lett., 29*(10), 1409, doi:10.1029/2001GL013938.

Locarnini, R. A., A. V. Mishonov, J. I. Antonov, T. P. Boyer, and H. E. Garcia (2006), World Ocean Atlas 2005, vol. 1, Temperature, *NOAA Atlas NESDIS, vol. 61*, edited by S. Levitus, NOAA, Silver Spring, Md, pp. 182.

Lukas, R. (1988), Interannual Fluctuations of the Mindanao Current Inferred from Sea-Level, *J. Geophys. Res. -Oceans*, *93*(C6), 6744-6748.

Loubere, P., (1994), Quantitative estimation of surface ocean productivity and bottom water oxygen concentration using benthic foraminifera, *Paleoceanography, 9*, 723-737, doi:10.1029/94PA01624.

Loubere, P., (1996), The surface ocean productivity and bottom water oxygen signals in deep water benthic foraminiferal assemblages, *Mar. Micropaleontol., 28*, 247-261, doi:10.1016/0377-8398(96)00004-7.

Lukas, R. (1988), Interannual fluctuations of the Mindanao Current Inferred from sea level, *J. Geophys. Res. , 93*(C6), 6744-6748, doi:10.1029/JC093iC06p06744.

Lukas, R., E. Firing, P. Hacker, P. L. Richardson, C. A. Collins, R. Fine, and R. Gammon (1991), Observations of the Mindanao Current during the Western Equatorial Pacific-Ocean Circulation Study, *J. Geophys. Res., 96*(C4),7089-7104, doi:10.1029/91JC00062.

Lynch-Stieglitz, J., and R. G. Fairbanks (1994), A conservative tracer for glacial ocean circulation from carbon isotope and paleonutrient measurements in benthic foraminifera. *Nature 369*, 308-310.

Lynch-Stieglitz, J., W. B. Curry, N. Slowey and G. A. Schmidt (1999), The overturning circulation of the glacial Atlantic: A view from the top, Reconstructing Ocean History: A Window into the Future, edited by Abrantes, F., and A. Mix, *Kluwer Academic/Plenum, New York*, 7-31.

Lyon, B., H. Cristi, E. R. Verceles, F. D. Hilario, and R. Abastillas (2006), Seasonal reversal of the ENSO rainfall signal in the Philippines, *Geophys. Res. Lett., 33*, L24710, doi:10.1029/2006GL028182.

Macdonald, A. M. (1993), Property Fluxes at 30-Degrees-S and Their Implications for the Pacific-Indian Throughflow and the Global Heat-Budget, *J. Geophys. Res. -Oceans*, *98*(C4), 6851-6868.

Mackensen, A., H. W. Hubberten, T. Bickert, G. Fischer, and D. K. Fütterer, (1993). $\delta^{13}C$ in benthic foraminiferal tests of *Fontbotia wuellerstorfi* (SCHWAGER) relative to $\delta^{13}C$ of dissolved inorganic carbon in Southern Ocean deep-water: implications for glacial ocean circulation models. *Paleoceanography, 8*, 587-610.

Manabe, S., and R. J. Stouffer (1999), Are two modes of thermohaline circulation stable?, *Tellus A*, *51*(3), 400-411.

Martin, P. A., and D. W. Lea (2002), A simple evaluation of cleaning procedures on fossil benthic foraminiferal Mg/Ca, *Geochem. Geophys. Geosyst., 3*(10), 8401, doi:10.1029/2001GC000280.

Martínez, I., L. Keigwin, T. T. Barrows, Y. Yokoyama, and J. Southon (2003), La Niña-like conditions in the eastern equatorial Pacific and a stronger Choco jet in the northern Andes during the last glaciation, *Paleoceanography, 18*(2), 1033, doi:10.1029/2002PA000877.

Masumoto, Y., and T. Yamagata (1991), Response of the western tropical Pacific to the Asian winter Monsoon: The generation of the Mindanao Dome, *J. Phys. Oceanogr., 21*(9), 1386-1398, doi:10.1175/1520-0485 (1991)021<1386:ROTWTP>2.0.CO;2.

Masuzawa, J. (1968), Second cruise for CSK, Ryofu Maru, January to March 1968, *Oceanogr. Mag., 20*, 173-185.

Matsumoto, K., T. Oba, J. Lynch-Stieglitz, and H. Yamamoto (2002), Interior hydrography and circulation of the glacial Pacific Ocean, *Quaternary Sci. Rev.*, *21*(14-15), 1693-1704, doi:10.1016/S0277-3791(01)00142-1.

Mazaud, A., (2005). User-friendly software for vector analysis of the magnetization of long sediment cores. *Geochem. Geophys. Geosystems, 6,* doi:10.1029/2005GC001036.

McCartney, M. S. (1977), Subantarctic Mode Water. A Voyage of Discovery, M. V. Angel, *Ed., Pergamon*, 103-119.

McCartney, M. S. and L. D. Talley (1982) The Subpolar Mode Water of the North Atlantic Ocean. *J. Phys. Oceanogr., 12*, 1169-1188.

McCave, I. N., and I. R. Hall (2006), Size sorting in marine muds: Processes, pitfalls, and prospects for paleoflow-speed proxies, *Geochem. Geophys. Geosyst.*, 7, Q10N05, doi:10.1029/2006GC001284.

McCave, I. N., B. Manighetti, and S. G. Robinson (1995), Sortable silt and fine sediment size/composition slicing: Parameters for paleocurrent speed and paleoceanography, *Paleoceanography, 10,* 593-610.

McCave, I. N., L. Carter, I. R. Hall (2008), Glacial-interglacial changes in water mass structure and flow in the SW Pacific Ocean, *Quater. Sci. Rev., 27 (19-20)*, 1886-1908, doi:10.1016/j.quascirev.2008.07.010.

McCorkle, D. C., L. D. Keigwin, B. H. Corliss, S. R. Emerson (1990), The influence of microhabitats on the carbon isotopic composition of deep-sea benthic foraminifera. *Paleoceanography, 5,* 161-185.

McCreary, J. P., and P. Lu (2001), Influence of the Indonesian throughflow on the circulation of

Pacific intermediate water, *J. Phys. Oceanogr.*, *31*(4), 932-942, doi: 10.1175/1520-0485(2001)031<0932:IOTITO>2.0.CO;2.

McPhaden, M. J. (1999), Genesis and evolution of the 1997-98 El Niño, *Science*, *283*(5404), 950-954, doi: 10.1126/science.283.5404.950.

Meissner, K. J., E. D. Galbraith, and C. Völker (2005), Denitrification under glacial and interglacial conditions: A physical approach, *Paleoceanography*, *20*, PA3001, doi:10.1029/2004PA001083.

Mikolajewicz, U., T. J. Crowley, A. Schiller, and R. Voss (1997), Modelling teleconnections between the North Atlantic and North Pacific during the Younger Dryas. *Nature, 387*, 384-387, doi:10.1038/387384a0.

Mix, A. C., N. G. Pisias, R. Zahn, W. Rugh, C. Lopez and K. Nelson, (1991). Carbon-13 in Pacific deep and intermediate waters, 0-370 ka: implications for ocean circulation and Pleistocene CO_2. *Paleoceanography, 6*, 205-226.

Mix, A. C., N. G. Pisias, W. Rugh, J. Wilson, A. Morey and T. Hagelberg (1995). Benthic foraminiferal stable isotope record from Site 849, 0-5 Ma: Local and global climate changes. In: Pisias, N. G., L. Mayer, T. Janecek, A. Palmer-Julson, T. H. van Andel (eds.), *Proc. ODP, Scientific Results 138, College Station, TX (Ocean Drilling Program),* 371-412.

Molfino, B., and A. McIntyre (1990), Precessional forcing of nutricline dynamics in the Equatorial Atlantic, *Science, 249* , 766-769.

Mohtadi, M., S. Steinke, J. Groeneveld, H. G. Fink, T. Rixen, D. Hebbeln, B. Donner, and B. Herunadi (2009), Low-latitude control on seasonal and inter-annual changes in planktonic foraminiferal flux and shell geochemistry off south Java: A sediment trap study, P*aleoceanography, 24*, PA1201, doi:10.1029/2008PA001636.

Müller, A., and B. N. Opdyke (2000), Glacial-interglacial changes in nutrient utilization and paleoproductivity in the Indonesian Throughflow sensitive Timor Trough, easternmost Indian Ocean, *Paleoceanography, 15*(1), 85-94, doi:10.1029/1999PA900046.

Muller, J. -P., et al., (2000) 'The LANDMAP project for the automated creation and validation of multi-resolution orthorectified satellite image products and a 1" DEM of the British Isles from ERS tandem SAR interferometry'. *Remote Sensing Society Annual Conference*, Leicester University, UK.

Muratli, J. M., Z. Chase, A. C. Mix, and J. McManus (2010), Increased glacial-age ventilation of the Chilean margin by Antarctic Intermediate Water, *Nat. Geosci.*, *3*(1), 23-26, doi:10.1038/ngeo715.

Murtugudde, R., A. J. Busalacchi, and J. Beauchamp (1998), Seasonal-to-interannual effects of the

Indonesian throughflow on the tropical Indo-Pacific Basin, *J. Geophys. Res.*, 103(C10), 21,425-21,441, doi:10.1029/98JC02063.

Nadeau, M. J., M. Schleicher, P. M. Grootes, H. Erlenkeuser, A. Gottdang, D. J. W. Mous, J. M. Sarnthein, and H. Willkomm (1997), The Leibniz-Labor AMS facility at the Christian-Albrechts Univ., Kiel, Germany, *Nucl. Instrum. Methods Phys. Res., Sect. B, 123*(1-4), 22-30, doi:10.1016/S0168-583X(96)00730-6.

Nakatsuka, T., N. Harada, E. Matsumoto, N. Handa, T. Oba, M. Ikehara, H. Matsuoka, and K. Kimoto (1995), Glacial-interglacial migration of an upwelling field in the Western Equatorial Pacific recorded by sediment $^{15}N/^{14}N$, *Geophys. Res. Lett., 22*, 2525-2528, doi:10.1029/95GL02544.

Nitani, H., (1972) Beginning of the Kuroshio. In: Stommel, H. and K. Yoshida, Editors, Kuroshio: its physical aspects of the Japan Current, *University of Washington Press*, 129-163.

Nürnberg, D. (1995), Magnesium in tests of Neogloboquadrina pachyderma (sinistral) from high northern and southern latitudes, *J. Foraminiferal Res., 25*, 350-368, doi: 10.2113/gsjfr.25.4.350.

Nürnberg, D., J. Bijma, and C. Hemleben (1996a), Assessing the reliability of magnesium in foraminiferal calcite as a proxy for water mass temperatures. *Geochim. Cosmochim. Acta 60*(13), 803-814, doi:10.1016/0016-7037(96)82893-6.doi:10.1016/0016-7037(95)00446-7

Nürnberg, D., J. Bijma, and C. Hemleben (1996b) Erratum: Assessing the reliability of magnesium in foraminiferal calcite as a proxy for water mass temperatures. *Geochim. Cosmochim. Acta 60*(13), 2483-2484, doi:10.1016/0016-7037(96)82893-6.

Ono, A., K. Takahashi, K. Katsuki, Y. Okazaki, and T. Sakamoto (2005), The Dansgaard-Oeschger cycles discovered in the up stream source region of the North Pacific Intermediate Water formation, *Geophys. Res. Lett.*, 32, L11607, doi:10.1029/2004GL022260.

Oppo, D. W., and Y. B. Sun (2005), Amplitude and timing of sea-surface temperature change in the northern South China Sea: Dynamic link to the East Asian monsoon, *Geology, 33*(10), 785-788, doi:10.1130/G21867.1.

Oppo, D. W., B. K. Linsley, Y. Rosenthal, S. Dannenmann, and L. Beaufort (2003), Orbital and suborbital climate variability in the Sulu Sea, western tropical Pacific, *Geochem. Geophys. Geosyst., 4*(1), 1003, doi:10.1029/2001GC000260.

Oppo, D. W., G. A. Schmidt, and A. N. LeGrande (2007), Seawater isotope constraints on tropical hydrology during the Holocene, *Geophys. Res. Lett., 34*, L13701, doi:10.1029/2007GL030017.

Pahnke K., and R. Zahn (2005), Southern hemisphere water mass conversion linked with north Atlantic climate variability, *Science, 307,* 1741-1745, doi: 10.1126/science.1102163.

Paillard, D., L. Labeyrie, and P. Yiou (1996), Macintosh program performs time-series analysis,

Eos Trans. AGU, 77, 379.

Partin, J. W., K. M. Cobb, J. F. Adkins, B. Clark, and D. P. Fernandez (2007), Millennial-scale trends in West Pacific Warm Pool hydrology since the Last Glacial Maximum, *Nature, 449*, 452-455, doi:10.1038/nature06164, doi:10.1038/nature06164.

Peña, M. A., M. R. Lewis, and J. J. Cullen (1994), New production in the warm waters of the tropical Pacific Ocean*, J. Geophys. Res., 99*, 14,255-14,268.

Pouthiers J., and E. Gonthier (1978) Sur la susceptibilité magnétique des sédiments, indicateurs de la dispersion du matériel volcanoclastique à partir de l'Islande et des Faeroes, *Bull. Inst. Géologie d'Aquitaine, 23*, 214-226.

Qiu, B., and R. Lukas (1996), Seasonal and interannual variability of the North Equatorial Current, the Mindanao Current, and the Kuroshio along the Pacific western boundary*, J. Geophys. Res., 101*, 12,315-12,330.

Qu, T. D., and E. J. Lindstrom (2004), Northward intrusion of Antarctic intermediate water in the western Pacific, *J. Phys. Oceanogr.*, *34*(9), 2104-2118, doi: 10.1175/1520-0485(2004)034<2104:NIOAIW>2.0.CO;2.

Qu, T. D., H. Mitsudera, and T. Yamagata (1998), On the western boundary currents in the Philippine Sea, *J. Geophys. Res.*, 103(C4), 7537-7548, doi:10.1029/98JC00263.

Qu, T. D., H. Mitsudera, and T. Yamagata (1999), A climatology of the circulation and water mass distribution near the Philippine coast, *J. Phys. Oceanogr., 29*(7), 1488-1505, doi:10.1175/1520-0485(1999)029<1488:ACOTCA>2.0.CO;2.

Qu, T. D., J. Gan, A. Ishida, Y. Kashino, and T. Tozuka (2008), Semiannual variation in the western tropical Pacific Ocean, *Geophys. Res. Lett., 35*, L16602, doi:10.1029/2008GL035058.

Rahmstorf, S., and A. Ganapolski (1999), Long-term global warming scenarios computed with an efficient coupled climate model. *Climatic Change 43,* 353-367, doi: 10.1023/A:1005474526406.

Rahmstorf, S. (1996), On the Freshwater Forcing and Transport of the Atlantic Thermohaline Circulation. *Climate Dynamics 12*, no. 12, 799-811.

Ramsey, M. H., P. J. Potts, P. C. Webb, P. Watkins, J. S. Watson and B. J. Coles (1995), An objective assessment of analytical method precision: comparison of ICP-AES and XRF for the analysis of silicate rocks, *Chem. Geol. 124*, 1-19.

Ravelo A. C., R. G. Fairbanks, and S. G. H. Philander (1990), Reconstructing tropical Atlantic hydrography using planktonic foraminifera and an ocean model*. Paleoceanography. 5*, 409-431.

Ravelo, A. C., and R. G. Fairbanks (1992), Oxygen isotopic composition of multiple species of planktonic foraminifera: Recorders of the modern photic zone temperature gradient, *Paleoceanography, 7*, 815-832, doi:10.1029/92PA02092.

Rees, A. I. (1961), The effects of water currents on the magnetic remanence and anisotropy of susceptibility of some sediments, *Geophys. J. R. Astron. Soc*., *6*, 235-251.

Rees, A. I. (1965), The use of anisotropy of magnetic susceptibility in the estimation of sedimentary fabric, *Sedimentology, 4,* 257-271.

Reid, J. L. (1965): Intermediate Waters of the Pacific Ocean. *The Johns Hopkins Oceanogr. Study*, *2*, pp. 85.

Reid, J. L. (1997), On the total geostrophic circulation of the Pacific Ocean: Flow patterns, traces and transports. *Progress in Oceanography, 39*, Pergamon, 263-325.

Reid, J. L., and A. W. Mantyla (1978), On the mid-depth circulation of the North Pacific Ocean. *J. Phys. Oceanogr., 8*, 946-951.

Richter, T. O., S. Van der Gaast, B. Koster, A. Vaars, R. Gieles, H. De Stigter, H. De Haas, and T. C. E. van Weering (2006), The Avaatech XRF core scanner: technical description and applications to NE Atlantic sediments. In: Rothwell, R.G. (Ed.), *New Techniques in Sediment Core Analysis. Special Publication, 267.* Geological Society, London, 39-50.

Rind, D. and D. Peteet (1985), Terrestrial conditions at the last. glacial maximum and CLIMAP sea-surface temperature estimates: Are they consistent? *Quaternary Res. 24*, 1-2.

Ropelewski, C. F., and M. S. Halpert (1986), North American precipitation and temperature patterns associated with the El Niño/Southern Oscillation (ENSO). *Mon. Wea. Rev, 114*, 2352-2362.

Rosenthal Y., E. A. Boyle, and N. Slowey (1997) Temperature control on the incorporation of magnesium, strontium, fluorine, and cadmium into benthic foraminiferal shells from Little Bahama Bank: Prospects for thermocline paleoceanography. *Geochim. Cosmochim. Acta, 61*, 3633-3643.

Rosenthal, Y., and A. J. Broccoli (2004), In search of paleo-ENSO, *Science*, *304*(5668), 219-221, doi: 10.1126/science.1095435.

Rosenthal, Y., D. W. Oppo, and B. K. Linsley (2003), The amplitude and phasing of climate change during the last deglaciation in the Sulu Sea, western equatorial Pacific, *Geophys. Res. Lett., 30*(8), 1428, doi:10.1029/2002GL016612.

Rosenthal, Y., et al., (2004), Interlaboratory comparison study of Mg/Ca and Sr/Ca measurements in planktonic foraminifera for paleoceanographic research, *Geochem. Geophys. Geosyst., 5*, Q04D09, doi:10.1029/2003GC000650.

Rousseau, D. D., N. Wu, Y. Pei, and F. Li (2009), Three exceptionally strong East-Asian summer monsoon events during glacial times in the past 470 kyr, *Clim. Past, 5*, 157-169, doi:10.5194/cp-5-157-2009.

Rudolf, B., A. Becker, U. Schneider, A. Meyer-Christoffer, and M. Ziese (2010), On the most recent gridded global data set issued in fall 2010 by the Global Precipitation Climatology Center (GPCC), *GPCC Status Report*, pp. 7.

Ruth, U., et al., (2007), "EDML1": A chronology for the EPICA deep ice core from Dronning Maud Land, Antarctica, over the last 150 000 years, *Clim. Past, 3*, 475-484, doi:10.5194/cp-3-475-2007.

Sadler J.C. (1975) The upper-tropospheric circulation over the global tropics. *Department of Meteorology, University of Hawaii, UHMET-75-05,* pp. 35.

Saikku, R., L. D. Stott, and R. Thunell (2009), A bi-polar signal recorded in the western tropical Pacific: Northern and Southern Hemisphere climate records from the Pacific warm pool during the last Ice Age, *Quat. Sci. Rev., 28*(23-24), 2374-2385, doi:10.1016/j.quascirev.2009.05.007.

Sajona, F. G., H. Bellon, R. C. Maury, M. Pubellier, R. D. Quebral, J. Cotton, F. E. Bayon, E. Pagado, and P. Pamatian (1997), Tertiary and Quaternary magmatism in Mindanao and Leyte (Philippines): geochronology, geochemistry and tectonic setting, *J. of Asian Earth Sci., 15(2-3),* 121-153.

Sakai, K., and R. Kawamura (2009), Remote response of the East Asian winter monsoon to tropical forcing related to El Niño-Southern Oscillation, *J. Geophys. Res., 114*, D06105, doi:10.1029/2008JD010824.

Sathiamurthy, E., and H. K. Voris (2006), Maps of Holocene sea level transgression and submerged lakes on the Sunda Shelf, *Nat. Hist. J. Chulalongkorn Univ. Suppl. 2*, 1-43.

Schleicher, M., P. M. Grootes, M. J. Nadeau, and A. Schoon (1998), The carbonate ^{14}C background and its components at the Leibniz AMS facility, *Radiocarbon, 40*(1), 85-93.

Schmidt, M. W., H. J. Spero, and D. W. Lea (2004), Links between salinity variation in the Caribbean and North Atlantic thermohaline circulation, *Nature, 428*, 160-163, doi:10.1038/ nature02346.

Schmittner, A., K. J. Meissner, M. Eby, and A. J. Weaver (2002), Forcing of the deep ocean circulation in simulations of the Last Glacial Maximum, *Paleoceanography, 17*(2), 1015, doi:10.1029/2001PA000633.

Schott, F. A., and J. P. McCreary (2001), The monsoon circulation of the Indian Ocean, *Prog Oceanogr*, *51*(1), 1-123, doi:10.1016/S0079-6611(01)00083-0.

Schott, F. A., M. Dengler, and R. Schoenefeldt (2002), The shallow overturning circulation of the Indian Ocean, *Prog. Oceanogr.*, *53*(1), 57-103, doi:10.1016/S0079-6611(02)00039-3.

Schrag, D. P., G. Hampt, and D. W. Murray (1996), Pore fluid constraints on the temperature and oxygen isotopic composition of the glacial ocean, *Science, 272*, 1930-1932.

Schulz, M., and M. Mudelsee (2002), REDFIT: estimating red-noise spectra directly from unevenly spaced paleoclimatic time series, *Comput Geosci-Uk*, *28*(3), 421-426, doi:10.1016/S0098-3004(01)00044-9.

Seidov, D., E. Barron, and B. J. Haupt (2001), Meltwater and the global ocean conveyor: Northern versus southern connections. *Global Planet. Change, 30*, 257-270, doi:10.1016/S0921-8181(00)00087-4.

Seltzer, G. O., D. T. Rodbell, P. A. Baker, S. C. Fritz, P. M. Tapia, H. D. Rowe, and R. B. Dunbar (2002a), Early warming of tropical South America at the last glacial-interglacial transition. *Science, 296*, 1685-1686, doi*:* 10.1126/science.1070136.

Seltzer, G. O., D. T. Rodbell, P. A. Baker, S. C. Fritz, P. M. Tapia, H. D. Rowe, and R. B. Dunbar (2002b), Early deglaciation in the tropical Andes - Response, *Science*, *298*(5591), doi: 10.1126/science.298.5591.7a.

Shackleton, N. J. (1967), Oxygen isotope analyses and Pleistocene temperature reassessed. *Nature, 215*, 15-17.

Shackleton, N.J. (1977): Carbon-13 in Uvigerina: Tropical rain forest history and the equatorial Pacific carbonate dissolution cycle.- In: Andersen, N. R., and A. Malahoff, (eds.), The Fate of Fossil Fuel in the Oceans, *Plenum, New York*, 401-427.

Shackleton, N. J., and N. D. Opdyke (1973), Oxygen isotope and palaeomagnetic stratigraphy of equatorial Pacific core V28-238: Oxygen isotope temperatures and ice volumes on a 100 kyrs and 1000 kyrs scale, *Quat. Res., 3*(1), 39-54, doi:10.1016/0033-5894(73)90052-5.

Sigman, D. M., J. Granger, P. J. DiFiore, M. M. Lehmann, R. Ho, G. Cane, and A. van Geen (2005), Coupled nitrogen and oxygen isotope measurements of nitrate along the eastern North Pacific margin, *Global Biogeochem. Cycles, 19*, GB4022, doi:10.1029/2005GB002458.

Sigman, D. M., K. L. Casciotti, M. Andreani, C. Barford, M. Galanter, and J. K. Böhlke (2001), A bacterial method for the nitrogen isotopic analysis of nitrate in seawater and freshwater, *Anal. Chem., 73*, 4145-4153, doi: 10.1021/ac010088e.

Sijp, W. P, and M. H. England (2009) Southern Hemisphere westerly wind control over the ocean's thermohaline circulation. *J. of Climate. 22*, 1277-1286, doi: 10.1175/2008JCLI2310.1.

Singer, B. S., H. Guillou, B. R. Jicha, C. Laj, C. Kissel, B. L. Beard, and C. M. Johnson (2009), $^{40}Ar/^{39}Ar$, K-Ar and ^{230}Th -^{238}U dating of the Laschamp excursion: A radioisotopic tiepoint for ice core and climate chronologies, *Earth Planet. Sci. Lett., 286*(1-2), 80-88, doi:10.1016/j.epsl.2009.06.030.

Song, Q., A. L. Gordon, and M. Visbeck (2004), Spreading of the Indonesian throughflow in the Indian Ocean, *J. Phys. Oceanogr.*, *34*(4), 772-792.

Song, Q., and A. L. Gordon (2004), Significance of the vertical profile of the Indonesian Throughflow transport to the Indian Ocean, *Geophys. Res. Lett.*, *31*, L16307, doi:10.1029/2004GL020360.

Spero, H. J., and D. W. Lea (2002), The cause of carbon isotope minimum events on glacial terminations, *Science*, *296*(5567), 522-525, doi: 10.1126/science.106940.

Steinke, S., M. Mohtadi, J. Groeneveld, L.-C. Lin, L. Löwemark, M.-T. Chen, and R. Rendle-Bühring (2010), Reconstructing the southern South China Sea upper water column structure since the Last Glacial Maximum: Implications for the East Asian winter monsoon development, *Paleoceanography, 25*, PA2219, doi:10.1029/2009PA001850.

Stocker, T. F., and A. Schmittner (1997), Influence of CO_2 emission rates on the stability of the thermohaline circulation, *Nature, 388*, 862-865.

Stott, L. D., C. Poulsen, S. Lund, and R. Thunell (2002), Super ENSO and global climate oscillations at millennial time scales, *Science, 297*, 222-226, doi:10.1126/science.1071627.

Stott, L. D., K. Cannariato, R. Thunell, G. H. Haug, A. Koutavas, and S. Lund (2004), Decline of surface temperature and salinity in the western tropical Pacific Ocean in the Holocene epoch, *Nature, 431*, 56-59, doi:10.1038/nature02903.

Stott, L. D., A. Timmermann, and R. Thunell (2007a), Southern Hemisphere and deep-sea warming led deglacial atmospheric CO_2 rise and tropical warming, *Science, 318*, 435-438, doi:10.1126/science.1143791.

Stott, L. D. (2007b), Comment on "Anomalous radiocarbon ages for foraminifera shells" by W. Broecker et al.: A correction to the western tropical Pacific MD9821-81 record, *Paleoceanography, 22*, PA1211, doi:10.1029/2006PA001379.

Stuijts, I., J. C. Newsome and J. R. Flenley (1988) Evidence for Late Quaternary vegetational change in the Sumatran and Javan highlands. *Review of Palaeobotany and Palynology, 55*. 207-216.

Svensson, A., et al.,(2008), A 60 000 year Greenland stratigraphic ice core chronology, *Clim. Past, 4*, 47-57, doi:10.5194/cp-4-47-2008.

Sverdrup, H. U., M. W. Johnson, and R. W. Fleming (1942), The Oceans: Their Physics, Chemistry and General Biology. *Prentice-Hall, Englewood, NJ*, pp. 1060.

Széréméta, N., F. Bassinot, Y. Balut, L. Labeyrie, and M. Pagel (2004), Oversampling of sedimentary series collected by giant piston corer: Evidence and corrections based on 3.5 kHz chirp profiles, *Paleoceanography, 19*, PA1005, doi:10.1029/2002PA000795.

Takahashi, T. (1959), Hydrographical researches in the western equatorial Pacific, *Mem. Fac. Fish. Kagoshima Univ., 7*, 141-147.

Takahashi, K. (1998), The Bering and Okhotsk Seas: modern and past paleoceanographic changes and gateway impact. *Journal of Asian Earth Sciences, 16*(1), 49-58.

Talley, L. D. (1991), An Okhotsk Sea water anomaly: implications for sub-thermocline ventilation in the North Pacific. *Deep-Sea Res., 38*, 171-190.

Talley, L. D. (1993), Distribution and Formation of North Pacific Intermediate Water, *J. Phys. Oceanogr.*, *23*(3), 517-537.

Talley, L. D. (1999), Some aspects of ocean heat transport by the shallow, intermediate and deep overturning circulations. In Mechanisms of Global Climate Change at Millenial Time Scales, *Geophys. Mono. Ser., 112*, American Geophysical Union, ed. Clark, Webb and Keigwin, 1-22.

Talley, L. D. (2003), Shallow, intermediate, and deep overturning components of the global heat budget, *J. Phys. Oceanogr.*, *33*(3), 530-560, doi: 10.1175/1520-0485(2003)033<0530:SIADOC>2.0.CO;2.

Talley, L. D. (2007) Hydrographic Atlas of the World Ocean Circulation Experiment (WOCE). Volume 2: Pacific Ocean (eds. M. Sparrow, P. Chapman and J. Gould), *International WOCE Project Office, Southampton, U.K.*, ISBN 0-904175-54-5.

Talley, L. D., and T. M. Joyce (1992), The Double Silica Maximum in the North Pacific, *J Geophys. Res.-Oceans*, *97*(C4), 5465-5480.

Thevenon, F., E. Bard, D. Williamson, and L. Beaufort (2004), A biomass burning record from the West Equatorial Pacific over the last 360 ky: Methodological, climatic and anthropic implications, *Palaeogeogr. Palaeoclimatol. Palaeoecol., 213*(1-2), 83-99, doi:10.1016/j. palaeo.2004.07.003.

Thunell, R. C., and L. A. Reynolds (1984), Sedimentation of planktonic foraminifera: Seasonal changes in species flux in the Panama Basin, *Micropaleontology, 30*, 243-262, doi:10.2307/ 1485688.

Thunell, R. C., and A. B. Kepple (2004), Glacial-Holocene $\delta^{15}N$ record from the Gulf of Tehuantepec, Mexico: Implications for denitrification in the eastern equatorial Pacific and changes in atmospheric N_2O, *Global Biogeochem. Cycles, 18*, GB1001, doi:10.1029/2002GB002028.

Toole, J. M., R. C. Millard, Z. Wang, and S. Pu (1990), Observations of the Pacific North Equatorial Current Bifurcation at the Philippine Coast, *J. Phys. Oceanogr., 20*(2), 307-318, doi:10.1175/1520-0485(1990)020<0307:OOTPNE>2.0.CO;2.

Tozuka, T., T. Qu, and T. Yamagata (2007), Dramatic impact of the South China Sea on the Indonesian Throughflow, *Geophys. Res. Lett.*, 34, L12612, doi:10.1029/2007GL030420.

Tozuka, T., T. Kagimoto, Y. Masumoto, and T. Yamagata (2002), Simulated multiscale variations in the western tropical Pacific: The Mindanao Dome revisited, *J. Phys. Oceanogr., 32*(5), 1338-1359, doi:10.1175/1520-0485(2002)032<1338:SMVITW>2.0.CO;2.

Tsuchiya, M. (1991), Flow path of the Antarctic Intermediate Water in the western equatorial South Pacific Ocean, *Deep Sea Res., Part A, 38,* S273-S279.

Tsuchiya, M. (1968). Upper waters of the intertropical Pacific Ocean. *The Johns Hopkins Oceanographic Studies, No. 4. The Johns Hopkins Press, Baltimore, Md*., pp. 50.

Tsuchiya, M., (1981). The origin of the Pacific Equatorial 13°C water. *J. Phys. Oceanogr., 11*(6) 794-812.

Tsuchiya, M., and L. D. Talley (1996), Water-property distributions along an eastern Pacific hydrographic section at 135W, *J. Mar. Res.*, *54*(3), 541-564.

Tudhope, A. W., C. P. Chilcott, M. T. McCulloch, E. R. Cook, J. Chappell, R. M. Ellam, D. W. Lea, J. M. Lough, and G. B. Shimmield (2001), Variability in the El Niño-Southern oscillation through a glacial-interglacial cycle, *Science*, *291*(5508), 1511-1517, doi: 10.1126/science.1057969.

Turk, D., M. R. Lewis, G. W. Harrison, T. Kawano, and I. Asanuma (2001), Geographical distribution of new production in the western/central equatorial Pacific during El Niño and non-El Niño conditions, *J. Geophys. Res.*, 106, 4501-4515, doi:10.1029/1999JC000058.

Udarbe-Walker, M. J. B., and C. L. Villanoy (2001), Structure of potential upwelling areas in the Philippines, *Deep Sea Res., Part I, 48*(6), 1499-1518, doi:10.1016/S0967-0637(00) 00100-X.

Ueki, I., Y. Kashino, and Y. Kuroda (2003), Observation of current variations off the New Guinea coast including the 1997-1998 El Niño period and their relationship with Sverdrup transport, *J. Geophys. Res.*, 108(C7), 3243, doi:10.1029/2002JC001611.

Urey, H. C. (1947), The Thermodynamic Properties of Isotopic Substances. *J. Chem. Soc.,* 562-581. doi:10.1039/JR9470000562.

van der Zwaan, G. J., I. A. P. Duijnstee, M. den Dulk, S. R. Ernst, N.T. Jannink, and T. J. Kouwenhoven, (1999), Benthic foraminifers: Proxies or problems? A review of paleoecological concepts. *Earth-Science Reviews, 46*, 213-236, doi:10.1016/S0012-8252(99)00011-2.

van Geen, A., R. G. Fairbanks, P. Dartnell, M. McGann, J. V. Gardner, and M. Kashgarian (1996), Ventilation changes in the northeast Pacific during the Last Deglaciation, *Paleoceanography*, 11(5), 519-528, doi:10.1029/96PA01860.

van Scoy, K. A., R. A. Fine and H. G. Ostlund (1991): Two decades of mixing tritium into the North Pacific Ocean, *Deep-Sea Res., 38*, Suppl., S191-S219.

Vellinga, M., and R. A. Wood (2008), Impacts of thermohaline circulation shutdown in the twenty-first century, *Climatic Change*, *91*(1-2), 43-63, doi: 10.1007/s10584-006-9146-y.

Vidal, L., R. Schneider, O. Marchal, T. Bickert, T. F. Stocker, and G. Wefer (1999), Link between the North and South Atlantic during the Heinrich events of the last glacial period, *Climate Dynamics 15*, 909-919, doi: 10.1007/s003820050321.

Visser, K., R. Thunell, and L. Stott (2003), Magnitude and timing of temperature change in the Indo-Pacific warm pool during deglaciation, *Nature, 421*, 152-155, doi:10.1038/nature01297.

Visser, K., R. Thunell, and M. A. Goni (2004), Glacial-interglacial organic carbon record from the Makassar Strait, Indonesia: implications for regional changes in continental vegetation, *Quaternary Sci. Rev.*, *23*(1-2), 17-27, doi:10.1016/j.quascirev.2003.07.001.

Vranes, K., A. L. Gordon, and A. Ffield (2002), The heat transport of the Indonesian Throughflow and implications for the Indian Ocean heat budget, *Deep-Sea Res. Pt. Ii.*, *49*(7-8), 1391-1410, doi: 10.1016/S0967-0645(01)00150-3.

Vranes, K., and A. L. Gordon (2005), Comparison of Indonesian Throughflow transport observations, Makassar Strait to eastern Indian Ocean, *Geophys Res. Lett.*, *32*(10), doi: 10.1029/2004GL022158.

Waelbroeck, C., L. Labeyrie, E. Michel, J. C. Duplessy, J. F. McManus, K. Lambeck, E. Balbon, and M. Labracherie (2002), Sealevel and deep water temperature changes derived from benthic foraminifera isotopic records, *Quat. Sci. Rev., 21*(1-3), 295-305, doi:10.1016/S0277-3791(01)00101-9.

Wainwright, L., G. Meyers, S. Wijffels, and L. Pigot (2008), Change in the Indonesian Throughflow with the climate shift of 1976/77. *Geophys. Res. Lett., 35*, L03604, doi:10.1029/2007GL031911.

Wajsowicz, R. C. (2002), Air-sea interaction over the Indian Ocean due to variations in the Indonesian throughflow, *Clim. Dynam.*, *18*(5), 437-453, doi: 10.1007/s00382-001-0187-7.

Wajsowicz, R. C., and E. K. Schneider (2001), The Indonesian throughflow's effect on global climate determined from the COLA coupled climate system, *J. Climate*, *14*(13), 3029-3042, doi: 10.1175/1520-0442(2001)014<3029:TITSEO>2.0.CO;2.

Waliser, D. E., and C. Gautier (1993), A Satellite-Derived Climatology of the ITCZ, *J. Climate*, *6*(11), 2162-2174.

Wang, B., I. S. Kang, and J. Y. Lee (2004), Ensemble simulations of Asian-Australian monsoon variability by 11 AGCMs, *J. Climate., 17*(4), 803-818, doi:10.1175/1520-0442 (2004)017<0803:ESOAMV>2.0.CO;2.

Wang, B., R. G. Wu, and X. H. Fu (2000), Pacific-East Asian teleconnection: How does ENSO affect East Asian climate?, *J. Climate, 13*(9), 1517-1536, doi:10.1175/1520-0442 (2000)013<1517:PEATHD>2.0.CO;2.

Wang, C., R. G. Prinn, and A. Sokolov (1998), A global interactive chemistry and climate model: Formulation and testing, *J. Geophys. Res.*, 103(D3), 3399-3417, doi:10.1029/97JD03465.

Wang, F, and H. Dunxin (1998), Dynamic and thermohaline properties of the Mindanao Undercurrent, part I: dynamic structure. *Chin. J. Oceanol. Limnol., 16*, 122-127, doi: 10.1007/BF02845177.

Wang, F, and H. Dunxin (1998), Dynamic and thermohaline properties of the Mindanao Undercurrent, part II: thermohaline structure. *Chin. J. Oceanol. Limnol., 16*, 206-213, doi: 10.1007/BF02848724.

Wang, L., M. Sarnthein, H. Erlenkeuser, J. O. Grimalt, P. Grootes, S. Heilig, E. Ivanova, M. Kienast, C. Pelejero, and U. Pflaumann (1999), East Asian monsoon climate during the Late Pleistocene: high-resolution sediment records from the south China Sea, *Mar. Geol.*, *156*(1-4), 245-284, doi:10.1016/S0025-3227(98)00182-0.

Wang, P. (2009), Global monsoon in a geological perspective, *Chinese Science Bull., 54(7),* 1113-1136.

Wang, P. X., S. Clemens, L. Beaufort, P. Braconnot, G. Ganssen, Z. M. Jian, P. Kershaw and M. Sarnthein (2005), Evolution and variability of the Asian monsoon system: state of the art and outstanding issues, *Quater. Sci. Rev*., 24, 595-629, doi:10.1016/j.quascirev.2004.10.002.

Weaver, A. J., M. Eby, F. F. Augustus, and E. C. Wiebe (1998), Simulated influence of carbon dioxide, orbital forcing and ice sheets on the climate of the Last Glacial Maximum, *Nature*, *394*(6696), 847-853, doi:10.1038/29695.

Webster, P. J., and N. A. Streten (1978), Late Quaternary Ice-Age Climates of Tropical Australasia: Interpretations and Reconstructions. *Quat. Res., 10*, 279-309.

Weeks, R., C. Laj, L. Endignoux, M. Fuller, A. Roberts, R. Manganne, E. Blanchard, W. Goree (1993), Improvements in long-core measurement techniques : applications in palaeomagnetism and palaeoceanography, *Geophys. J. Int., 114*, 651-662.

Weltje, G. J., and R. Tjallingii (2008), Calibration of XRF core scanners for quantitative geochemical logging of soft sediment cores, *Geochim. Cosmochim. Ac.*, *72*(12), A1014-A1014, doi:10.1016/j.epsl.2008.07.054.

Wijffels, S. E., M. M. Hall, T. Joyce, D. J. Torres, P. Hacker, and E. Firing (1998), Multiple deep gyres of the western North Pacific: A WOCE section along 149°E, *J. Geophys. Res.*, 103(C6), 12,985-13,009, doi:10.1029/98JC01016.

Wijffels, S., E. Firing, and J. Toole (1995), The Mean Structure and Variability of the Mindanao Current at 8°N, *J. Geophys. Res., 100*(C9), 18421-18435, doi:10.1029/95JC01347.

Wright, D. G., and T. F. Stocker (1993), Younger Dryas experiments. In: Ice in the Climate System, Peltier, R.W. (ed), *NATO ASI I12, Kluwer*, 395-416.

Wyrtki, K. (1961), Physical oceanography of the southeast Asian waters. *Univ. Calif., NAGA Rept., No. 2*, pp. 195.

Xiang, R., Y. Sun, T. Li, D. W. Oppo, M. Chen, and F. Zheng (2007), Paleoenvironmental change in the middle Okinawa Trough since the last deglaciation: Evidence fromthe sedimentation rate and planktonic foraminiferal record, *Palaeogeogr. Palaeoclimatol. Palaeoecol., 243*, 378-393, doi:10.1016/j.palaeo.2006.08.016.

Xiao, J. L., Z. S. An, T. S. Liu, Y. Inouchi,H. Kumai, S. Yoshikawa, and Y. Kondo (1999), East Asian monsoon variation during the last 130,000 Years: Evidence from the Loess Plateau of central China and Lake Biwa of Japan, *Quat. Sci. Rev., 18*(1), 147-157, doi:10.1016/S0277-3791(97)00097-8.

Xie, P. P., and P. A. Arkin (1997), Global precipitation: A 17-year monthly analysis based on gauge observations, satellite estimates, and numerical model outputs, *B. Am. Meteorol. Soc.*, *78*(11), 2539-2558.

Xie, S. P., K. M. Hu, J. Hafner, H. Tokinaga, Y. Du, G. Huang, and T. Sampe (2009), Indian Ocean Capacitor Effect on Indo-Western Pacific Climate during the Summer following El Niño, *J. Climate*, *22*(3), 730-747, doi: 10.1175/2008JCLI2544.1.

Xu, J., A. Holbourn, W. Kuhnt, Z. M. Jian, and H. Kawamura (2008), Changes in the thermocline structure of the Indonesian outflow during Terminations I and II, *Earth Planet Sc. Lett.*, *273*(1-2), 152-162, doi:10.1016/j.epsl.2008.06.029.

Xu, J., W. Kuhnt, A. Holbourn, N. Andersen, and G. Bartoli (2006), Changes in the vertical profile of the Indonesian Throughflow during Termination II: Evidence from the Timor Sea, *Paleoceanography, 21*, PA4202, doi:10.1029/2006PA001278.

Xu, J., W. Kuhnt, A. Holbourn, M. Regenberg, and N. Andersen (2010), Indo-Pacific Warm Pool variability during the Holocene and Last Glacial Maximum, *Paleoceanography, 25*, PA4230, doi:10.1029/2010PA001934.

Yamagata, T., Y. Shibao, and S. Umatani (1985), Interannual Variability of the Kuroshio Extension and its relation to the Southern Oscillation/El Niño, *J. Oceanogr. Soc. Jpn., 41*, 274-281, doi:10.1007/BF02109276.

Yancheva, G., N. R. Nowaczyk, J. Mingram, P. Dulski, G. Schettler, J. F. W. Negendank, J. Liu, D. M. Sigman, L. C. Peterson, and G. H. Haug (2007), Influence of the intertropical convergence zone on the east Asian monsoon, *Nature, 445*, doi:10.1038/nature 05431.

Yaremchuk, M., and T. D. Qu (2004), Seasonal variability of the large-scale currents near the

coast of the Philippines, *J. Phys. Oceanogr.*, *34*(4), 844-855, doi: 10.1175/1520-0485(2004)034<0844:SVOTLC>2.0.CO;2.

Yoshikawa, C., Y. Yamanaka, and T. Nakatsuka (2006), Nitrate-nitrogen isotopic patterns in surface waters of the western and central equatorial Pacific, *J. Oceanogr., 62*, 511-525.

Zhang, Y. G., J. F. Ji, W. Balsam, L. W. Liu, and J. Chen (2009), Mid-Pliocene Asian monsoon intensification and the onset of Northern Hemisphere glaciation, *Geology, 37*(7), 599-602, doi:10.1130/G25670A.1.

Zhang, Y. G., J. Ji, W. L. Balsam, L. Liu, and J. Chen (2007), High resolution hematite and goethite records from ODP 1143, South China Sea: Co-evolution of monsoonal precipitation and El Niño over the past 600,000 years, *Earth Planet. Sci. Lett., 264*(1-2), 136-150, doi:10.1016/j.epsl.2007.09.022.

Zheng, W., P. Braconnot, E. Guilyardi, U. Merkel, and Y. Yu (2008), ENSO at 6 ka and 21 ka from ocean-atmosphere coupled model simulations, *Clim. Dyn., 30*, 745-762, doi: 10.1007/s00382-007-0320-3.

Zuraida, R., A. Holbourn, D. Nürnberg, W. Kuhnt, A. Dürkop, and A. Erichsen (2009), Evidence for Indonesian Throughflow slowdown during Heinrich events 3-5, *Paleoceanography, 24*, PA2205, doi:10.1029/2008PA001653.

Zuvela-Aloise, M. (2005), Modelling of the Indonesian Throughflow on glacial- interglacial timescales. Ph.D. thesis. *Institute for Geosciences, University of Kiel*.

Academic Career

Timothé Bolliet
25/04/1983
Citizenship: French
tb@gpi.uni-kiel.de / timprobox@googlemail.com

University Qualifications

2006-2010: PhD: West Pacific climate and circulation over the last 160 kyr: A palaeontological and geochemical multiproxy reconstruction within the inflow path of the Indonesian Throughflow
Supervised by Prof. Dr. W. Kuhnt and Dr. A. Holbourn
Kiel CAU University, Germany.
Mark: GOOD

2004-2006: Master degree SET (Sciences of Terrestrial Environment), speciality Geosystems:
A 60 000-year record of the palaeoenvironmental conditions in the West Pacific Warm Pool from coccoliths assemblages and morphometry.
Supervised by Dr. L.Beaufort.
Aix-Marseille university U3 Paul Cézanne in collaboration with CEREGE, France.

2003-2004: Licence STU (Sciences de la Terre et de l´Univers; Earth and Universe Sciences)
Aix-Marseille University U3 Paul Cézanne

2001-2003: D.E.U.G. (Diplôme d´Etudes Universitaires Générales) STU (Sciences de la Terre et de l´Univers; Earth and Universe Sciences)
Aix-Marseille University U3 Paul Cézanne

2001-2001: Baccalauréat S (Scientific). Speciality: Earth and living sciences.

Seagoing experience

IMAGES XII-PECTEN (2005, L. Beaufort, A. Droxler and M.T. Chen), N.O. Marion Dufresne.
12.06.2005 (Bitung, Indonesia)- 08.07.2005 (Darwin, Australia).